Ice Loads

The effect of climate change on Arctic offshore structure design

G. Ordeman

Technische Universiteit Delft

TU Delft

Ice Loads

The effect of climate change on Arctic offshore structure design

by

G. Ordeman

to obtain the degree of Master of Science
at the Delft University of Technology,
to be defended publicly on Tuesday August 4, 2020 at 02:00 PM.

Student number:	4351649	
Project duration:	November 11, 2019 – August 4, 2020	
Thesis committee:	Prof. DSc. K. A. Riska,	TU Delft, Committee Chairman
	Dr. ir. H. Hendrikse,	TU Delft, Supervisor
	Dr. ir. A. Jarquin Laguna,	TU Delft, Supervisor
	R. Bridges,	Total S.A, Supervisor.

This thesis is confidential and cannot be made public until August 4, 2025.

TU Delft

Abstract

For the development of Arctic offshore structures, design ice loads are required. These design loads represent the ice loads a structure may be exposed to for specified requirements. The design ice loads depend on magnitude of the ice loads and on the probability of exposure to the ice loads. Both are impacted by local sea ice conditions.

Climate change affects the sea ice conditions causing change in the ice loads Arctic offshore structures are expected to experience. To obtain accurate design loads, the effect of climate change should be considered in defining those.

Conventional methods to determine design ice loads are based on historical data and assume this data can be used to represent the loads during the lifetime of the structure. However, historical data cannot represent future ice conditions if climate change is considered as sea ice conditions will change. This means that the effect of climate change is not incorporated in the design ice loads when these are based on conventional methods. To include the effect of climate change a new method needs to be developed.

In this thesis, such a new method is proposed that enables to include the effect of climate change into the design ice loads. Instead of historical data, the new method considers the future ice conditions. The method allows to base the design ice loads on sea ice conditions that change over time.

To determine design ice loads, extremal distributions are used. Extremal distributions describe the probability of seasonal maximum ice loads. Commonly, the extremal distribution is based on data covering multiple seasons and cannot properly include inter-seasonal change in sea ice conditions. The new method allows to determine the design ice loads based upon changing extremal distributions. The extremal distributions are determined for seasons separately based on sea ice conditions of one season only.

For the proposed method, a concept referred to as an 'ice state' is introduced. Ice states describe a period of time in which the sea ice conditions are assumed to be constant. When sea ice conditions are constant, the corresponding short-term ice load distributions and the ice load frequency can be determined. Both are required to be able to determine the extremal distribution for one season.

According to the new method, increase of drift speeds causes increase of design ice loads whereas the decrease of ice concentration, thickness and compressive strength causes decrease of the design ice loads. Based upon expected future climate change scenarios, the new method indicates that design ice loads are lower when compared to the design ice loads according to the conventional method.

Preface

This thesis is the result of my graduation project, the final step in completing the master program Offshore and Dredging Engineering specialization Bottom Founded Offshore Structures, Arctic and Wind at Delft University of Technology.

The work presented in this report has been conducted in collaboration with the Total S.A. ice engineering department. I want to express my gratitude to Total S.A. for offering the opportunity to perform my work at the headquarters in La Défense, France for six months.

I would like to express my gratitude especially to my supervisors Robert Bridges from Total S.A. and Kaj Riska, Hayo Hendrikse and Antonio Jarquin Laguna from the TU Delft for providing guidance and sharing their expertise in ice engineering during the research. Their advice and comments have been of great help pursuing the thesis objective.

Also, I would like to thank my family, friends and especially my parents and my girlfriend for their support and sincere interest in this thesis project.

G. Ordeman
Delft, July 2020

Contents

1 Introduction

Nowadays, climate change is a great concern in our society. Due to human economical activities, anthropogenic forcing is considered to have contributed significantly to global warming since the start of the industrial revolution [1]. Consequences of climate change include, among others, extreme weather conditions like droughts, floods, cyclones and sea level rise. These consequences reveal the vulnerability of ecosystems and human systems [2].

Climate change also impacts the Arctic environment. Warming at roughly twice the rate of the global average has been reported in the Arctic region [3]. Warming severely affects Arctic sea ice conditions as it drives ice melting during the melt season and slows down ice growth during the freezing season.

A well-known example of the impact of climate change in the Arctic is the change in sea ice extent. In September, the sea ice extent reaches its seasonal minimum. As can be seen in Figure 1.1, the September sea ice extent has been rapidly declining. Besides extent, other sea ice properties like ice thickness, ice concentration and drift speeds are also affected by climate change.

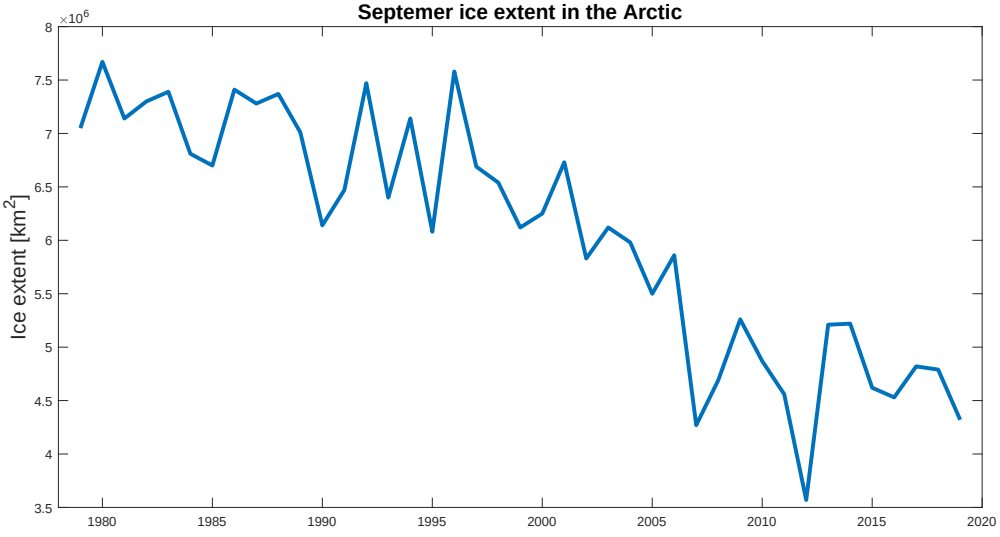

Figure 1.1: September ice extent obtained from the National Snow and Ice Data Center [4].

Arctic offshore structures are exposed to drifting sea ice. Sea ice, colliding with a structure, exerts a load on the structure. In order to prevent failure of the structure, ice loads should be taken into account for design of Arctic offshore structures [5].

Offshore structures are designed to withstand extreme loads because the structure should be able to resist the highest load it will experience during its life time. For different failure modes of the structure, different design loads are defined that represent the extreme loads [6]. However, due to climate change the extreme loads are expected to change. If the extreme loads change, this change should be considered for design of the offshore structures.

How climate change impacts design loads is not straight forward. Not only the magnitude of the loads but also to probability of exposure to the loads play an important role in determining the design loads. Both these aspects are impacted by climate change but how they are impacted is unclear.

Accurate design loads are needed in order to ensure safety of personnel and to prevent environmental damage and economic loss [5]. In order to be able to determine the change in design ice loads, caused by climate change, a new method has yet to be developed.

1.1. Objective

The objective of this thesis is to develop a method to determine design ice loads of Arctic offshore structures including the effect of climate change.

1.2. Scope

Different methods for design of structures exists. In this report, only the limit state design method is considered. This method is the most commonly used method in Arctic offshore structure design.

Focus will be on the impact of climate change on extreme conditions. Most failure modes of a structure are determined by extreme loads. However, failure due to fatigue is not based on extreme loads only and is therefore not in the scope of this thesis.

Depending on the type of ice-structure interaction, the ice load is limited by different limiting mechanisms. The impact of an ice feature is limited by the momentum of the ice. If an ice feature lies still against the structure and does not fail, the ice load is limited by the forces driving the ice feature. If the ice fails, the ice load is limited by the maximum stress the ice can handle before it fails. In this thesis, focus is on ice loads due to failure of ice.

How sea ice fails during interaction with a structure has great impact on the magnitude of the load the ice exerts on the structure. The type of structure influences the failure mode of the ice. For structures with vertical walls, the ice will fail due to compression. In that case, crushing is considered to be the failure mode of ice causing the highest ice loads. For structures with sloped walls, the ice will most likely fail due to bending. Ice loads due to bending are generally assumed to be lower compared to ice loads due to crushing and both depend differently on ice characteristics. Even though bending is important for the design of sloping structures, this thesis will only focus on ice loads due to crushing.

The effect of climate change is believed to be especially large in the Arctic. Therefore, mainly sea ice in the Arctic region is considered in this thesis. However, in other regions offshore structures are also exposed in sea ice. The developed methodology is also applicable to structures in these regions.

1.3. Thesis outline

The first part of this thesis consist of the literature study. In Chapter 2, climate change and its impact on sea ice in the Arctic is discussed. In Chapter 3, methodology for determining design loads and ice loads is described. Additionally, the types of offshore structures are discussed.

The other chapters are part of the core of this thesis. Chapter 4 describes how design loads can be determined if a trend in ice loads exists. In Chapter 5, methodology suitable for determining extremal distributions in case of climate change is discussed. Extremal distributions are needed in order to be able to determine design loads. Chapter 6 describes ice states and how they are used in order to

determine the extremal distribution. Chapter 7 focusses on ice events. How ice events are defined, has great impact on the extremal distribution. Two methods are suggested. Chapter 8 presents a complete overview of the method to determine the impact of climate change on design loads. In Chapter 9, an example case is presented in order to illustrate the full method.

2

Climate change in the Arctic

The climate has been changing on a global level. The impact of climate change is believed to be even bigger in the Arctic compared to the global average. Therefore, major changes in sea ice are to be expected in the future. These changes in sea ice will cause change in ice loads the offshore structures experience. Therefore, the change in sea ice will impact the design ice loads. In order to study the impact of climate change on ice loads, it is import to know how the ice will change in the future and what is causing this change.

2.1. Climate change

Nowadays, more and more research is done into climate change. The cryosphere is a big part of this research because large changes have been observed especially in the Arctic and also because these changes are assumed to amplify the climate change on a global scale [7]. Models have been developed in order to make predictions on near future changes in the climate. Some models predict winter warming will be at least 40% greater by 2100 in northern high latitude regions compared to the global mean [8]. In order to take climate change into account for design of Arctic offshore structures, it is important to know the impact of climate change on different sea ice properties over time.

2.1.1. Arctic amplification

Positive feedback mechanisms are believed to cause amplification of the greenhouse-induced warming in the Polar regions. Therefore, trends in temperature in the Arctic region tend to be larger than trends for the globe as a whole. This is often referred to as Arctic amplification [3]. The impact of different positive feedback mechanisms is still debated but include: ice and snow melt causing decrease of surface albedo, increase of water vapour in the Arctic atmosphere, atmospheric stability trapping temperature anomalies near to the surface, changes in total cloudiness in summer [9].

2.1.2. Intergovernmental Panel on Climate Change

The Intergovernmental Panel on Climate Change (IPCC) was created in 1988 in order to provide assessment reports about climate change for policy makers. This panel only assesses existing literature and does not carry out any research themselves.

The first assessment report originates from 1990 and the fifth report from 2014 is the most recently finished report. IPCC is a body of the United Nations and provides reports for governments to determine climate policies. IPCC now uses the Coupled Model Intercomparison Project Phase 5 (CMIP5) models of the World Climate Research Programme to asses climate change. This project brings together different climate model simulations from all over the world.

Representative concentration pathways (RCPs) characterise different climate change scenarios of anthropogenic forcing. They represent future concentrations of greenhouse gases and are defined by the total amount of radiative forcing in the year 2100 compared to 1850. There are four scenarios considered: RCP2.6 [10], RCP4.5 [11] [12] [13], RCP6.0 [14] [15] and RCP8.5 [16] which correspond to a

radiative forcing increase of 2.6 Wm^{-2}, 4.5 Wm^{-2}, 6.0 Wm^{-2} and 8.5 Wm^{-2} respectively. These RCPs are used in CMIP5 as input to model different climate change scenarios.

IPCC report 'Climate Change 2013: The Physical Science Basis' is part of the fifth assessment and assesses the global climate [2]. Chapter 4 of this report focuses on the observed changes in cryosphere and Chapter 11 focuses on the modelling and predicting the future climate, including a brief description on forecasts of sea ice conditions in the cryosphere.

In 2019, IPCC published the report: 'IPCC Special Report on the Ocean and Cryosphere in a Changing Climate' [17]. This report provides updated information on the climate change in the Cryosphere and is part of the new sixth assessment cycle of IPCC. Both IPCC reports use the same CMIP5 models and RCP scenarios.

Some observed and forecasted changes of sea ice reported by IPCC will be discussed in Section 2.4.

2.1.3. Representative concentration pathways

The report 'The representative concentration pathways: an overview' provides a more in-depth review of the characteristics of the RCPs [18]. RCPs are used as input for climate change models in order to make prediction on how the climate will change in the near future. These models provide insights in how the climate may change with respect to socio-economic change, technological change, energy use, land use and emissions of greenhouse gases and air pollutants. The RCP scenarios include the impact of different climate policies (RCP2.6, RCP4.5 and RCP6.0) and the no-climate-policy (RCP8.5).

For the fifth assessment of IPCC a new set of scenarios was required. The scenarios include more detailed information and different climate policies. That way, one common set of scenarios can be used for various models. These scenarios are not developed by IPCC but by the research community. The scenarios have been selected from existing literature on the concentration levels, this means that there is no consistent design for different (socio-economic) parameters in the four scenarios.

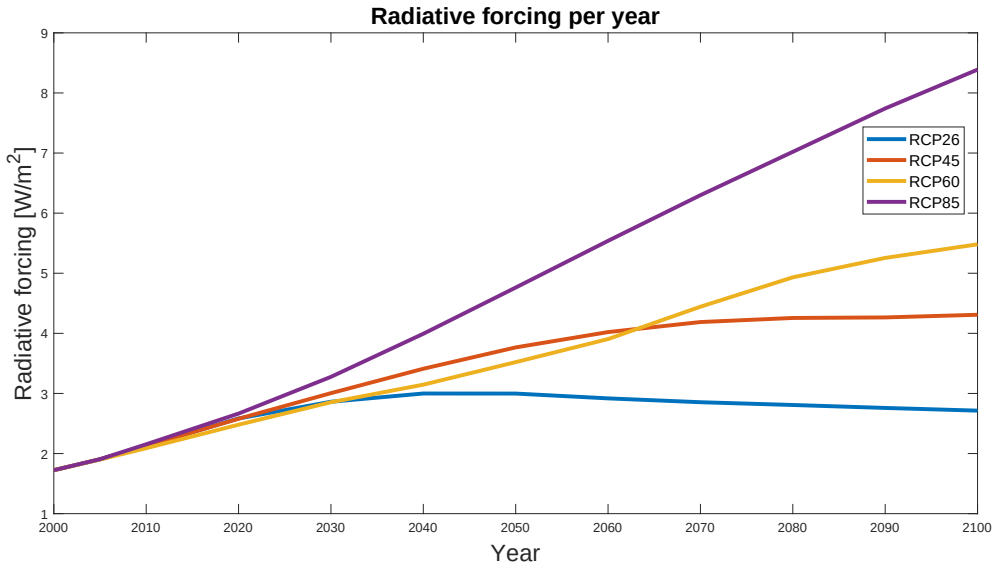

Figure 2.1: Global radiative forcing per year for RCP scenarios obtained from the RCP Database [19].

RCP2.6 is the most optimistic scenario where radiative forcing will mitigate. First the radiative forcing will peak at 3.0 Wm^{-2} but thereafter it declines. In RCP4.5 and RCP6.0 the radiative forcing will stabilize. RCP4.5 stabilizes around year 2100 at 4.2 Wm^{-2} but RCP6.0 stabilizes after the year 2100 around 6.0 Wm^{-2}. RCP8.5 represents a scenario with very high greenhouse gas emissions and the

radiative forcing does not stabilize at all. For all pathways as function of time, see Figure 2.1.

Regarding energy use, RCP2.6, RCP4.5 and RCP6.0 are consistent with intermediate scenarios in the literature. This corresponds to almost doubling today's energy usage to 750 – 900 EJ. Due to expected carbon capture and storage technologies, in all scenarios a greater amount of coal and/or natural gas usage is assumed in the year 2100 compared to 2000. Usage of oil is more-or-less the same in 2100 for the scenarios, except for RCP2.6 it is much lower. The use of renewable resources increases in all scenarios.

The carbon dioxide (CO_2) emission differ for all scenarios, see Figure 2.2. Because the scenarios are selected on the greenhouse gas concentrations, CO_2 emissions correspond well to the literature. RCP8.5 is in the high range of non-climate policy scenarios from literature whereas RCP6.0 is just below most of these non-climate policy scenarios. RCP4.5 is comparable to climate policy and low-emissions scenarios. RCP2.6 corresponds to the lowest scenarios with stringent climate policies.

Emissions of methane (CH_4) and nitrous oxide (N_2O) are highly dependent on the assumed climate policies, see Figure 2.2. For RCP8.5 there is big increase in emissions. For RCP6.0 CH_4 is fairly stable but N_2O increases over time. For RCP4.5 both gas emissions remain quite stable and for RCP2.6 both emissions reduce over time.

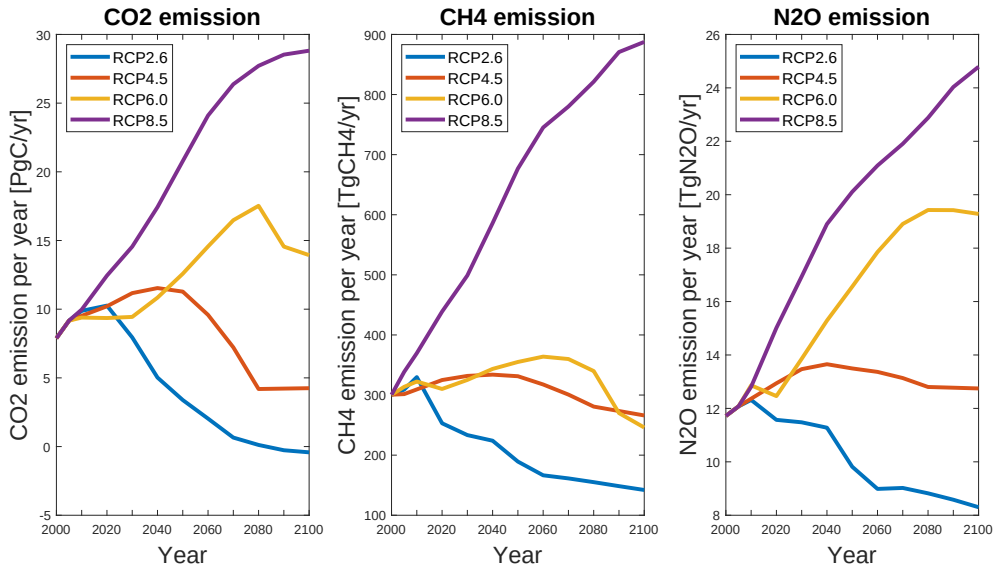

Figure 2.2: Yearly emissions for different scenarios [19].

The RCPs should be interpreted as a set of possible developments and not as a forecast or absolute bounds. There are no probabilities allocated to the RCPs so there is no most-likely scenario. The RCPs only represent ranges of radiative forcing and emissions pathways consistent with scientific literature.

2.1.4. Coupled climate models

The World Climate Research Programme, a program to coordinate international global climate research, initiated the Coupled Model Intercomparison Project (CMIP) to form a framework of most of the existing coupled climate models from modelling groups worldwide. Phase five (CMIP5) is the most recently completed phase of the project and freely provides data including more than 50 climate models from more than 20 institutes. Phase 6 has not been completed yet.

One of the main intentions of CMIP5 was to address some of the questions, that arose in the fourth

assessment report of IPCC, for evaluation in the fifth assessment report. The models are not meant to be comprehensive and do not include all components of the Arctic climate system [20]. Therefore, errors may arise in the simulations. However, the simulated climate futures can still be used as the basis for exploring climate change impacts.

The models focus on two different time scales. The long-term experiments focus on century time scale. The historical runs of these experiments usually start mid nineteenth century to near present so they cover most of the industrial period. Future projections, using the RCP scenarios, of these models start at the present up to the year 2100, some are extended to the year 2300. The near-term experiments start in the year 1960 and go up to the year 2035 [21].

The models are categorized into three different types:

1. Atmosphere-ocean global climate models
2. Earth system models of intermediate complexity
3. Earth system models

The atmosphere-ocean models are considered to be the most simple models. These models only include the exchange of heat and water between the atmosphere and ocean whereas the earth system models also include the carbon cycle. However, for the earth system models of intermediate complexity, the carbon cycle is not considered fully closed because biochemical components are not included.

These models are made to asses climate change at a global scale and the resolution of these models are relatively coarse. Therefore, on a local scale, the model outcomes may not be as detailed as desired. Regional climate models also exist, these focus on one specific area and may provide more detailed high-resolution simulations.

2.2. Arctic environment

Sea ice conditions are impacted by the environment. Different elements of both the atmosphere and the ocean have influence on ice growth and movement. Knowing how these elements impact the sea ice helps understanding how the sea ice changes.

2.2.1. Surface air temperature

The surface air temperature is the main driver of sea ice growth and is therefore important to consider. Because of the Arctic amplification, global climate models project that the Arctic will warm at a greater rate over the coming decades and century compared with other regions of the planet, see Figure 2.3 [22].

2.2.2. Seasonality

Seasonality describes the the annual time and duration of ice advance and retreat. IPCC states that strong regional changes of seasonality have been observed in the Arctic. Most regions show an increase in duration of the melt season. According to the reports, there is high confidence that the Arctic melt season has been extended by ten days per decade since 1979. The melt season starts three days per decade earlier because of earlier melt onset and seven days per decade later because of later freeze-up. The areas between the East Siberian Sea and the western Beaufort Sea show one of the most rapid changes. Here, between 1979 and 2011 the duration of the melt season became three months (90 ± 16) longer, sea ice advance occurred (41 ± 6) days later and sea ice retreat occurred (49 ± 7) days earlier.

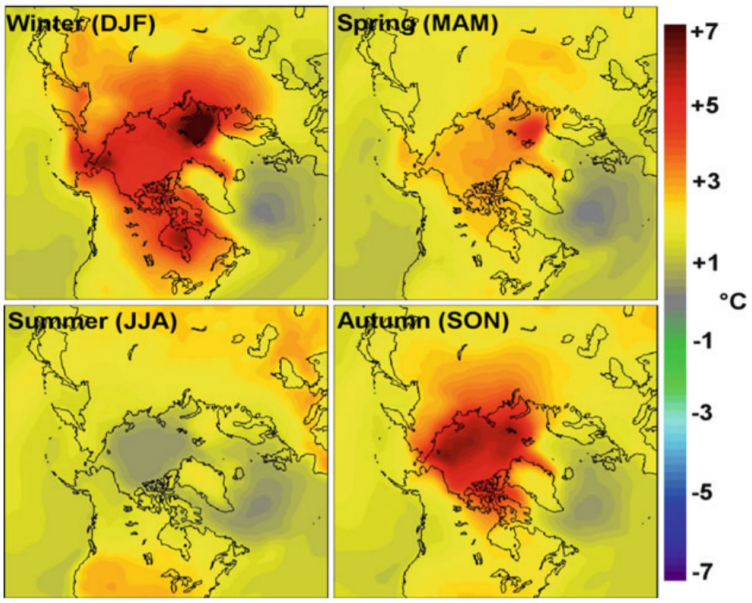

Figure 2.3: Projected changes of temperature by season for 2070–2090 relative to the 1981–2000 mean according to IPCC Fourth Assessment [23].

2.2.3. Snow

Snow has a big impact on sea ice. The insulation by accumulations of snow protects the ice from melting but also limits the growth. If the snow accumulation is sufficiently thick, the weight of the snow will push the ice below the sea surface and snow-ice will form. This process may become more common in the Arctic because of the thinning of sea ice. Both positive and negative temporal trends of snow days have been observed regionally. However, in general, data clearly show a snow decrease throughout the whole Arctic [24].

2.2.4. Wind

In the Arctic, winds force movement of sea ice directly but winds also drive ocean currents, which themselves also force ice movement. In the Arctic as a whole, a small positive trend of only 1% to 2% per decade of averaged wind speed has been observed between the years 1992 and 2009. Regionally, in a large fraction of the Central Arctic, positive trends up to 9 % per decade have been observed in the same time period [25].

2.2.5. Ocean currents

Ocean currents also force movement of sea ice but to a lesser extent compared to wind. The Beaufort Gyre and the Transpolar Drift Stream are considered to be the two governing ocean currents in the Arctic. The Beaufort Gyre causes sea ice to stay in the Arctic Basin and grow old, whereas the Transpolar Drift Stream transport the ice into the Atlantic Ocean where the ice melts.

Literature does not describe a general trend in ocean currents. In 1979, the Beaufort gyre covered a larger area compared to 1994 causing less recirculation and more export of ice through the Fram Strait [26]. On the other hand, circulation in the Beaufort Gyre increased between 2007-2010 relative to 2003-2006 and currents in the south-west Beaufort Gyre even doubled in strength between 2003 and 2014 [27].

2.3. Sea ice conditions

In order to understand how ice is evolving, it is important to understand how conditions of sea ice are described by different ice properties. Some properties are related to each other and some have direct influence on the magnitude of ice loads. How these properties change determines the change in ice loads on structures.

2.3.1. The age of ice

Sea ice is divided in first-year ice and old ice because age influences different properties like thickness, porosity and strength [28]. Old ice is subdivided in second-year ice and multiyear ice. Second-year ice can be seen as a two layered system where the upper layer survived one summer and lower layer is similar to first-year ice. Multiyear ice is, in some ways, more comparable to freshwater and glacial ice than to fist-year ice because of low salinity.

2.3.2. Ice concentration

Sea ice concentration is defined as the surface area of all ice at a given location relative to the total surface area of this location. Ice concentration is measured in order to be able to determine ice areas and ice volumes. The concentration can be determined by ship and aircraft observations and satellite imagery.

2.3.3. Ice cover

Approximately 7 percent of the world ocean is covered by ice [29]. Lots of research is dedicated to the extent of the ice cover for several reasons. One main reason is that the ice cover is considered to have big influence of the global climate because of the albedo effect [7]. Another reason is that the reduction of ice extent, making shipping routes considerably shorter, introduces opportunities for marine traffic around the Arctic. First satellite measurements were already taken in 1972.

Coverage of sea ice in a certain region can be measured as ice extent and as ice area. Commonly, ice area is simply the surface area of all ice in the considered region and can be calculated as the product of the ice concentrations and the surface area of the considered region. Ice extent is the sum of the surface area of all ice in the considered region with concentrations of at least 15% [2].

2.3.4. Ice thickness

Sea ice grows vertically in two different ways: mechanically and thermally. Mechanical growth occurs due to colliding ice sheets (ice ridging and rubbling), thermal ice growth occurs due to heat loss from the ice into the atmosphere.

Ice starts to grow as soon as the surface air temperature gets below the freezing temperature of the sea water. The ice mainly grows at the ice-seawater interface at the bottom. Here the heat from the seawater is conducted through the ice and snow and released into the atmosphere. The process is different for sea water compared to fresh water because of different freezing points. The freezing point of water is well understood and can be calculated as function of pressure and salinity [30]. Because of salinity, the freezing point of sea water is roughly $-1.8\,^{\circ}\mathrm{C}$ [5]. To determine the thickness of ice, not only the surface temperature needs to be taken into account but also the duration of the freezing process.

Stefan's law is commonly used to calculate thickness of first-year ice [31]. Details are described in Appendix B.1. In this method the thickness is a function of Freezing Degree Days (FDD), which combines the air temperature and the duration of freezing into one parameter. FDD should include all days of the considered freezing period.

For multiyear ice, determining the thickness is more complex because mechanical growth plays a big role. Because of the mechanical growth, multiyear ice can be get much thicker than first-year ice. Average ice floe thickness of 11.3 m has been reported [28].

As soon as the surface air temperature gets above the freezing point of sea water, the ice starts to melt. The melting process is far less understood. Literature about the ice melting process and methods for calculating the melting rate of sea ice as function of surface air temperature are limited.

2.3.5. Ice drift

The drift speed of ice is, for the most part, governed by wind. Sea ice drift speeds are normally about 1% to 2% of the wind speed. However, the ice motions also depend on other environmental elements. The momentum of sea ice can be determined using Equation (2.1) where the left-hand side is the derivative to the ice momentum [32]:

$$\frac{D}{Dt}(m\vec{u}) = \vec{\tau_a} + \vec{\tau_w} - mf\vec{k} \times \vec{u} - mg\vec{\nabla}H - \nabla\dot{\sigma} \tag{2.1}$$

Here, m is the mass of the ice feature and $\vec{u}$ is the velocity of the ice. The first two terms on the right-hand side of the equation, τ_a and τ_w, are the atmospheric and oceanic surface drag, respectively. The third term is the Coriolis force, the fourth term the ocean surface tilt and the last term is the ice internal stress. The Coriolis force and the sea-surface-tilt terms can normally be neglected so the ice momentum mainly depend on the atmospheric drag, oceanic drag and the internal friction. These terms relate to sea ice concentration, sea ice thickness, wind and oceanic surface currents.

2.4. Observed changes in sea ice

The IPCC reports provide, among other literature, detailed observations in changes of different sea ice properties. It is useful to know how these properties have changed in order to know how (design) ice actions have changed.

2.4.1. The age of ice

IPCC distinguishes ice into perennial (also called second-year ice) and multiyear ice, where perennial ice survives one summer and multiyear ice survived at least two summers. For perennial ice negative trends between 1979 and 2012 very likely were $-11.5 \pm 2.1\,\%$ and $-12.5 \pm 2.1\,\%$ per decade for the ice extent and ice area respectively [2]. For multiyear ice, the trend of ice extent and area between 1979 and 2012 very likely were $-13.5 \pm 2.5\,\%$ and $-14.7 \pm 3.0\,\%$ [2].

According to the IPCC report of 2019, the average age of sea ice in the Arctic has been decreasing between 1979 and 2018. The proportion of at least five year old ice decreased from 30% to 2%, whereas the proportion of first-year sea ice increased from 40% to 60-70%.

2.4.2. Ice concentration

Observations of larger decline in ice area compared to ice extent imply that ice concentration in the Central Arctic also has been declining. Trends in sea ice concentration differ per location and season. For the seasons February to April (winter) and August to October (summer), the trends in ice concentrations are persistent. In this winter period, between 1979 and 1993, positive trends have been seen in the Labrador sea and the Bering Sea and negative trends in the Greenland Sea and the Barents Sea [33]. Later, from 1993 till 2007, also in the winter season a negative trend is observed in all marginal seas of the Arctic Ocean.

Overall, seasonal trends in sea ice concentration have been negative for all areas, except the Bering sea. From 1979 till 2006, the largest declines of sea ice concentrations can be found in waters extending from Laptev Sea to the Beaufort Sea.

2.4.3. Ice cover

The extent of sea ice has shown an inter-annual downward trend for all months since October 1978 [20] [34]. Changes in summer ice extent have been more significant compared to changes in the winter. The downward trend of September has been the largest and seems to have steepened with time, see Figure 1.1. In the years 2002, 2005, 2007 and 2012 record low ice extents have been observed. In 2011 the extent was reduced with more than 30% compared to 1970 [35] .

According to IPCC, the sea ice cover is a prominent indicator for climate change. The increase of greenhouse gasses cause approximately half of all summer sea ice loss. The ice extent in September shows a trend of $-83\,000\,\text{km}^2$ per year between 1979 and 2018 and in March a trend of $-41\,000\,\text{km}^2$

per year between 1979 and 2019. The main declines of summer ice extent happened in the East Siberian Sea, Beaufort Sea, Chukchi Sea, Laptev Sea and Kara sea. Loss of winter ice extent only mainly occurred in Barents Sea.

The seasonal trends for ice extent are $-2.3 \pm 0.5\,\%$ (winter), $-1.8 \pm 0.5\,\%$ (spring), $-6.1 \pm 0.8\,\%$ (summer) and $-7.0 \pm 1.5\,\%$ (autumn) per decade in the entire Northern Hemisphere. According to IPCC, future shrinking of the Arctic sea ice cover is very likely. For the RCP8.5 scenario a nearly ice-free Arctic Ocean (less than $1 \times 10^6\,\mathrm{km}^2$ sea ice for at least five years) in September is likely to be expected before year 2050.

2.4.4. Ice thickness

Available data of sea ice thickness is limited both in space and time. Estimates on ice thickness are made using both ice draft and freeboard measurements. The first available data originates from submarine records using upward-looking sonar to measure the ice draft [32]. The US navy started executing the first submarine surveys in 1958. Since the year 2000, very little data has been provided from these submarine surveys. Measurements from anchored moorings systems in the Farm Strait and Beaufort Sea have been using the same upward looking sonar, see for example Figure 2.4 [36] [37]. Later, data on ice freeboard from aircraft, helicopter and satellite records became available. Since 2002 Envisat (ESA) and since 2003 ICESat (NASA) spacecrafts have been providing broad data on ice freeboard. Nowadays, both the Envisat and ICESat have been shut down and their successors, CryoSat-2 and ICESat-2, have been launched in 2010 and 2018 respectively.

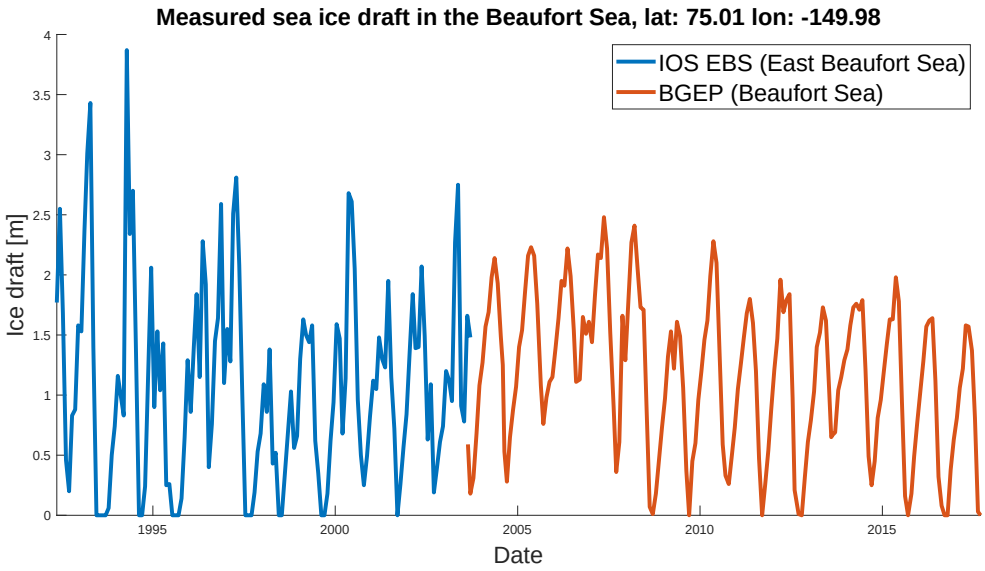

Figure 2.4: Monthly mean ice draft measurements using moored upward looking sonar for two different locations in the Beaufort Sea [38].

Studies have been dedicated to combining the data of the different data sets, trying to find a trend in the ice thickness. These studies report decline in annual mean basin-average ice thickness over the period 2000-2012 from 2.12 to 1.41 meter, a linear trend of -0.58 ± 0.07 m per decade [39]. Including the submarine surveys from 1975 and onward indicates a linear trend of -0.69 ± 0.03 m per decade. However, these submarine surveys only cover almost 38 percent of the Arctic ocean.

In the Arctic, an environmental shift from multiyear to first-year ice domination has been observed [40]. Because older ice generally is thicker, this shift in ice regime contributed to the thinning of the Arctic ice cover. In the Beaufort Sea, this led to a decrease of 44% in mean ice thickness between 2001 and 2007 [41].

Currently the CryoSat-2 satellite provides the main data on ice thickness, giving the opportunity to get insights on how the sea ice thickness is changing on a large spatial scale. The data currently available from this satellite is however limited in time because first data originates from 2010 but first findings imply no (declining) trend [42]. In the 2013/2014 season there is even an increase noticeable.

According to IPCC, land-fast ice thickness has also been decreasing. Since mid-1960s declines in ice thickness of 0.11 m per decade in the Barents Sea, 0.035 m per decade in the Canadian Arctic Archipelago and 0.033 m per decade along the Siberian Coast have been observed.

2.4.5. Ice drift

The earliest measurements of ice drift speed originate from the end of the 19th century. During expeditions schooners were locked in the ice pack so they would drift away along with the ice. The positions of the ships were measured and so drift speeds could be determined [36]. Currently, the same expedition is carried out by the Multidisciplinary drifting Observatory for the Study of Arctic Climate (MOSAiC). More continuous record originates from the International Arctic Buoy Program (IABP). This program uses buoys, which are trapped in the ice sheets, to determine drift speeds. The first measurements are from 1978. Nowadays, broad drift data can also be retrieved from satellite records. The highest drift speeds are observed in October and the lowest in April [37].

Records indicate that sea ice velocities have been increasing over the last few decades, see monthly mean drift speeds of IABP in Figure 2.5. These drift speeds cover the full central Arctic, only the Laptev Sea is poorly covered [43]. Multiple studies have looked into this, trying to find the cause of this observation. No significant trend of wind speeds is noticeable in wind records, so this cannot explain the upward trend of drift speed.

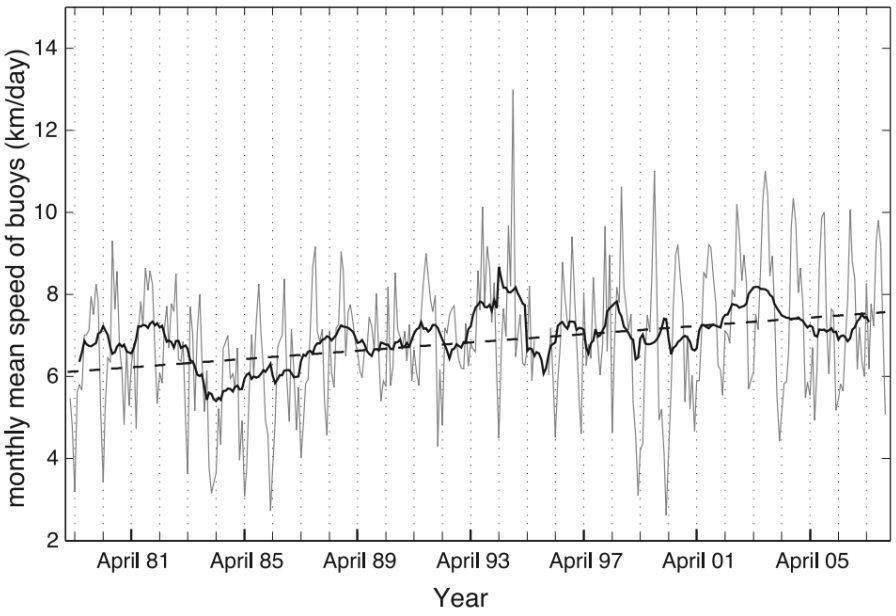

Figure 2.5: Mean drift speed for IABP buoys from 1979 to 2007 in the central Arctic. [43].

According to IPCC, between 1978 and 2007, an increase in drift speed of $17 \pm 4.5\,\%$ per decade in the winter and an increase of $8.5 \pm 2.0\,\%$ per decade in the summer has been recorded. Satellite data between 1992 and 2008 show an increase in average winter drift speed of $10.6 \pm 0.9\,\%$ per decade. The largest increase of drift speed occurred during the second half of this period [2].

The cause for increased drift speeds differs for different seasons [32]. Changes in ice concentra-

tions are assumed to be the main driver from June to November. From December till March the ice concentration is rather constant and shows little change. The decrease in ice thickness, causing the ice to fracture more easily, is likely to be the main driver of increasing drift speeds. In April and May both ice thickness and ice concentration remain nearly constant but drift speeds show strong increases. This is probably caused fracturing of the ice. During this period the fractures will not refreeze as much as it used to and the densely packed ice will weaken as a whole.

2.5. Future changes in sea ice

In order to estimate how ice loads will change in the future, it is important to know how the sea ice will change in the future. How the ice will change is uncertain but can be predicted. Historical observed trends can be extrapolated into the near future but this does not include the physics behind climate change. So, changes in drivers of climate change, like emissions of greenhouse gasses, are not included. Climate models that consider the physics behind climate change, can also be used to predict changes in ice.

2.5.1. Climate model projections

Coupled climate models, like the CMIP5 models, provide insights about expectations of change in sea ice. Unfortunately, the IPCC reports do not state detailed expectations in change of certain ice properties, like thickness or drift speeds, based on these models. However, model output data is available for different ice properties. For example see Figure 2.6, here the sea ice thickness in 2050 according to the model is plotted for the full northern hemisphere. On the left-hand side, the contours of Scandinavia and Russia can be seen, on the right-hand side the contours of Alaska, Canadian Archipelago and Greenland. According to the model, sea ice is much thinner and the ice extent is much smaller for the RCP8.5 scenarios compared to the RCP2.6 scenario.

Studies have been dedicated to asses the quality of different climate models for different ice properties [44]. The performance of the different models can be checked by comparing the models with historical data. Important is that these models are not made to predict change of sea ice on local level. The sea ice is an important mechanism of the bigger global climate and is therefore extensively included in the climate models. In these models, focus lays more on the effect of sea ice change on global scale rather than on the local changes of the ice itself.

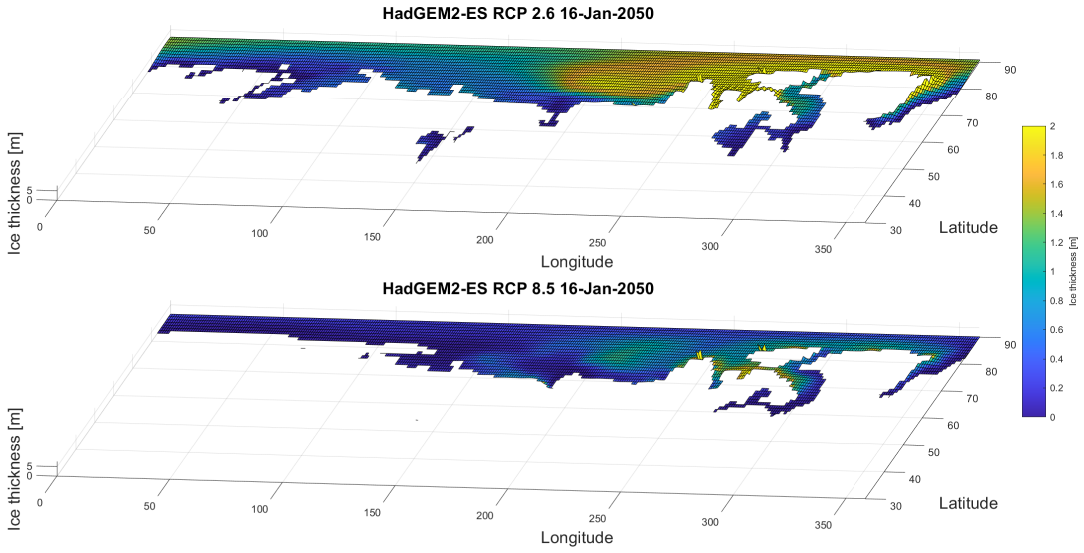

Figure 2.6: Projected global sea ice thickness for the full Northern Hemisphere mapped for the RCP2.6 and RCP8.5 scenario according to earth system coupled climate model from the Met Office Hadley Centre [45].

3

Arctic offshore structure design

Design loads are used to base the design of offshore structures on. The structure should have enough resistance to withstand all loads it experiences during its lifetime. These loads are represented by the design loads. For offshore structures in the Arctic, this also includes loads caused by interactions with sea ice. These ice loads change because the sea ice changes due to climate change and therefore the design ice loads for the structures may also change.

In order to determine how the design loads change, two aspects should be studied. First of all, one should know how the design loads are determined based on the ice loads. Secondly, it is important to know how the ice loads are determined. How they depend on sea ice determines how the change in sea ice causes change in design ice loads.

3.1. Design standards for Arctic offshore structures

Different design codes have been developed over the years. The objective of these standards is to provide guidance in design, construction, installation, transportation, and decommissioning. Requirements are specified to ensure that the structures provide an appropriate level of reliability to govern safety, protect the environment and protect asset value. Some well-known standards related to Arctic offshore design are:

1. API RP 2N [46]
2. CAN/CSA-S471-04 [47]
3. ISO 19906 [5]
4. SNiP 2.06.04-82 [48]

Before ISO 19906, only regionally accepted standards existed which provided different guidance for design of offshore structures. In order to obtain one internationally accepted standard, ISO 19906 has been developed. In the European Economic Area the standard has been adopted. In Canada, ISO 19906 has replaced CAN/CSA-S471-04. In the United States of America, API recommends ISO 19906 and API RP 2N has been withdrawn. In Russia, ISO 19906 has been translated for usage [49].

3.1.1. ISO 19906

The International Organization for Standardization (ISO) is an organisation that provides international standards for almost every industry. The standard ISO 19906 is part of the ISO 19900 series for offshore structures that is developed for the petroleum and natural gas industries [5]. ISO 19906 focuses on offshore structures in the Arctic and in environments with similar characteristics. It is the most commonly known standard in the field of Arctic engineering, the most recent edition originates from July 2019.

The main method of ISO 19906 of ensuring safety, is by ensuring that the resistance of the structure is larger than the ice actions the structure experiences. This includes guidance on determining design loads.

3.2. Design methods

The working stress design method and the limit state design method are the two most commonly used design method for structures. Limit state design method is suggested by ISO 19906 and is often used in offshore structure design [50]. Therefore, only the limit state design method is considered for determining the effect of climate change on Arctic offshore structure design.

3.2.1. Working stress design

The workings stress design method, also referred to as the allowable stress design method, considers the stress developed in the structural members and connections. This stress should not exceed the yield or buckling stress divided by a safety factor [51]. The method does not allow plastic deformation of the structure members and may therefore lead to a design with unnecessary high structure resistance.

There is great variability in loads and structure resistance. The safety factor should account for the variability of both these aspects. For different conditions, the variability of the loads and the resistance may be different. Therefore, it is difficult to define one safety factor for different conditions. Also, the method uses one safety factor for several failure modes acting together leading to irrationality of the safety factors [51]. Therefore, the safety factor may also lead to a design with unnecessary high structure resistance.

3.2.2. Limit state design

The limit state design method, also called the load and resistance factor design method, is different compared to the working stress design method in two ways.

The limit state design method addresses the variability of the loads and the resistance separately. Two safety factors are used, one for the load variability and one for the variability of the structure resistance. This way, the method allows to use different safety factors for different types of loads. This may be useful because, for example, dead loads have less variability compared to live loads [52].

Instead of combining different failure modes like the working stress method, this method considers limit states. These limit states are defined as a condition beyond which a structure or a part of a structure exceeds a specified design requirement [6] [50]. Because different limit states consider different design requirements, for some limit states plastic deformation is allowed. In Section 3.3.2, the different limit states suggested by ISO 19906 are described.

3.3. Design loads

Design values represent a certain variable for a specified time period. Besides loads, design values can also be determined for other properties like ice thickness or ice drift speed. However, one should be careful using these design values because they do not necessarily correspond to the design load of that time period. For example, an ice feature with the maximum ice thickness within a hundred year time period may exert less pressure on a structure compared to an ice feature which is slightly thinner but has higher compressive strength. In this study main focus will be on design loads.

Different design loads should be determined for different failure modes of the offshore structure. Extreme loads should be considered for plastic deformation of structure members whereas repetitiveness of loads leading to elastic deformations determine design loads for fatigue failure. Main focus in this report is on design loads for extreme conditions.

3.3.1. Return period

The design of a structure should have sufficient capacity to resist the greatest load this structure will experience during its lifetime. Therefore, when characterising design values, often 'return periods' are

used. For design values for extreme loads, this return period corresponds to the average time to the first exceedance of this load.

The probability of event X taking place during a trial can be calculated using Equation (3.1). If the event happened during the trial, it is considered to be a success. The probability of the event ($P(X)$) is calculated as the number of successes ($n_{successes}$) divided by the total number of trials (n_{trials}).

$$P(X) = \frac{n_{successes}}{n_{trials}} \tag{3.1}$$

So, if the probability of an ice load being exceeded ($P(F > F_x)$) is known, the average number of trails needed to have one success (the ice load (F_x) is exceeded once), can simply be calculated using Equation (3.2):

$$n_{trials} = \frac{n_{exceedances}}{P(F > F_x)} = \frac{1}{P(F > F_x)} \tag{3.2}$$

Using the average number of trials, the return period of the load can be calculated. For design loads, the return period (t_R) is the average time to the first exceedance of this load. One trial is considered to be one season with the duration (t_{trial}) of one year. Therefore the return period is expressed in years. So, the number of trials can be expressed as a function of the return period, see Equation (3.3):

$$n_{trials} = \frac{t_R}{t_{trial}} = \frac{t_R}{1\,\text{year}} \tag{3.3}$$

The design load (F_D) corresponding to a given return period in years can be determined using Equation (3.4):

$$P(F > F_D) = \frac{1\,\text{year}}{t_R} \tag{3.4}$$

Because the the return period is the average time to exceedance, there is still a certain probability the load is being exceeded before the end of this return period. For design values, often the maximum load is required. Therefore, the probability used in Equation (3.4) should be the probability of a load being the maximum load of that year. In order to find this load, the probability density function of annual maximum loads is required. This probability distribution is often referred to as the 'extremal distribution', see Figure 3.1.

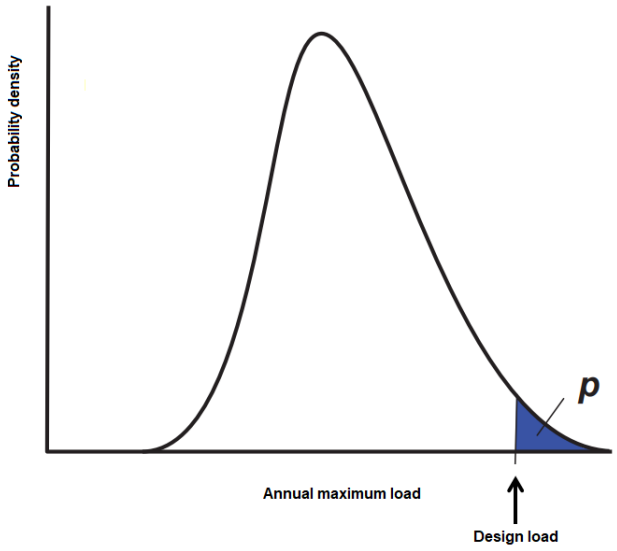

Figure 3.1: Design value as function of the extremal distribution.

For this method to be valid, the extremal distribution should represent all years considered in the return period. This could be, but only if the climate could be considered constant over this time span. So, when the impact of climate change is studied, this assumption cannot be made.

In case of a changing climate, the extremal distribution should be determined for smaller time periods where the environmental conditions can be assumed constant. So multiple distributions are required to cover the return period. How design loads can be determined based on multiple different extremal distributions is described in Chapter 4.

3.3.2. Limit States

In order to ensure that the structure withstands all ice loads it experiences, different limit states should be considered for design. In ISO 19906, return periods are allocated to the different limit states. How these return periods are determined so they correspond with the limit states is not clearly stated. The return period may vary for different types of structure but there is no dependency of the design lifetime even though the lifetime has a great impact on the probability of exposure to extreme ice loads.

Ultimate Limit State

The ultimate limits state (ULS) is associated with prevention of impairment of the structure function. Evacuation and suspension of operations is possible but the structure should have sufficient resistance to withstand the ULS load without any damage impacting the functionality of the facility.

The ULS design value is based on extreme conditions. The ULS load represents the maximum load with a return period of 100 years. Thus, this 100-year load corresponds to exceedance probability of the annual maximum load of 1%.

Accidental Limit State

The accidental limit state (ALS), also called abnormal limit state is also based on extreme conditions. In general, the return period for ALS loads is 10.000 years. ALS requires the structure to survive the accidental load. Damage is possible but should not lead to undesirable events.

ISO 19906 suggests for manned platforms with evacuation possibilities or platform that are not considered as high-consequence platforms, a return period of 1000 years. For unmanned and low-consequence platform ALS does not have to be considered.

Serviceability Limit State

The serviceability limit state (SLS) requirements ensure adequate performance under normal operations. The SLS load may corresponds to a return period of 10 years but exact SLS specifications are generally seen as responsibility of the owner.

Fatigue Limit State

The fatigue limit state (FLS) covers the accumulated effect of repetitive ice loads on the structure. Therefore, not only extreme ice loads but all loads need to be considered for this limit state. This may also include loads during transportation and installation of the structure. Because FLS is based on a different methodology, main focus of this report is on the other limit states.

3.3.3. Extremal ice load distribution

The extremal distribution should give the probability of the annual maximum ice load the structure could experience. How this distribution for ice loads is determined and how this distribution is affected by environmental parameters is generally unclear. Neither ISO 19906 and other design standards nor literature suggest specific methods for determining probability distributions of ice loads.

The extremal distribution should be based on ice loads. How these loads are determined seems a bit obscure. For example, if one piece of ice interacts with a structure a continuous load is applied on the structure for as long as the interaction lasts. How the load profile looks like, highly depends on the failure mechanism of the ice. Somehow, to determine which loads to consider, a selection of loads

should be made based on this load profile.

The ice loads that should be selected, can be linked to an ice event. In ISO 19906 an ice event is defined as the occurrence of ice-structure interaction for which ice actions can be calculated. ISO 19906 also notes that this can be occurrences of peaks within a specified length or duration of the interaction process. How to select the length or duration of the interaction is key to select events but is not suggested in ISO 19906.

Furthermore, the impact of environmental conditions on the extremal distribution should be studied. That way, the impact of climate change on the extremal distribution can be determined. It seems obvious that for thicker ice due to more severe environmental conditions, ice loads are also more severe. However, thicker ice tends to be less dynamic and therefore the probability of exposure to these ice loads may be lower. How these probabilities are exactly impacted is unclear and should be determined in order to be able to study the impact of climate change.

3.3.4. ULS design load according to ISO 19906

In order to directly calculate the ULS design load due to ice crushing, ISO 19906 suggest the method described in Appendix B.7 [5]. This method calculates the upper bound load that should represent the global ice load during the extreme level ice event. Meaning that, this load should correspond to the ULS design load.

This load highly depends on the ice strength coefficient (C_R), see Equation (B.17). This coefficient should encompass both the strength of the ice as well as the probability of occurrence of the ice within the return period corresponding to ULS. Both are highly site specific. ISO 19906 suggests 3 different ways to determine this ice strength coefficient. However, none of those methods seem to include both site specific ice strength and the probability of exposure to the ice.

The first method is based on location, Arctic, subarctic and temperate regions are distinguished. This method assumes that the strength of ice and the number of expected events are the same in the whole Arctic even though they highly depend on the considered location.

The second method is based on the number of events per year the structure is exposed to and the return period of the strength coefficient. This approach seems more reasonable but the suggested values are only based on data from Baltic Sea and thus does not consider local ice strength.

The third method suggest to scale the strength coefficient with the local ice strength. This can be done using local uni-axial compressive strength measurements or borehole jack strengths. If this data is not available, an alternative is proposed. An average strength index can be calculated as function of the brine volume according to site specific data. Also the reference average strength index is given, so the strength coefficient (C_R) can be scaled using these values. So, this method includes local strength of the sea ice but does not consider site specific expected number of events.

3.4. Arctic offshore structures

Most of the Arctic offshore structures have been build as production facilities of hydrocarbons, see Figure 3.2. However, also bridge piers, lighthouses and wind turbines have been installed in Arctic regions. The type of structure affects how the ice and structure interact. Therefore, the structure type also has impact on the ice loads and is an important part of the design process. The Arctic offshore structures can be classified into three different types:

1. Artificial islands
2. Bottom founded structure
3. Floating structure

Artificial islands can be build non-retained or retained with sand bags, rocks or a caisson. They have great resistance to ice loads but can only be build in shallow coastal zones. Several artificial

islands have been build North off the coast of Alaska, see Figure 3.2a.

Bottom founded structures types include gravity based structures, piled structures and jack-ups. These structures can be build in moderate water depths. Jacket type piled structures are relatively simple but difficulties with ice have been encountered in the past leading to severe damage [53]. Gravity based structures, see Figure 3.2b, show better ice resistance but can be relatively expensive. Jack-ups do not have great ice resistance but they are mobile and can therefore be removed from site in case of severe ice loads.

Floating structures are suitable for deep waters. They can be moored or use dynamics positioning for station keeping. These structures are not fixed but drift because these structures are not rigidly fixed to the sea floor. Lots of different types of floating structures have been proposed like conical buoys (see Figure 3.2), ship-shaped units, tension leg platforms, single point anchor reservoir platforms and semi-submersibles. Only steel buoys, ships and semi-submersibles actually have been used. These structures do not have great ice resistance but they could be detached from mooring in case of severe ice threats.

(a) Artificial island Northstar (b) Gravity based structure Prirazlomnoye. (c) Floating conical buoy Kulluk

Figure 3.2: Offshore structures installed in the Arctic.

The shape of the structure at water level is an important feature for the structure regarding ice loads. Whether the structure is vertical or has an inclination determines the way the ice fails, see Figure 3.3. The ice will be compressed if it is pushed against a vertical wall. If structure has an inclined wall, the ice will be bend out-of-plane. Ice loads due to bending are generally assumed to be lower than ice loads due to compression.

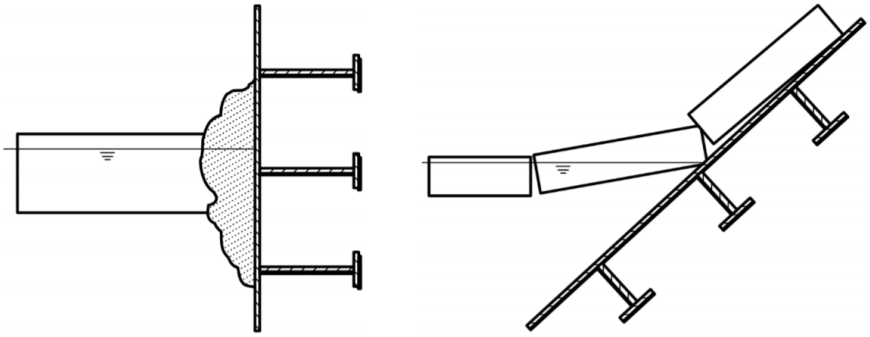

Figure 3.3: Ice failure illustrated for vertical and sloping structures [5].

3.5. Ice actions

Once an ice feature collides with an offshore structure either the piece of ice stays intact or it fails and interaction between the ice and the structure starts. During this interaction, the ice exerts a loads on the structure (and vice versa), often referred to as ice actions. During the interaction, the load is not constant but increases up to the point either the ice or the structure fails.

Whether the ice feature stays intact or fails depends on the momentum and the work done by failing the ice for the whole structure width [54]. If the kinetic energy is larger than the work done by failing, the ice fails. Otherwise, the ice stays whole, comes to standstill and remain at location or may drift away. If the ice comes to standstill, ice load can simply be calculated solving the energy balance. However, if the ice fails, calculating ice loads is much more complex.

3.5.1. Compression

Different failure modes exist for compression of ice. Which failure mode takes place depends on indentation speed, geometry and ice properties [55]. The geometry mainly determines whether the ice buckles or not. For relative thin ice (high aspect ratio between structure width and ice thickness), the ice tends to buckle. If the ice does not buckle, the ice can fail in two manners; viscous/plastic for slow indentation speeds (creep) or cracking/spalling for high indentation speeds (crushing). In Figure 3.4, the failure mechanisms are visualized and mapped to show for which regimes of indentation speed and aspect ratio each mechanism dominates [56].

Buckling

Buckling ice failure is failure due to out-of-plane flexure of the ice during compression. Therefore, this is actually a bending failure due to compression. Circumferential cracks form if the ice start to buckle causing short peak loads. Buckling only happens for high aspects ratios.

Creep

Creep of ice is failure in a ductile manner, the ice envelops the structure leading to an almost uniform pressure interface. From the start of the interaction the load increases gradually up to a point ice failure reaches a steady-state. Creep is mainly observed during low indentation speeds and low aspect ratios.

Crushing

Crushing is failure of ice due to fracture. It is a combination between pulverization, spalling, and radial cracking of the sea ice. This causes, instead of a uniform, a highly local contact and pressure interface. Because of the cracking, loads are rapidly oscillating around a mean load. Crushing mostly takes place at high indentation speeds and low aspect ratios.

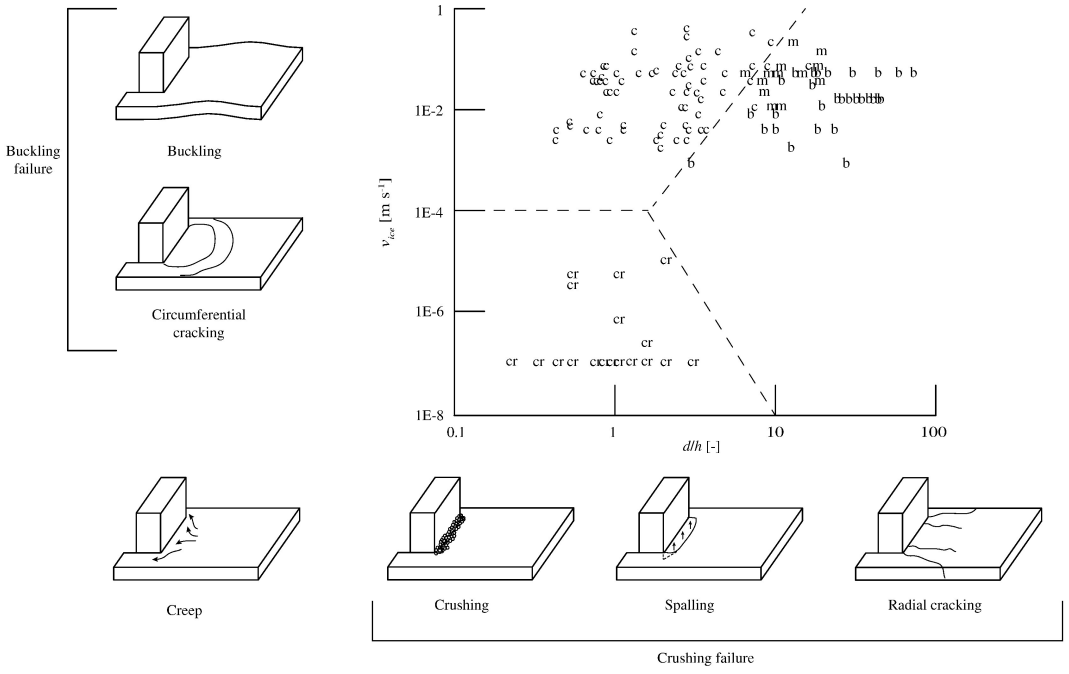

Figure 3.4: Ice failure map based on results of Timco 1991 [55]. B-Buckling, C-Crushing, M-Mixed crushing and buckling, and Cr-Creep failure [56].

Mixed mode
For certain conditions the ice fails both by buckling and crushing. In that case, the mechanism alternate, causing the load to build up, highly oscillate due to crushing and drop to zero because of buckling of the ice.

3.5.2. Bending
For sloping structures, sea ice will fail in flexural failure mode. In general, ice loads due to bending are assumed to be lower than ice loads due to compression. This interaction is complex because, besides failure of the ice, ride-up of broken ice pieces, accumulation of ice rubble on or under the slope, and subsequent clearing of the rubble also exert loads on the structure which should be taken into account. In ISO 19906 a detailed method is suggested to calculate ice load due to bending. Even though bending is an important part of the design of sloping structures, focus of this report is on ice loads due to crushing.

3.5.3. Crushing Load
For vertical structures, crushing is generally assumed to be the failure mechanism leading to the highest load. Therefore, it is important to consider the global crushing loads for design. Different method have been developed to determine these loads however they all seem to have their shortcomings.

One way of estimating the global crushing load is by using the uni-axial compressive strength of the ice and the contact area. For crushing, the actual contact area is considered to be much smaller than the interaction area (ice thickness multiplied by the structure width) [57]. The effect of non-simultaneous ice failure and the effect of spalling and radial cracking changing the ice geometry should be taken into account [58]. Because of spalling, the ice gets a wedged shaped front seen from the side reducing the contact area. Because of radial cracking, the ice also gets a wedged shaped front seen from above. To estimate the actual contact area Equation (B.14) in Appendix B can be used.

For crushing regimes the average value for C_{NS} is smaller than 0.25 and the upper-limit is around 0.4 [59]. For C_G, a value of 0.3 can be assumed [60]. The global crushing load can be estimated using Equation (B.15).

3.6. Engineering properties of sea ice
The strength of sea ice determines when the ice fails. Therefore, it has great impact on the ice loads. The strength of ice can be measured in different ways, for example: compressive, flexural, tensile and shear strength. Which type of strength is relevant depends on failure mechanism considered. Therefore, some types are more relevant for design than other. Ice strength highly depends on the structure and porosity of ice. The porosity itself is determined by the salinity and temperature of the ice.

3.6.1. Salinity
Because of the salinity of sea water, salt gets captured in sea ice when the sea water freezes. Salinity is measured as the fraction of the mass of the salt to the total mass of unit it is entrapped in. One way of measuring the salinity is by melting the sea ice and measuring the electrical conductivity of the melt water. In Appendix B.3, the method used to determine the salinity for first-year ice as function of thickness is elaborated [61]. This method is based on ice data from both the Arctic and the Antarctic.

3.6.2. Porosity
In contrast to pure ice, sea ice also consists of brine and gasses (mostly just air). The total porosity (ν_t) can be calculated as the sum of the relative brine volume (ν_b) and the relative air volume (ν_a). It is important to know the porosity of the ice because it has big impact on its strength.

When the sea water freezes, pure ice forms. This causes solutions of highly concentrated salt in sea water (brine) and solid salt crystals to get trapped in the ice. Some of this brine drains out of the ice. If the ice grows fast, more brine gets captured compared to slow growing ice. Besides brine, also

air gets trapped during the growing process.

The porosity is generally assumed to be a function of ice salinity, temperature, growth rate, structure and also density. However, the relative brine volume and relative air temperature can be estimated using the empirical functions that only includes salinity (S_i), temperature (T_i) and density(ρ) [62]. Details of this method are provided in Appendix B.4.

3.6.3. Compressive strength

Compressive strength is an important property of sea ice because the ice often fails due to compression during interaction with a structure. This is also the case for ice crushing which is one of the main governing mechanism determining design ice loads. Lots of research into compressive strength has been done.

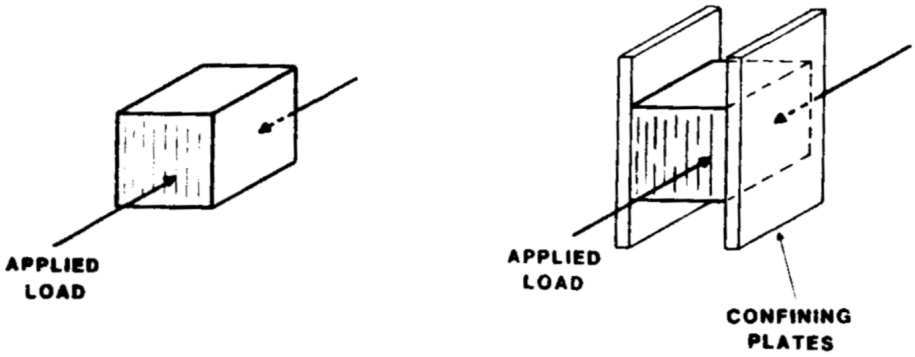

Figure 3.5: The considered unconfined and confined columnar sea ice [63].

The compressive strength can be measured unconfined (uni-axial) and confined (bi- and tri-axial) and highly depends on the structure of the ice. For granular ice, the confined compressive strength can be 19 percent higher compared to the unconfined compressive strength. For columnar ice, the confined compressive strength can be four times higher than the unconfined compressive strength, if the ice is horizontally loaded and the confinement is in the same plane as the applied load and the columnar structure of the ice, like in Figure 3.5 [64].

Whether confined or unconfined compressive strength should be considered for interactions between ice features and offshore structures seems not entirely clear. Two options seem reasonable depending on the geometry of the ice. If the ice is relatively narrow, so the ratio between thickness and width ($\frac{h}{w}$) of the ice is high, maybe the assumption could be made that the ice is unconfined and unrestricted to move horizontally and uni-axial strength is most appropriate. Otherwise, if the ice is relatively wide, the ice can be assumed to be confined and restricted to move in a horizontal direction and bi-axial compressive strength is more appropriate.

One way of calculating the uni-axial strength is by using the method of Timco and Frederking, see Appendix B.5 [65]. For this method, only the average air temperature (T_a), ice thickness (h_i) and strain rate ($\dot{\epsilon}$) are needed. The method suggests that the ice is divided in nine layers, see Figure 3.6. The top layer is assumed to be made of granular ice and the other layers of columnar ice.

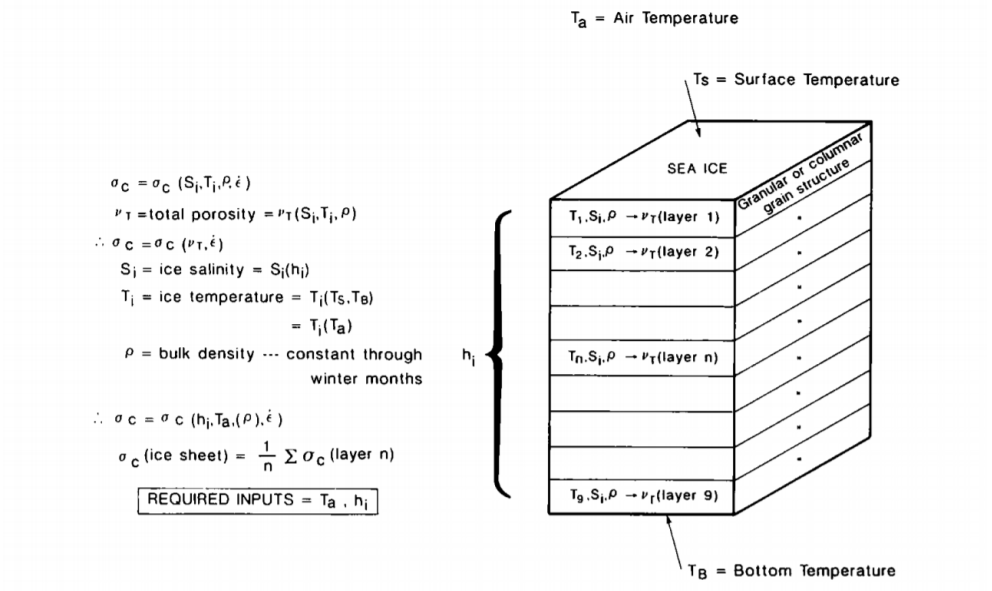

Figure 3.6: The compressive strength according to Timco and Frederking [65].

3.7. New method for design loads

Both existing methods described in Section 3.3.1 and Section 3.3.4 seem unable to include the effect of climate change in design loads. If that is the case, a new method needs to be developed that enables to include the effect of climate change in design ice loads. Two types of methods seem possible options.

First option is a method like the method defined in ISO 19906 [5]. This means a direct equation as function of different relevant ice properties. These ice properties should be linked to the considered return periods. In that case, the return periods of the ice properties are affected by climate change.

Second option is a method based on the site specific extremal distributions. Different extremal distributions are needed to cover the return period and include climate change. In this case, also a method needs to be developed to determine design loads based on changing extremal distributions.

The first method does not provide a clear insight in how the climate change affects the design loads. The second method explicitly includes extremal distributions. The extremal distributions are affected by climate change. Once is known how climate change exactly affects the extremal distribution, the effect of climate change on design loads can be studied more easily. Therefore, the second method is preferred.

4

Determining design loads

Commonly, design loads are based on historical data and the assumptions is made that there is no trend in the data. In order to determine design loads based on data having a trend a new method needs to be developed.

4.1. Common practice

The conventional way to determine design loads is based on historical data. Here, the seasonal maximum crushing loads from Figure 4.1 are used. How these seasonal maximum loads are determined, is described in Appendix A.4. Maximum values are selected for a certain frequency, commonly annual maximum values are used. Because sea ice only grows during the freezing season, it is convenient to consider a one year time period that covers a whole freezing process instead a calender year that covers two freezing seasons only partially. In this case, the maximum loads are selected in the period between August 1 and July 31 of all available seasons in the dataset. These loads are calculated according the method discussed in Appendix B.6.

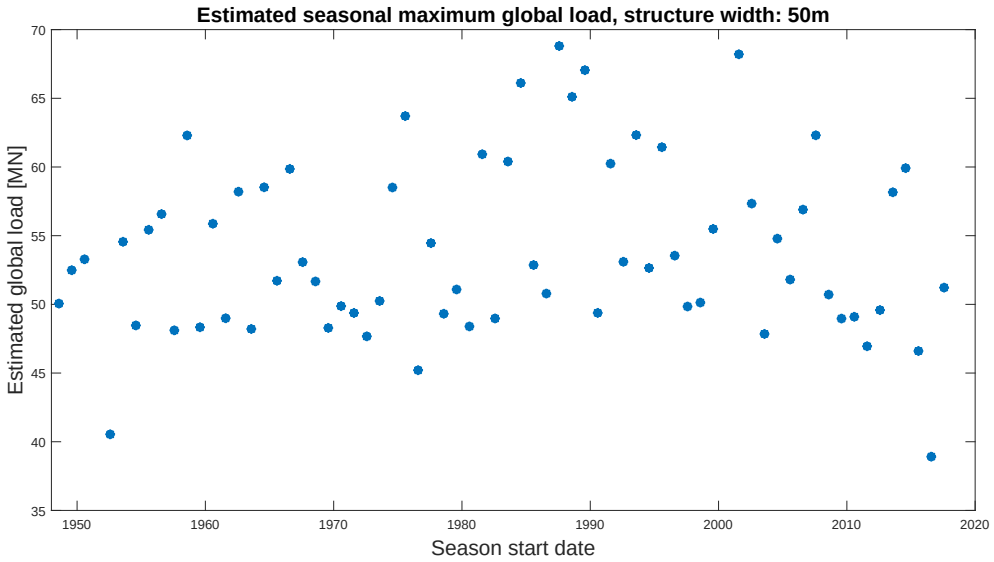

Figure 4.1: Estimate of seasonal maximum crushing load at Resolute Bay.

To determine the cumulative probability of the seasonal maximum ice loads, the following method is used [66]. The loads are arranged in ascending order. To each load n a cumulative probability is allocated using Equation (4.1). Here, N is the total amount of data points. The cumulative probability is plotted in Figure 4.2. Because the considered data are seasonal maximum loads, the plotted cumu-

lative probability is an approximation of the cumulative probability function of the extremal distribution. Therefore, this data can be used to fit the extremal distribution.

$$P(F_{max} \leq F_n) = \frac{n}{N+1} \tag{4.1}$$

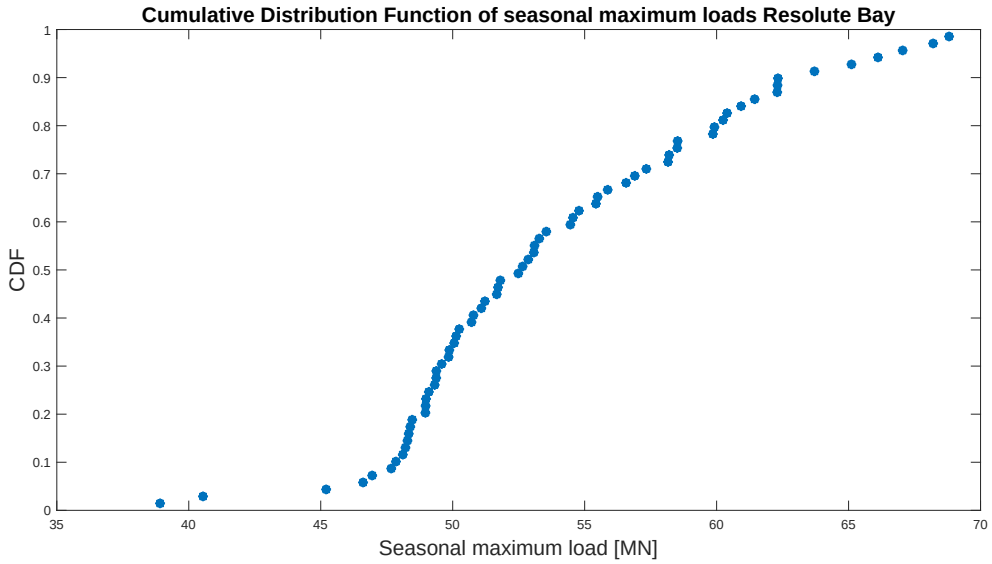

Figure 4.2: Cumulative Distribution Function based on of seasonal maximum crushing load at Resolute Bay.

Based on Equation (3.4), the return period for each load can be calculated using Equation (4.2). The conventional way of determining the return period of the considered design value, is fitting a curve to the return periods and extend this curve to the desired return period to determine the design load. For the purpose of illustration, a Generalized Extreme Value type I extremal distribution is fitted in Figure 4.3. Which type of curve is suitable depends on the nature of the considered parameter. This issue is discussed in more detail in Chapter 5. Based on the curve fit, the ULS design load at Resolute Bay is 69.76 MN.

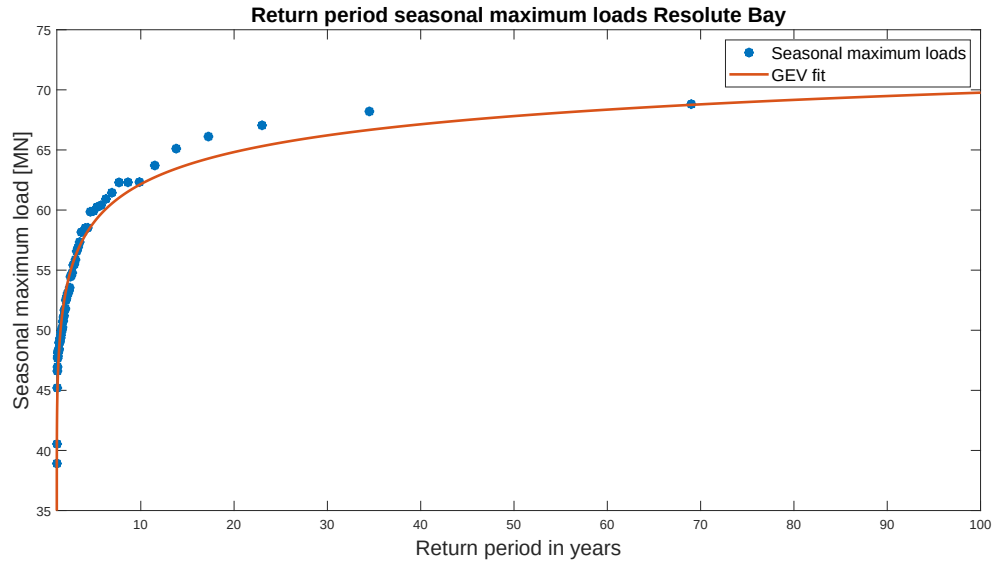

Figure 4.3: Return periods of seasonal maximum crushing loads at Resolute Bay.

$$t_R = \frac{1\text{ year}}{P(F_{max} > F_n)} = \frac{1\text{ year}}{1 - P(F_{max} \leq F_n)} \tag{4.2}$$

4.2. Data with trend

For the purpose of illustrating the problems that arise using the conventional method for data having a trend, a trend is added to the annual maximum loads retrieved from the Resolute Bay data. How the trend is applied to the data, is elaborated in Appendix A.5.

The data and the corresponding return periods are presented in Figure 4.4. According to the curve fit, the ULS design load is equal to 60.06 MN. In both graphs, data point fade from blue to red as time progresses. As can be seen in the lower graph, the data points in the beginning of the time interval mainly end up at the right hand side because they correspond to the largest return period. So, these data points have great impact on the right hand side of the curve fit and therefore on which load correspond to the return periods relevant for design loads. However, because of the trend in the data, these loads are less probable in the future.

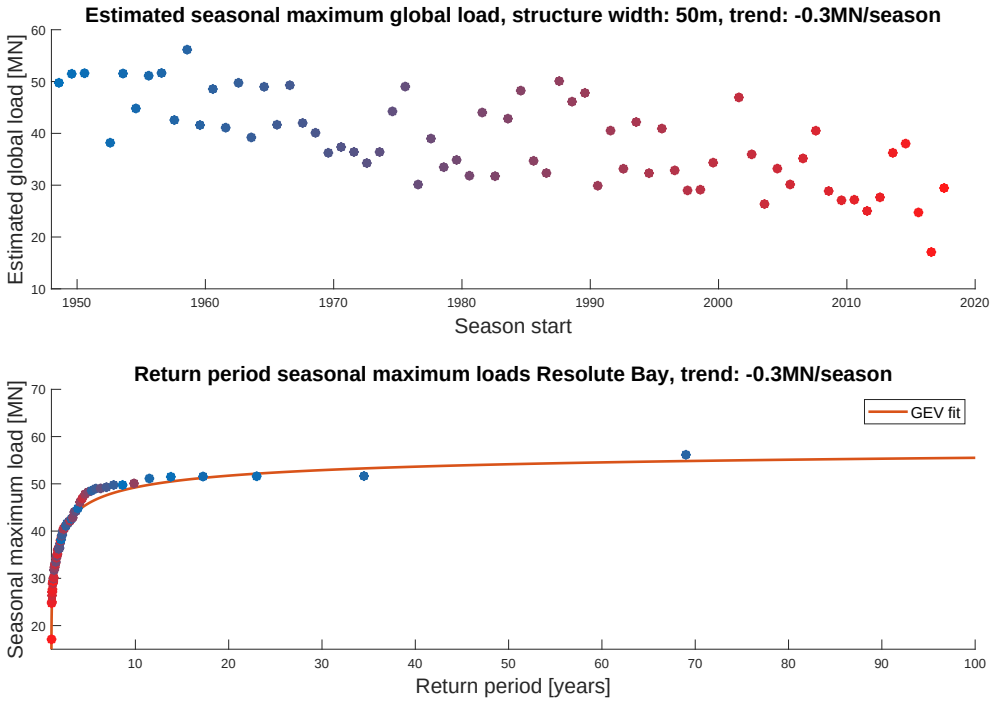

Figure 4.4: Seasonal maximum crushing loads with trend and corresponding return periods at Resolute Bay.

This method is not suitable for extrapolating the curve fit to determine return period of ice loads if the data has a trend. Therefore, if design loads are based on historical data with a downward trend, design loads for structures build after the time period of this historical data are overestimated. Vice versa, for data with an upward trend design loads will be underestimated.

The trend could be removed from the data, as described in Appendix A.5. That way the anomaly could be used to determine the a return period. However, here another problem arises. The trend should be included in the design loads. So, some load representing the trend should be added up to the load corresponding to the return period of the anomaly. However, because of the trend, the data is inconstant over the considered time period and therefore this cannot be properly done. Which value should be selected to represent the trend depends on the moment in time the extreme load corresponding to the return period occurs. However, this moment in time cannot be known.

In Figure 4.5, the trend and anomaly have been separated from the annual maximum loads. According to the exponential curve fit, the ULS design load anomaly is equal to 15.24 MN. The trend of the global load is extrapolated for forty years. This time period can be considered as the lifetime of an offshore structure. Which value of the trend forecasted during the lifetime of the structure should be added up to the design load according to the anomaly is unclear.

For a downward trend, the expected load at the start of the lifetime of the structure according to the trend may be used. This way, design should be safe because the most extreme possibility is considered. However, even in the case of a downward trend, the highest load case does not necessarily occur in the beginning of the lifetime of a structure. Therefore, this method seems conservative leading the overestimation of the design loads.

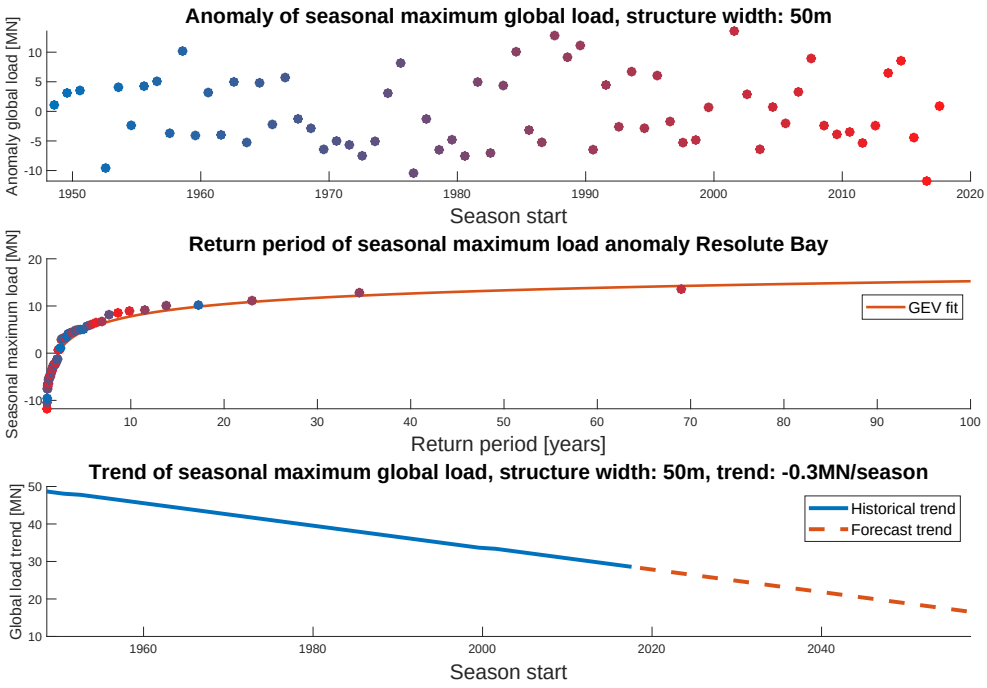

Figure 4.5: Separated trend and anomaly of seasonal maximum crushing loads at Resolute Bay.

The same holds for data having an upward trend. Here, the load expected according to the trend at the end of the lifetime of the structure can be used. This also covers the most extreme case leading to overestimated design loads.

So, this method cannot be used if a trend is to be expected in future loads. Furthermore, climate change may not only have impact on the trend but also on the anomaly of ice loads.

4.3. Multiple extremal distributions

For the conventional method, the assumption is made that an extremal distribution based on the historical data can also be used for probabilities of loads in the future. So, this extremal distribution is assumed to represent each season in the return period. However, one extremal distribution cannot represent multiple seasons if climate changes is considered. Because of climate change, the sea ice conditions change for each season. This means that the extremal distribution changes over time.

In Figure 4.6, the estimated seasonal extreme global loads for Resolute Bay are divided into two

intervals and for each interval an Generalized Extreme Value type I extremal distribution is fitted. If these extremal distributions are assumed to represent both intervals, they can be used to determine the probability of the loads for the whole time period.

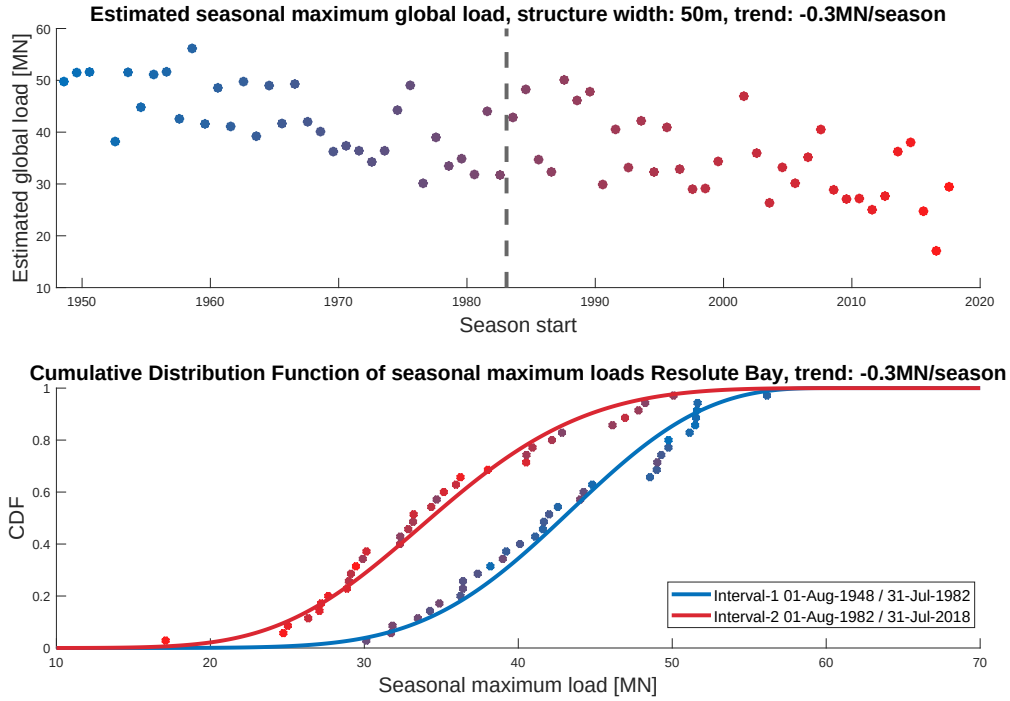

Figure 4.6: Cumulative extremal distribution fit for two intervals of seasonal maximum crushing loads at Resolute Bay.

So, to include the trend in the design load, multiple extremal distributions should cover the full return period. The smaller the time period the extremal distributions covers, the smaller the error in the design load will be. If each season is covered by one specific extremal distribution, the inter-seasonal trend is fully included.

Normally, the load with a 1% probability of being exceeded according to the extremal distribution is used as design load with a 100 year return period (ULS). Because this load has a 1% probability of being exceeded in one trial, on average 100 trails are needed before the load is exceeded and $n_{exceedances} = 1$ like in Equation (4.3).

$$n_{exceedances} = n_{trials} \cdot P(F > F_x) = 1 \tag{4.3}$$

In this case, one trial corresponds to one full season with a duration of one year. Therefore, 100 years is the average time period to the first exceedance of this extreme load with a 1% probability of being exceeded in one season. For this reasoning to be valid, the assumption is made that events of one year cause no change in probabilities of events in the next years and the extremal distribution is the same for all considered years.

If multiple extremal distributions are considered, this method no longer holds as the probability of a extreme load changes as time progresses. However, in order to determine the extreme load with an average of 100 trials to the first exceedance, the product of the probability of exceeding in each trial and the number of trials should still be 1 after 100 trials.

Instead of assuming that the probability of a load being exceeded is constant over the full time period, the changing probability of the different smaller intervals should be combined. However, the

condition $n_{exceedances} = 1$ should still hold after 100 years for the ULS design load. The average number of exceedances ($n_{exceedances}$) of a load (F) being exceeded for full time period can be calculated using Equation (4.4). The average number of exceedances is calculated as the sum of the product of probability in one trial in the specific interval (n) and the number of trials corresponding to that interval for all intervals (N). For a load corresponding to $n_{exceedances} = 1$, the average number of season before the load is expected to be exceeded is exactly equal to the duration of the considered time interval. So the return period of this load is equal to the considered time period. If $n_{exceedances} > 1$, the return period is smaller than the considered time interval and on average the corresponding load occurs more than once in the interval and if $n_{exceedances} < 1$, the return period is bigger than the considered time interval and on average the load occurs less than once in the interval.

$$n_{exceedances} = \sum_{n=1}^{N} \left(P_n(F_{max} > F) \cdot n_{trials,n} \right) = \sum_{n=1}^{N} \left(P_n(F_{max} > F) \cdot \frac{t_n}{1\,\text{year}} \right) \tag{4.4}$$

Here, N is the total number of intervals, $P_n(F_{max} > F)$ probability of the seasonal maximum load exceeding load F, $n_{trials,n}$ the number of trials in the considered interval n and t_n the duration in years of interval n. In Figure 4.7, the average number of exceedances of the ice loads for both intervals and for the full time period of the data set are plotted based the two extremal distributions in Figure 4.6. According to this method, the design load with a return period equal to the duration of the first (blue) interval is equal to 54.54 MN. For the second interval, the design load with a return period equal to the duration of the second (red) interval is equal to 49.37 MN. For the full time period, the design load with a return period equal to the duration of the full interval (yellow) is equal to 54.79 MN. The duration in this interval is 69 seasons. For comparison, the ice load with a return period also equal to 69 seasons according to the method described in Figure 4.4, is equal to 56.88 MN.

If an interval of 100 years is considered, the load with a return period of a 100 years could be determined using this method. However, the Resolute Bay does only provide data for 69 seasons, so the ULS design ice load cannot be determined for this data using this method.

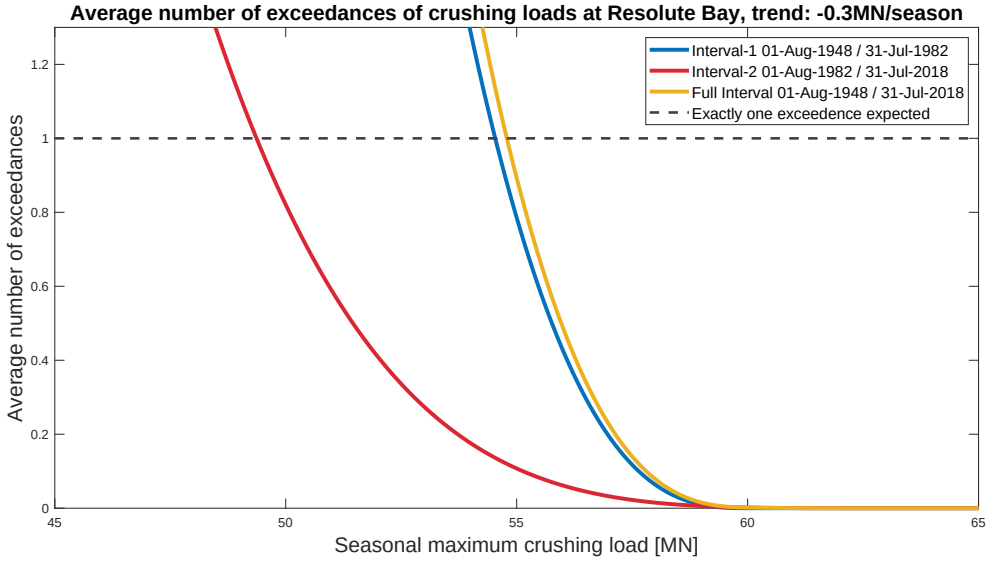

Figure 4.7: Average number of exceedances during the considered interval of seasonal maximum crushing ice loads at Resolute Bay based on two extremal distributions.

In this example the design load is based on historical data and only two extremal distribution are used. This method could also be used for more than two extremal distributions which should result in more accurate design loads. In order to determine design loads for future loads, the extremal distri-

bution covering future time intervals should be known. In that case, the extremal distributions should cover the future time period with the duration equal to the considered return period.

5

The extremal distribution

Extremal distributions are needed to determine the design loads. The extremal distribution represents the probability of maximum load events due to extreme conditions for a specified time interval.

Different methods to determine the extremal distribution exist. A common method is to fit a probability distribution to observed maximum values. However, the extremal distribution can also be based on the parent distribution. The parent distribution represents not only the maxima but includes all load events of the considered parameter.

In order to illustrate the methods for determining the design values, data from Resolute Bay in Canada is used. This data is assessed in Appendix A.

5.1. Extremal distribution based upon parent distribution

The parent distribution, also called the initial distribution, is in this context the probability density function of the loads of all events a structure is exposed to in a certain time period. The occurrence of one ice load event is assumed to not affect the probability of occurrence of other ice loads event. So, the ice loads are assumed to be independent. If all ice loads of one season are independent and have the same parent distribution, this parent distribution can be used to determine the extremal distribution. In order to get an adequate extremal distribution, an adequate parent distribution is crucial. Especially, the tails of these distributions have great influence on the extremal distributions and the design values.

The cumulative parent distribution function represent the probability of a load to be less than or equal to a given load. This cumulative distribution function (F_{parent}) can be determined with the probability density function (f_{parent}) of the parent distribution using Equation (5.1):

$$P(X \leq x) = F_{parent}(x) = \int_{-\infty}^{x} f_{parent}(x)dx \tag{5.1}$$

The probability of the loads of two events to be both less than or equal to a given load, is the product of probability for the load of each individual events to be less than or equal to this given load. Because for each event the probability is assumed to be the same, the probability of all loads X_n, for n event, to be less than or equal to load x can be calculated using Equation (5.2):

$$P(\text{all}X_n \leq x) = P(X_n \leq x)^n = F_{parent}(x)^n \tag{5.2}$$

If the number of events in a certain time period is known, the probability of all loads for all events in this time period being less than or equal to an given load can be determined. This probability is actually the cumulative distribution function of the extremal distribution of this time period. So, the cumulative distribution function of the extremal distribution can be determined using Equation (5.3):

$$F_{extremal}(x) = P(\text{all}X_n \leq x) = F_{parent}(x)^n \tag{5.3}$$

The probability density function of the extremal distribution can be determined using Equation (5.4). In Figure 5.1, the extremal distribution is determined for the season 1969 - 1970. The parent distribution is approximated with a kernel distribution fit to daily estimated crushing loads. How these loads are calculated is discussed in Appendix B.6. The number of events expected in the season should be determined as function of the ice conditions, more details in Section 6.2. For the purpose of illustration, the extremal distribution is presented for different number of events ($n = [10, 100, 200]$). As can be seen in the figure, for higher values of n the extremal distribution shifts to the right and tend to be more peaked.

$$f_{extremal}(x) = \frac{d}{dx}\left(F_{extremal}(x)\right) \tag{5.4}$$

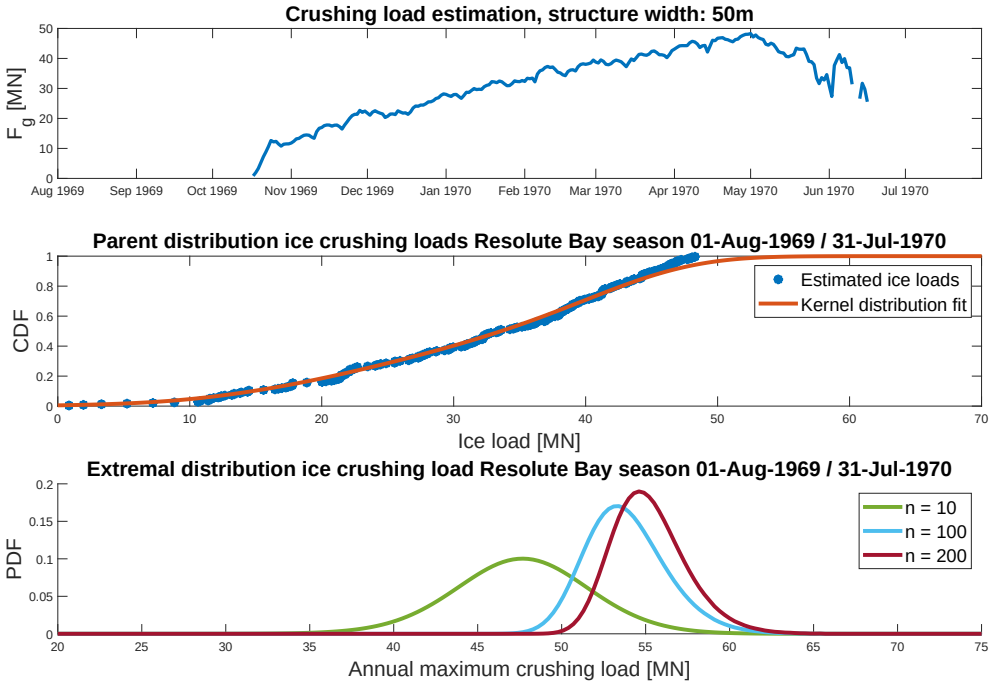

Figure 5.1: Extremal distribution based on daily data of one season at Resolute Bay.

So, in order to determine the extremal distribution for one season according to this method, the parent distribution and the expected number of events of that season are needed. Both are impacted by climate change.

5.2. Extreme value distribution fit

Using the method described in Section 5.1, commonly used parent distributions tend to an extremal distribution of the same form. If these forms are known, a direct fit to extreme values can be used to determine the extremal distribution without using the parent distribution itself. Therefore, the generalized extreme value distributions are developed. These distributions have these forms and can be fitted to data in order to approximate the extremal distribution. The generalized extreme value distribution family consist of three different types a distribution with each a different form:

1. Type I Gumbel
2. Type II Fréchet
3. Type III Weibull

These types are related to each other and the generalized extreme value distribution family can be expressed as one function, see Equation (5.5). Type I, II and III are obtained for $c = 0$, $c > 0$ and $c < 0$ respectively.

$$F_{GEV}(x) = \exp\left\{-\left[1 + c\left(\frac{x-\gamma}{\delta}\right)\right]^{-\frac{1}{c}}\right\} \qquad \text{for: } 0 \leq 1 + c\left(\frac{x-\gamma}{\delta}\right) \tag{5.5}$$

All three classes have distinct forms of behaviour, which is determined by the tail behaviour of the parent distribution. In Figure 5.2, type I is fitted to the seasonal maximum ice loads of Resolute Bay. The distribution is fitted using the maximum likelihood estimation method. This method maximises the likelihood that the process described by the model produced the actual input data.

Type I is by far the most commonly used type because it is suitable for most types of parent distributions. This type is suitable for parent distributions with tails that decays at least as fast as exponentially. The tail of this distribution will decline to zero.

Type II distribution is suitable for parent distributions with tails that decays not as fast as exponentially. The tail of this distribution will also decays to zero but not as quickly as type I.

Type III is suitable for limited parent distributions. So, the considered value of the parent distributions cannot be greater than certain maximum value. Therefore, this type extremal distribution is also limited to this maximum value. In essence, ice loads are limited because ice thickness is physically limited and compressive strength is limited because air temperatures. However, defining a maximum ice load is difficult. Therefore it may be better to treat the ice load to be unlimited and check whether the ice loads resulting from the extremal distribution are reasonable in magnitude.

All in all, the behaviour of the tail of the parent distribution is determinative for the type and shape of the extremal distribution.

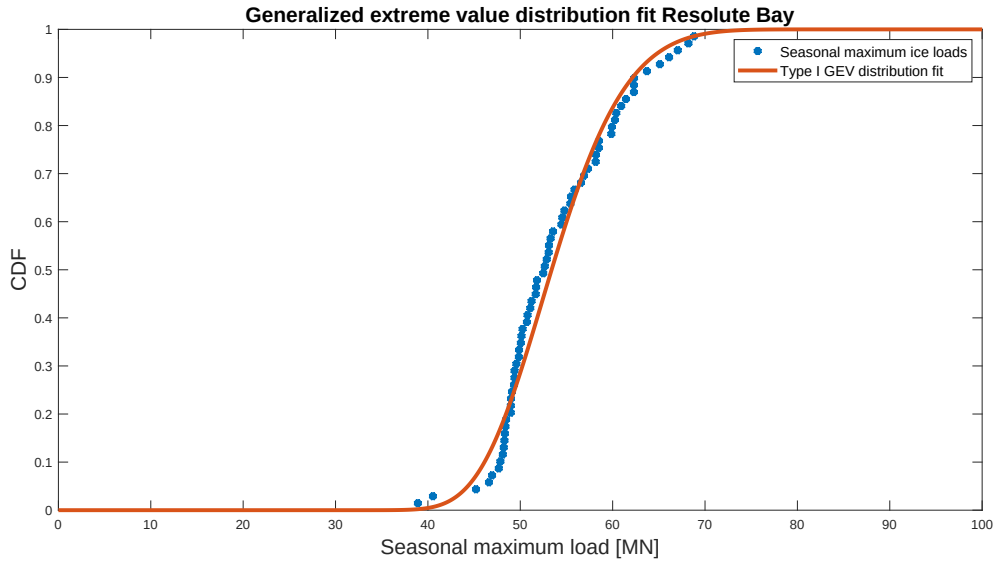

Figure 5.2: Cumulative distribution function of the generalized extreme value type I Gumbel distribution fit.

5.3. Extremal distribution for data with trend

The extreme value distribution fit is not a suitable method if a trend in the loads is to be expected because using this method determining multiple extremal distributions covering small time periods is not possible. For each season only one value can be used. Therefore, multiple years of data are necessary in order to be able to fit an extreme value distribution. Because these extreme distribution

covers multiple seasons, the impact of climate change on ice loads cannot properly be included in the distributions. Also, generalized extreme value distributions assume no trends in the ice loads.

Furthermore, this method is based on historical extreme loads and the assumptions is made that the distribution based on historical data could also represent probabilities of future loads. However, if climate change is considered, the parent distributions is different for each season. Therefore, the extremal distribution of one season cannot be used for another season. So, an extremal distribution based on historical data cannot be used for future seasons.

The preferred method for determining the extremal distribution is by using the parent distribution. The main advantage of this method is that the parent distribution already can be determined with data of only one season. Therefore, the extremal distribution of one season can already be determine on data of only one season. That means that for each individual season a specific extremal distribution can be determined. This is desirable because this makes it possible to properly capture a trend in data into the design loads. Therefore, using the parent distribution is recommended if a trend in the loads is to be expected.

Another advantage is that both magnitude of the loads and the number of events are explicitly included because both are affected by climate change. Therefore, the impact of these aspects can be examined individually. The difficulty in this method lies in determining the parent distribution and expected number of events.

6

The ice state

In order to determine the extremal distribution for a certain time interval, the parent distribution and the expected number of events for this whole interval are required. For ice loads, considering each season individually seems convenient. This way, the full seasonal cycle of sea ice evolvement is captured. The parent distribution is considered to be a long-term distribution because it covers a time span where governing conditions cannot be considered constant.

In order to be able to determine the long-term parent distribution and the expected number of events for a full season, the use of ice states is required. An ice state is defined as a time period in which the sea ice conditions are constant. Because the ice conditions during an ice state are assumed to be constant, for each ice state the short-term probability distribution and the event frequency can be determined. If is known which ice states are to be expected, the long-term parent distribution and seasonal number of events can be determined.

The ice state is characterised by the relevant ice properties that impact the extremal distribution. That means that the ice properties with an impact on the short-term distribution and the event frequency during the ice state should be considered. The short-term distribution is mainly impacted by the magnitude of the ice loads. According to the method discussed in Appendix B.6 the crushing load of sea ice depends on the ice thickness and the compressive strength of the ice. The event frequency is impacted by ice concentration, the dimensions of the ice feature and drift speed. How the short-term distribution and the event frequency are determined exactly is addressed in Chapter 7.

6.1. The parent distribution

In the field of ocean engineering, short-term distributions are used to determine long-term distribution [67]. For all sea states occurring in the long-term time span, a short-term distribution is determined. For these sea states, the sea characteristics are assumed to be constant. These short-term distributions are combined in order to get the long-term distribution.

This approach could also be applied for ice loads with the use of the state of the sea ice. First, for all ice states (N), occurring in the long-term time span, an short-term distribution should be determined, Then, the long-term probability distribution can be determined using the short-term distributions. The long-term parent distribution can be calculated using Equation (6.1):

$$f_{long-term} = \sum_{i=1}^{N} \left(w_i \cdot f_{short-term,i} \right) \tag{6.1}$$

Each short-term distribution is weighted by weight factors w_i.

6.2. Seasonal number of events

To determine the extremal distribution for one time interval, the expected number of events in the season should also be known. The number of events can be calculated as the product of the length of the period with sea ice and the event frequency during this season. Like with the short-term distributions, the seasonal event frequency should be linked to the ice states. If is known which ice states are to be expected in the season, the total number of events to be expected in the full season can be calculated using Equation (6.2):

$$n_{events} = t_s \cdot \eta_{long-term} = t_s \cdot \sum_{i=1}^{N} (w_i \cdot \eta_i) \tag{6.2}$$

Where, t_s is the length of the season with sea ice expressed in a unit of time, $\eta_{long-term}$ the weighted event frequency for the full season, w_i the weight factor and η_i the event frequency corresponding to the ice state i calculated for all ice states N. In Figure 6.1, a schematic overview of using the ice states to determine the parent distribution and seasonal event frequency is presented.

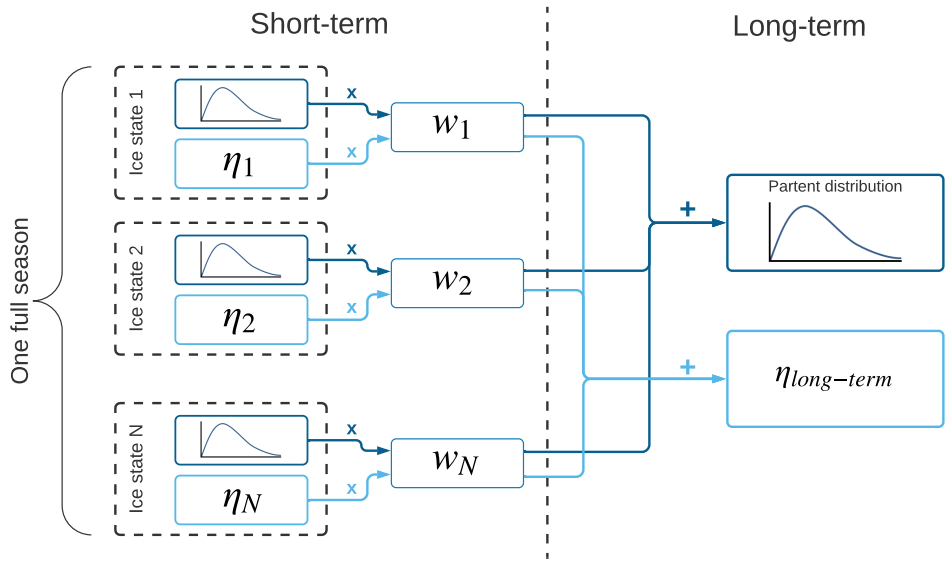

Figure 6.1: Schematic overview of determining the parent distribution and seasonal event frequency.

6.3. Weight factor

For each ice state, also the weight factor needs to be determined so the long-term parent distribution and the expected number of events for the full season can be calculated. The weight factor scales the short-term term distribution and the event frequency with the exposure to the considered ice state relative to the total exposure to all ice states. For these weight factors, the condition in Equation (6.3) should hold.

$$\sum_{i=1}^{N} w_i = 1 \tag{6.3}$$

One way to determine this weight factor is using the probability of the ice state. Because the parent distribution covers one full season, the probability distribution of the ice states should also cover this full season. The probability of an ice state is the same as the joint probability of the governing ice properties of that ice state. In this case, that means the joint probability of the ice thickness, compressive strength, concentration, drift speed and the dimensions of the ice features. How the joint probability of those ice

properties can be determined exactly is unclear and should be examined. This is complex because the different ice properties are dependent on each other. For example, compressive strength is a function of the ice thickness. The correlation between the different ice properties should be determined before the joint probability of the ice properties can be obtained.

An easier way of determining the weight factor is by using the frequency of the ice states. If future data is used where the frequency of occurrence of the ice states is known, this frequency can be directly be used as weight factor of the ice states. The condition in Equation (6.3) should still hold.

6.4. Impact of climate change

The distributions of the considered ice properties are impacted by the environmental conditions. Here, climate change comes into play because climate change impacts the environmental conditions. Therefore, the weight factor of the ice states are impacted by climate change.

The parent distribution will change because the weight factor of the different ice states will change. Depending on the impact of the climate change on the probability of the different ice states, contribution of the different short-term load distributions to the long-term parent distribution will be change.

The expected number of events for the full the season will also be impacted by climate change. Because of the rising temperatures, the freezing season will be shorter. So there will be a shorter period of time when there is sea ice. The number of events is also impacted by the changing weight factor like the parent distribution.

7

Ice events

Events are selected ice loads during ice-structure interaction. How an ice event is defined determines which values of the load during the interaction are selected. How the ice event is defined is not generally agreed upon but does affects the shape and scale of the short-term distributions and also the event frequency for the ice states.

7.1. Short-term distribution

The short term distribution should include all events that occur during a specific ice state. The type, shape and scale of the short-term distribution needs to be determined.

The magnitude of ice loads mainly determine the scale of this distribution. Considering Appendix B.6, the magnitude of the ice loads depends on the ice thickness and compressive strength of the ice and the width of the interaction zone. The width of the interaction zone is limited by the width of the structure or, if the ice feature is smaller than the structure, the width of the ice feature. These ice properties therefore impact the scale of the distribution.

Which loads are selected also impacts the shape of the short-term distribution. Which type and shape distribution gives a good fit should be determined for the specific selection criteria.

Once the type and shape of the short-term distribution are known, the distribution can be scaled using the magnitude of the expected load corresponding to the ice state. For example the method discussed in Appendix B.6 can be used to estimate the ice load, this load can be used as the mean or mode of the distribution.

7.2. Ice state event frequency

The ice state event frequency ($\eta_{ice-state}$) represents the number of ice load events per unit of time during an ice state and depends on two aspects:

1. The events frequency during an ice-structure interaction η_{events}
2. The exposure rate to sea ice during the ice state $r_{exposure}$

To determine the event frequency for an ice state, the events frequency during an ice-structure interaction and the exposure rate to sea ice during the ice state can directly be multiplied. The exposure rate to sea ice represents the fraction of time the structure is exposed to ice during the ice state. The exposure rate is calculated as the product of interaction frequency and the duration of the interactions, see Equation (7.1):

$$\eta_{ice-state} = r_{exposure} \cdot \eta_{events} = \eta_{interactions} \cdot t_{interaction} \cdot \eta_{events} \tag{7.1}$$

In Figure 7.1, a schematic example is presented. The interactions frequency ($\eta_{interactions}$) represents the number of interactions per unit of time during the ice state. In this example, the number of interactions divided by the duration of the ice state (t_T). The average duration of the three interactions (t_1, t_2, t_3) can be used for the duration of the interactions ($t_{interaction}$). The event frequency during the interaction (η_{events}) represents the number of ice load events during the interaction and depends on which ice loads are selected as events (red dots) during the interaction.

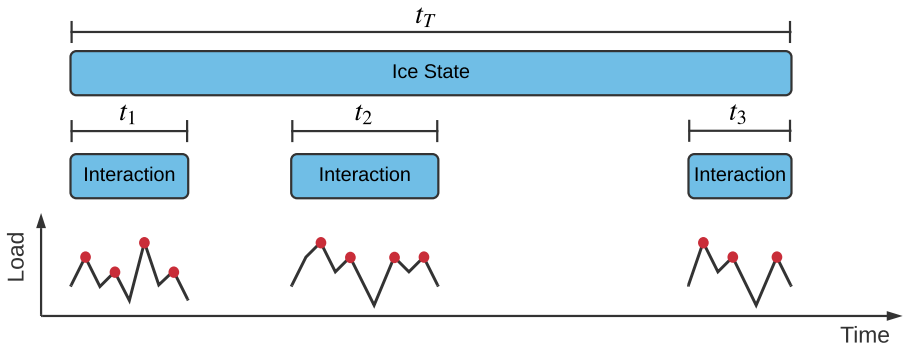

Figure 7.1: Schematic overview of determining the event frequency.

7.2.1. Interaction frequency

The ice-structure interaction frequency depends on the ice concentration, ice drift speed and the dimensions of the ice features. A method is needed to be able to to calculated the number of interactions. In ISO 19906, a method is suggested for this. In this method Equation (7.2) is used to calculate the rate of interactions per unit time:

$$\eta_{interaction} = \rho_A \left(\bar{D} + w\right) \bar{v} \tag{7.2}$$

Here, ρ_A is the areal density (number per unit area) of the ice features, w is the width of the structure, $\bar{D}$ is the average width or diameter of the ice features expected in the region and $\bar{v}$ is the average drift speed over the region.

The areal density can be expressed as function of the sea ice concentration and the average surface area of the ice features, see Equation (7.3). The areal density is calculated as the number of ice features ($n_{features}$) in the considered region divided by the total surface area of this region (A_{region}). The number of ice features can be calculated as the total surface area of all ice in the region (A_{ice}) divided by the average area of one ice feature ($A_{feature}$). The surface area of all ice itself can be calculated as the product of the sea ice concentration (C_{ice}) and the total area of the region.

$$\rho_A = \frac{n_{features}}{A_{region}} = \frac{A_{ice}}{A_{region} \cdot A_{feature}} = \frac{A_{region} \cdot C_{ice}}{A_{region} \cdot A_{feature}} = \frac{C_{ice}}{A_{feature}} \tag{7.3}$$

So, the interaction frequency can already be determined if the ice concentration, average ice feature area, average ice feature width and the structure width are known, see Equation (7.4).

$$\eta_{interactions} = \frac{C_{ice}}{A_{feature}} \left(\bar{D} + w\right) \bar{v} \tag{7.4}$$

The interactions frequency only represents the number of encounters of ice [68]. This method does not consider ice-structure interaction once the ice feature has hit the structure. So, the method does not suggest a method to determine the duration of the interactions.

7.2.2. Event frequency

The frequency of events during interaction between ice and the structure depends on how the event loads are selected. The average frequency of the events can simply be calculated using the number of events (n_{events}) selected in an interval and the duration of this interval ($t_{interval}$), see Equation (7.5):

$$\eta_{events} = \frac{n_{events}}{t_{interval}} \tag{7.5}$$

7.3. Selecting events

The purpose of selecting events is filtering the ice loads so irrelevant ice loads are disregarded and only relevant ice loads are considered. As discussed in Section 3.5, when an ice feature is driven against a structure, the ice loads increases up to the point the ice fails. Once the ice has failed, the ice loads decreases. So, as soon as the ice start to fail, the ice load peaks. Because the ice loads around the peaks are lower, these loads are irrelevant and can be disregarded. So, only these peaks should be selected as ice load events. The following methods for selecting ice events are considered:

1. Maximum values for a given frequency
2. Rayleigh separation

Using the maximum values for a given frequency is useful if the peaks occur around a certain frequency and this frequency is known. If this frequency is known it could be used to select the maximum values in time intervals corresponding to this frequency. This means that this frequency directly can be used as frequency of the events.

As discussed in Section 3.5.1, for ice crushing ice fails in different ways. The failure of ice cause the peaks in the ice loads. Because there are different ways of failure, identifying a specific peak frequency may be difficult.

If the event frequency is unknown or the frequency between the peak loads is unclear, another method is required. The method of Rayleigh separation can be used to identify different peaks in a signal regardless the frequency of the peaks [69]. This methods select peaks by comparing maximum with minimum values. If the minimum load between two maximum loads is smaller than the smallest maximum load multiplied by the separator value ξ, than both maximum loads are considered as load events.

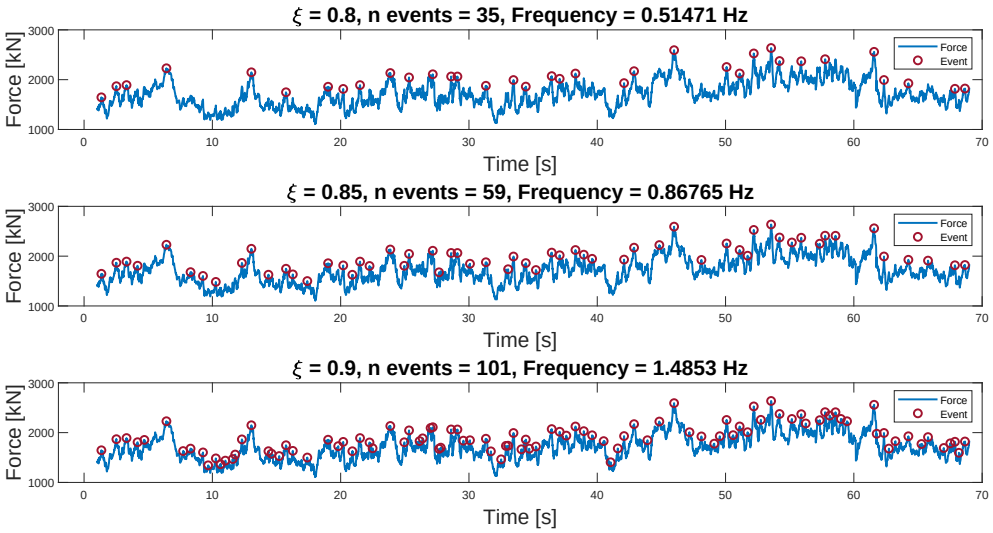

Figure 7.2: Rayleigh separation of load events for different values of ξ.

Crushing failure is a combination between pulverization, spalling, and radial cracking of sea ice. Because the ice fails in different ways, some load peaks may be smaller than others and may therefore be irrelevant and should not be selected as ice load event. The separator value ξ of Rayleigh separation method can be adjusted in order to select only ice load peaks that are considered relevant.

For the purpose of illustrating the selection of events, data from the Norströmsgrund lighthouse in the Baltic Sea is used. This data originates from the STRICE 2003 campaign, for more information about this data see reference [70]. An interval should be selected that resembles an ice state. Therefore, an interval is selected where the ice thickness anomaly is small. In this case, an interval where the thickness varies between 0.59 m and 0.92 m is selected. This is quite a wide range but the available data does not provide better intervals. For the purpose of illustration it should suffice. In Figure 7.2 events are selected using Rayleigh separation for different values of the separator value ξ.

Once the events are selected the data can be used to determine the short-term distribution and the average frequency of the events. The frequency of the events is calculated using Equation (7.5).

In order to determine the short-term distribution, the distribution type with the best fit should be determined. As discussed in Chapter 5, the tail of the parent distribution have great influence on the extremal distribution. Therefore, a good fit at the tail of the short-term distribution is crucial. In Figure 7.3, different distribution types are fitted to the selected events in Figure 7.2 for $\xi = 0.9$. In this example, the log-normal and gamma distribution seem to have reasonable fits, the tail of the Weibull distribution does not give a good representation of the data.

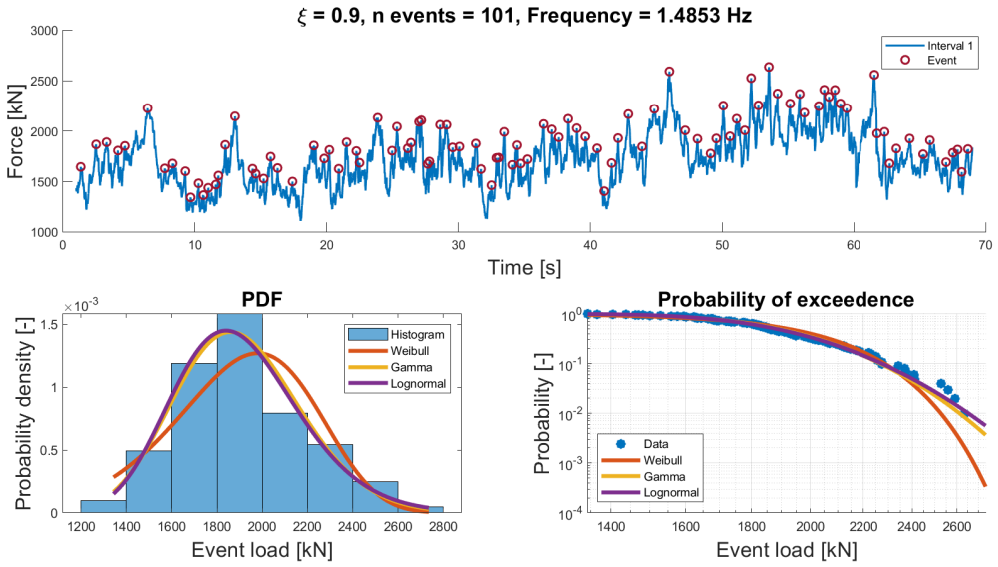

Figure 7.3: Short-term distribution fits of selected event loads.

8

Method overview

This chapter provides an overview of the complete method to determine the impact of climate change on the design loads. This method combines the methods discussed in previous chapters.

8.1. Schematic overview

Figure 8.1 provides a schematic representation of this method. The procedure describes all steps to be taken in order to determine the impact of climate change on the design loads. The input of the procedure describes what data should be known in order to be able to determine the design loads. The design loads depend both on the climate change scenario and characteristics of the offshore structure. The characteristics of the offshore structure include dimensions and location. The output simply consists of the design loads according to the input climate change.

8.2. Procedure details

To obtain an extremal distribution for each season, all seasons need to be considered individually. So, for all season in the considered time period, the procedure should be repeated. The extremal distribution could also cover multiple seasons but this would lead to less accurate results because the inter-seasonal change of ice loads due to climate change is not properly included in the extremal distribution, as discussed in Chapter 4.

This first step of the procedure, once the climate change scenario and location of the structure are known, is to determine the relevant sea ice characteristics and how they are expected to change for the different seasons. This step is needed in order to known which ice states are to be expected in the considered seasons.

Once the expect sea ice characteristics are known, the duration of the freezing period should be determined. This period represent the period in which the structure may experience ice loads. This period can be based on the temperature data of the season. If available, ice thickness data could also be used to determine the freezing period.

In order to weigh the short-term distributions and the event frequency, the weight factors for all ice states should be determined, as described in Section 6.3. The weight factor represents the probability or frequency of occurrence of the ice states. So, the weight factor describes which ice states should be considered.

For all these ice states, the short-term distribution and number of events should be determined according to the characteristics of the ice state, as described in Section 7.1 and Section 7.2 respectively. Both the short-term distribution and number of events depend on the dimensions of the structure.

Once these four aspects of each season are known, the long-term parent distribution and the number of events for each season can be determined. The long-term parent distribution depends on the

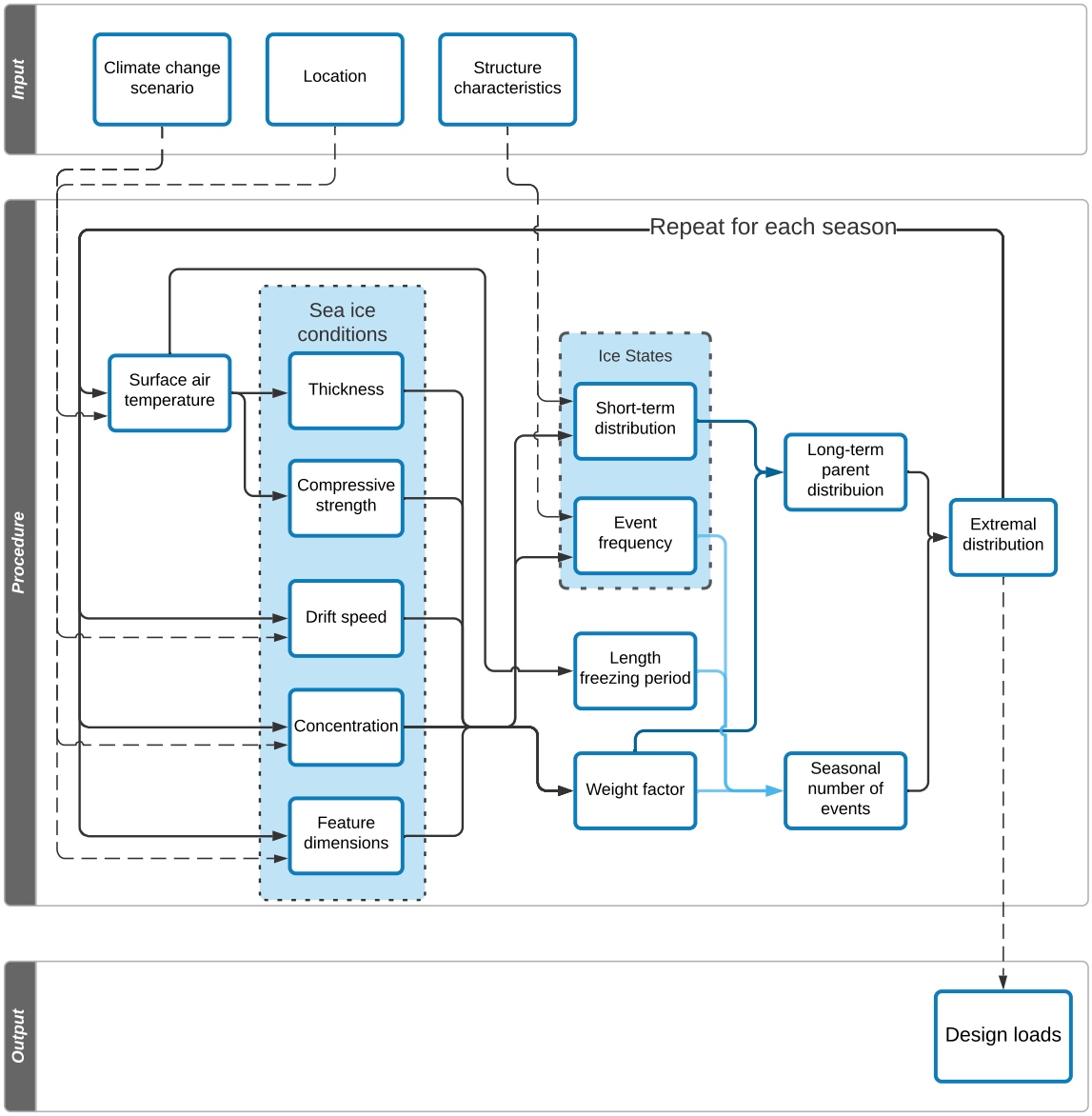

Figure 8.1: Schematic overview of the method to determine the impact of climate change on the design loads.

short-term distributions and the weight factor, as described in Section 6.1. The seasonal number of events depends of the number of events during the ice state, the weight factor and the duration length of the freezing season, described in Section 6.2.

The final step of the procedure is to determine the extremal distribution for each season, as described in Section 5.1. The extremal distribution can be determined if the parent distribution and the number of events are known. If the extremal distributions of all considered seasons are known, the design load of the considered time period can be determined, as described in Section 4.3.

9

Example case

For the purpose of illustration, in this chapter the method to determine the design loads under changing climate will be applied to an example case. In this example, the ULS design load will be determined. To be able to do this, a hundred seasons of data are required. This example will follow the steps according to the procedure presented in Chapter 8. In Section 9.5, the results of the new method are compared with the ULS design loads according to the conventional method and the method suggested by ISO 19906.

For this example, data of future sea ice conditions are required in order to know how the sea ice conditions will change in the future. For this example, the data from the earth system coupled climate model of the Met Office Hadley Centre is used [45]. For different climate change scenarios, daily data of the surface air temperature and all required sea ice properties are available. This model is part of CMIP5 used for IPCC assessment reports. The output of this model are the projections of the models according to the considered climate change scenario.

9.1. RCP2.6

In this section, the ULS design ice load will be determined for the RCP2.6 scenario. For the purpose of illustrating the method, all intermediate results are presented.

9.1.1. Assumptions

In order to calculate the design load for this example case, assumptions have to be made. The assumptions are explained in detail below. The assumptions are:

1. The structure is vertically walled.
2. The structure width is $w = 50\,\text{m}$.
3. The sea ice states last one full day.
4. The failure mechanism of ice is crushing.
5. Short-term distribution is a gamma distribution with a shape parameter of $\alpha = 46.18$.
6. The mode of short-term distribution is equal to the estimated global load.
7. The ice features are round ice floes.
8. The average diameter of the ice floes is $\bar{D} = 50\,\text{m}$.

9.1.2. Input

The input required for the procedure consist of the considered climate change scenario, the location of the structure and the structure dimensions.

For the climate change scenario, the RCP2.6 scenarios is used. The RCP scenarios are discussed in Section 2.1.3. In the RCP2.6 scenario, climate change forcing is the lowest from all RCP scenarios. The climate change will mitigate because of strict climate policies. Oil consumption will be much lower whereas usage of renewable energy will have increased by the year 2100. According to this scenario, global radiative forcing will already peak around the year 2040 and will gradually decrease thereafter.

A location in the Kara Sea is chosen. The coordinates of this location are 75°N and 73.1250°E, see Figure 9.1. The boundaries of the grid cell are 74.3750°N and 75.6250°N latitudinally and 72.1875°E and 74.0625°E longitudinally. The grid cell dimensions at the location are roughly 75 km in North-South direction and 29 km in East-West direction.

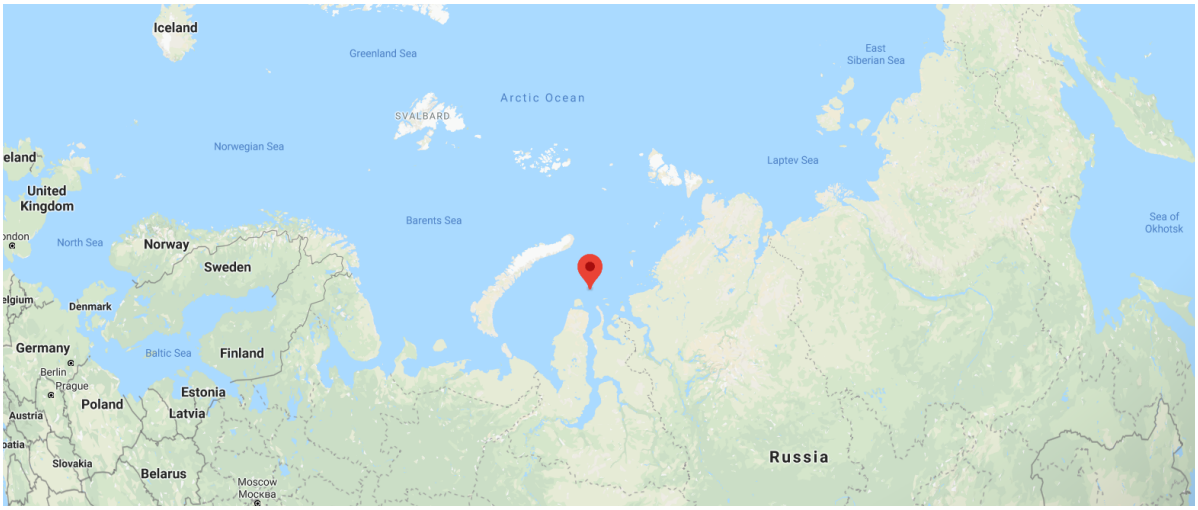

Figure 9.1: Considered location in Kara Sea [71].

The ice loads are calculated as function of the structure width, therefore a structure width needs to be selected. As described above, a structure width of 50 m is assumed.

9.1.3. Ice conditions

Once the input data is known, the future sea ice conditions need to be determined. In this case, the projections of the coupled climate change model are used. The interval from season 2006-2007 till season 2105-2106 is considered. The model output provides daily data of surface air temperature, sea ice thickness, sea ice concentration and sea ice drift speed.

The uni-axial compressive strength is calculated using the method described in Appendix B.5 using the daily surface air temperature and sea ice thickness. The method used to determine the compressive strength is only valid for air temperatures below $-2\,°C$. However, if there is sea ice, this ice also has some compressive strength. For each interval of days with sea ice but an air temperature above $-2\,°C$, the compressive strength is determined with a linear fit between the compressive strength corresponding to the last day before and the first day after this interval. If this interval is at the beginning or end of the season and there is no day before or after the interval where the compressive strength is known, the minimum compressive strength of that season is used.

The climate model provides data of the North-South and the East-West component of the drift speed. The absolute sea ice drift speed is calculated applying the Pythagorean theorem to to both components. In Figure 9.2, the sea ice properties are plotted during different seasons.

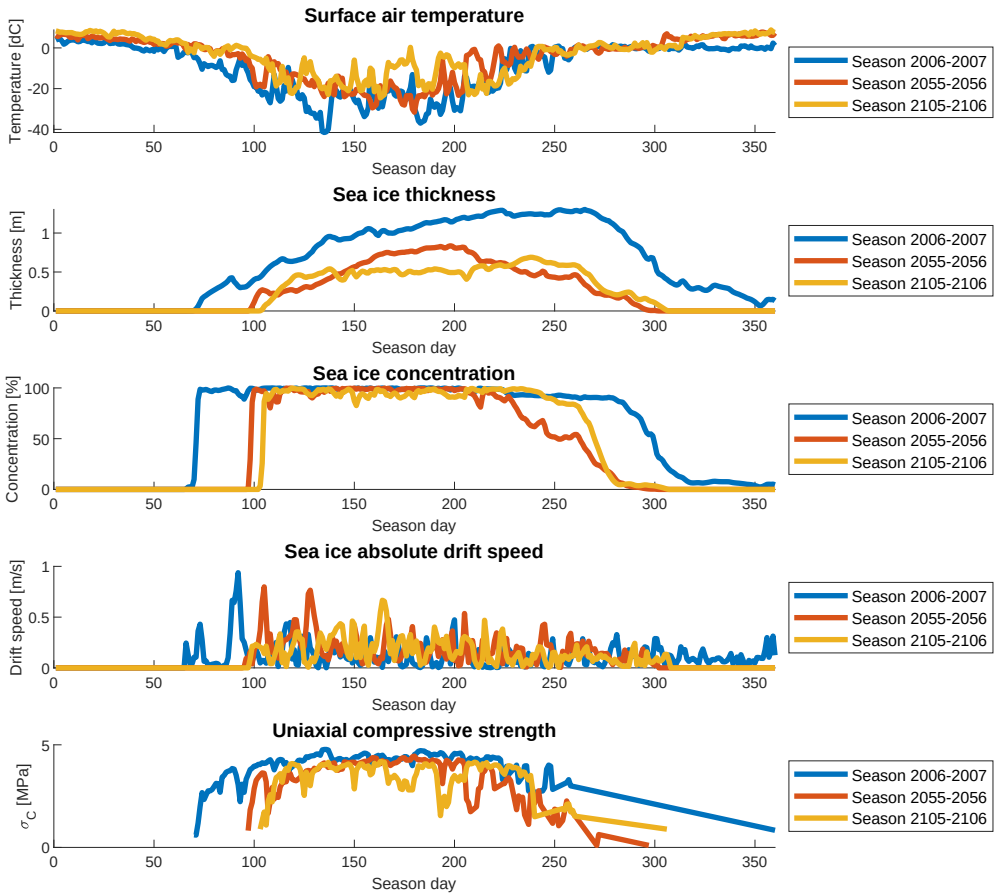

Figure 9.2: Overview of sea ice properties according to earth system climate model from the Met Office Hadley Centre for RCP2.6 [45].

In Figure 9.3, the seasonal mean value is plotted for all seasons. The surface air temperature shows an upward trend, thickness and concentration a downward trend and drift speed and compressive strength do not show a clear trend.

9.1.4. Length freezing period

The next step is to determine the length of the freezing period. This period should include all days when there is sea ice that could interact with the structure. For each season, the number of days with sea ice is determined. For the number of days with sea ice for each season, see Figure 9.4.

9.1.5. Weight factor

The weight factor need to be determined for all ice states to weigh the short-term distribution and the event frequency. Because only daily data is available, the sea ice states are assumed to last one full day. That way, the daily data characterizes the ice state and determines the short-term distribution and number of events for each ice state.

The weight factor weighs the short-term distribution and the load event frequency according to the frequency of occurrence of the ice state. Because each ice state is considered to last a full day, the weight factor of each ice state can simply be calculated as one day divided by the total number of days with sea ice in the considered season. This is equal to one day divided by the length of the freezing season in days (presented in Figure 9.4).

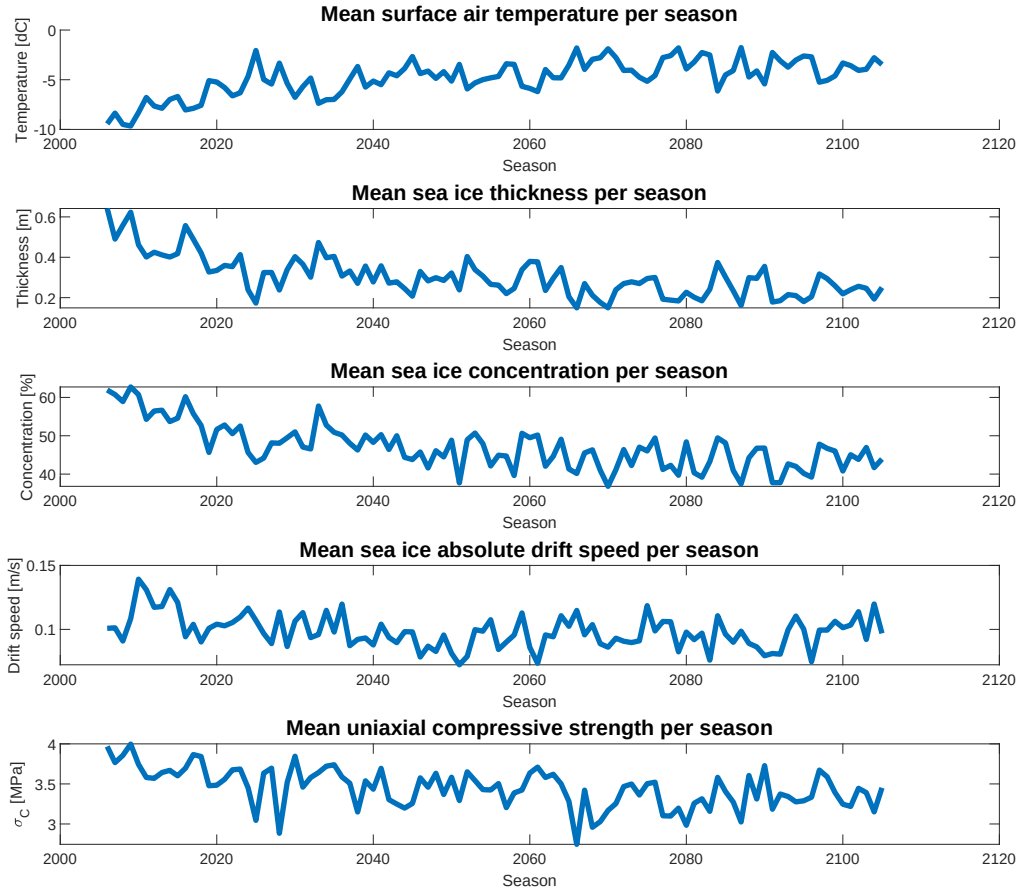

Figure 9.3: Seasonal mean of the sea ice properties according to earth system coupled climate model from the Met Office Hadley Centre for RCP2.6 [45].

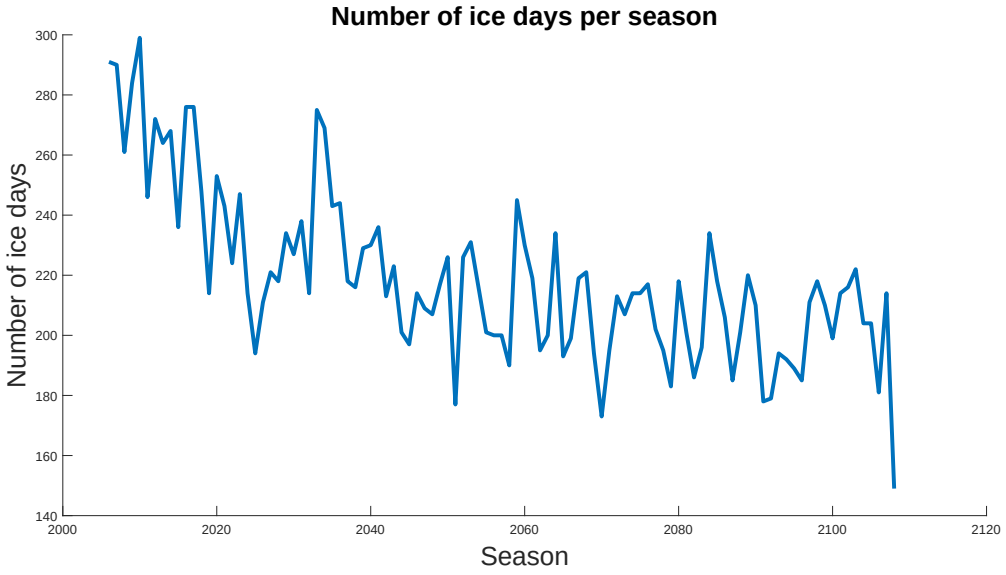

Figure 9.4: Number of days with sea ice for each season for RCP2.6.

9.1.6. Short-term distribution

The short-term distribution needs to be determined for each ice state. In this example, the short-term distribution is based on the results of Chapter 7 corresponding to an separator value of $\xi = 0.9$. The gamma distribution is used as short-term probability distribution, this distribution is given by Equation (9.1):

$$f(x) = \frac{x^{\alpha-1}e^{-\frac{x}{\beta}}}{\beta^{\alpha}(\alpha-1)!} \qquad \text{for } x, \alpha, \beta > 0 \tag{9.1}$$

Here,α is the shape parameter and β is the scale parameter. For the shape parameter, a value of $\alpha = 46.18$ is used. The scale parameter is based on the global ice crushing load (F_G) estimated with the method described in Appendix B.6 using the ice thickness and uni-axial strength of the ice state. The assumption is made that this estimated load is the mode of the short-term distribution. In other words, the load with the highest probability. The scale parameter can be expressed as function of the mode and is calculated using Equation (9.2):

$$\beta = \frac{F_G}{\alpha - 1} \tag{9.2}$$

The global load is calculated using Equation (B.15). In Figure 9.5, all short-term distributions of the last season are shown.

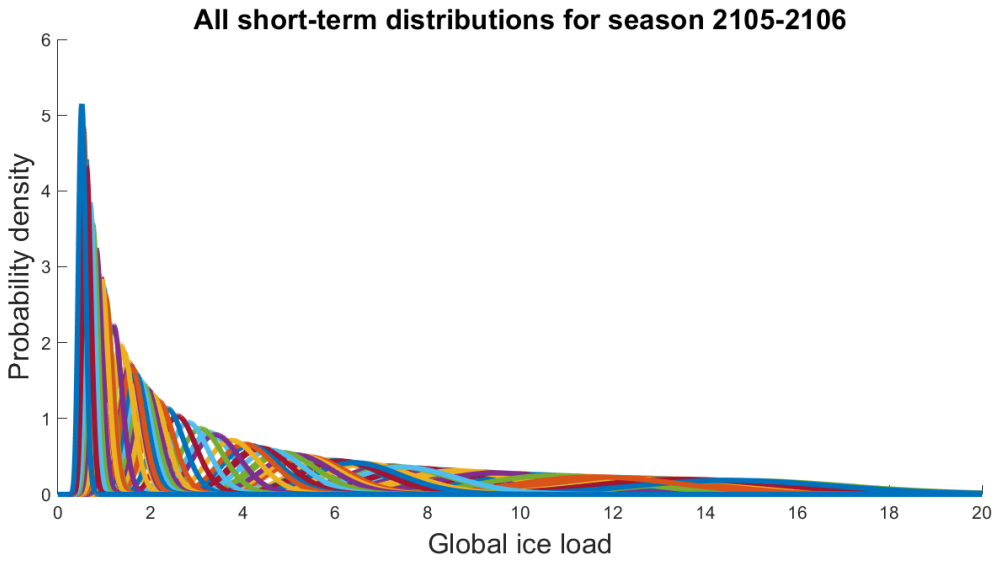

Figure 9.5: Short-term distribution for season 2105-2106 for RCP2.6.

9.1.7. Event frequency

For each ice state, also the corresponding event frequency needs to be determined. The frequency of events during an interaction is, like the the short-term distribution, based on the results of Chapter 7 corresponding to an separator value of $\xi = 0.9$. According to these results, $\eta_{events} = 1.49$ Hz.

The method suggested in Section 7.2 is used to calculate the interaction frequency. The interactions frequency during the ice state depends on the concentration, drift speed and dimensions of the ice. Drift speed and concentration data is available but size and shape of the ice features are unknown.

If a certain average width and shape of the ice features are assumed, the average area of the ice features can also be calculated. In this example the ice features are assumed to be round ice floes with an average diameter of $\bar{D} = 50$ m. The interaction frequency is calculated using Equation (9.3). In

Figure 9.6, the interaction frequency of each day of the last season is plotted.

$$\eta_{interactions} = \frac{4C_{ice}}{\pi \bar{D}^2}\left(\bar{D} + w\right)\bar{v} \tag{9.3}$$

Also, the average duration of the interactions is unknown and needs to be determined. In this example, the duration is estimated using Equation (9.5). Because the average diameter and velocity of the ice floe are known, the duration of the ice floe crossing the structure can be estimated under the assumption that ice feature maintains its speed during the interaction. However, because the number of interactions during the ice state is already known, the maximum duration of the interactions can also be calculated, see Equation (9.4). The average maximum duration of the interactions is equal to the duration of the ice state ($t_{icestate}$) divided by the number of interactions ($n_{interactions}$). The number of interactions can be calculated as the interaction frequency ($\eta_{interactions}$) multiplied by the duration of the ice state.

$$t_{interaction,max} = \frac{t_{icestate}}{n_{interactions}} = \frac{t_{icestate}}{\eta_{interactions} t_{icestate}} = \frac{1}{\eta_{interactions}} \tag{9.4}$$

$$t_{interaction} = \min\left(\frac{\bar{D}}{v_{ice}}, \frac{1}{\eta_{interactions}}\right) \tag{9.5}$$

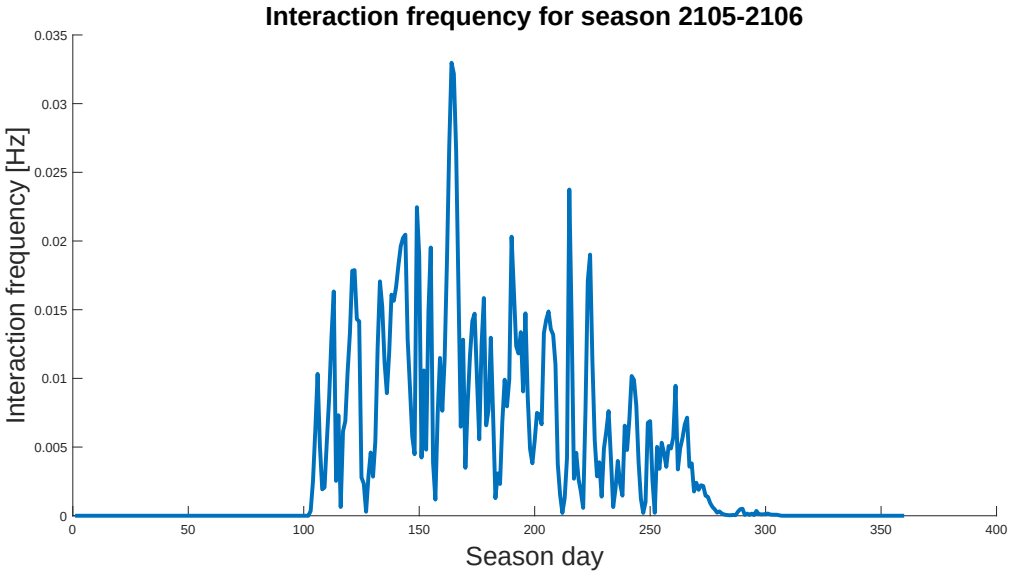

Figure 9.6: Daily interaction frequency for the last season for RCP2.6.

The events frequency per ice state is calculated using equation Equation (7.1). Because of the high concentration of sea ice in this example, for most ice states the interaction duration is limited by the interaction frequency $\eta_{interactions}$. Therefore, for most of the ice states the event frequency of the ice state ($\eta_{ice-state}$) is equal to the event frequency of the interaction (η_{events}), see Figure 9.7.

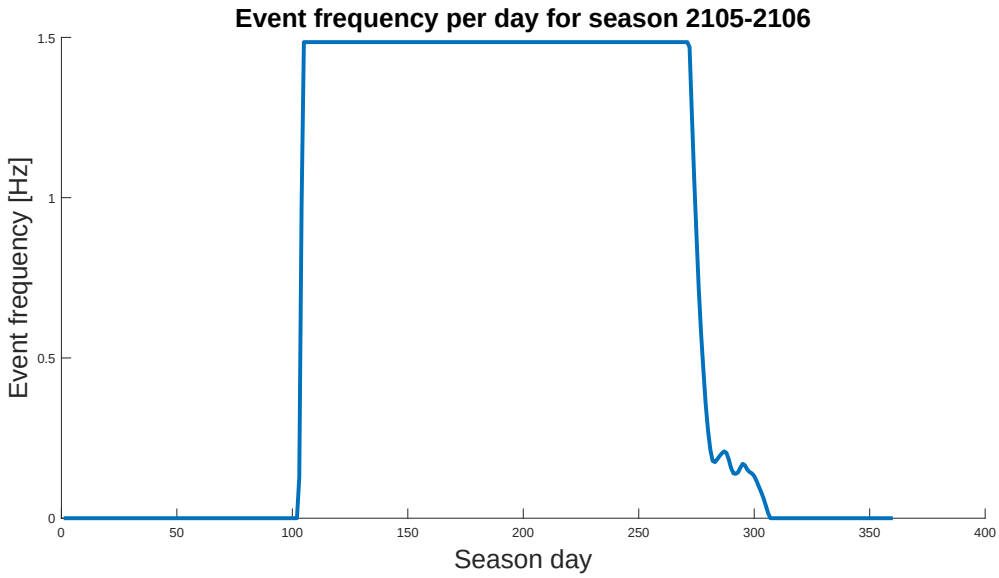

Figure 9.7: Daily event frequency for the last season for RCP2.6.

9.1.8. Long-term parent distribution

Once the short-term distributions and the weight factors are known, the long-term parent distributions for each season can be determined. The parent distribution is calculated using Equation (6.1). All short-term distributions in each season are weighted and added up. In Figure 9.8, the $CDF = 0.50$ (median), $CDF = 0.95$ and $CDF = 0.99$ ice loads according to the parent distribution are plotted for each season. All show a downward trend in the ice loads.

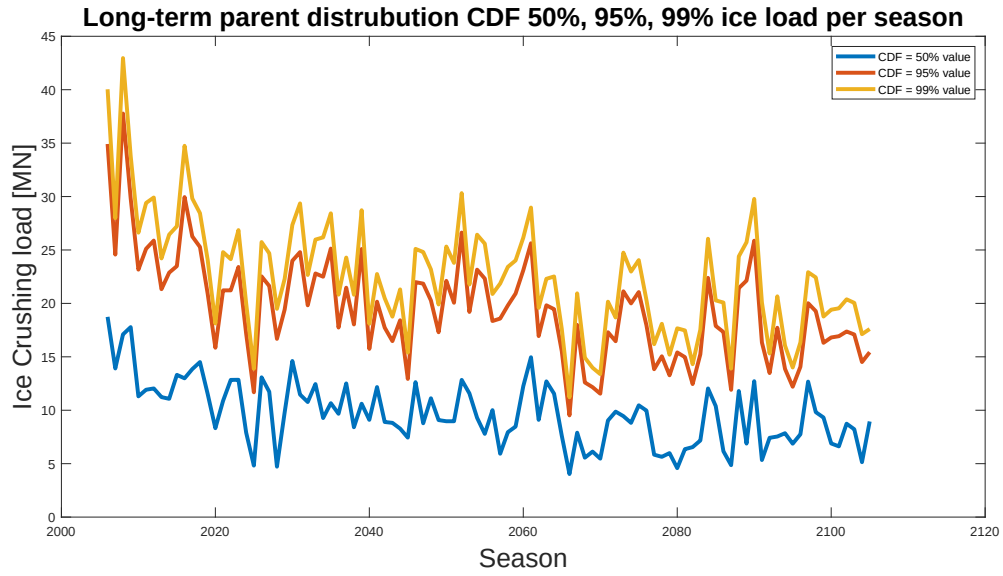

Figure 9.8: Median, 95% and 99% ice loads for each season in the considered time period for RCP2.6.

9.1.9. Seasonal number of events

The number of events per season is calculated according to Equation (6.2). In Figure 9.9, the number of events per season are presented. The load event frequency is weighted by the weight factor first. Then, the sum of the weighted event frequencies is multiplied by the duration of the freezing period. In this case, the number of events per season also shows a downward trend.

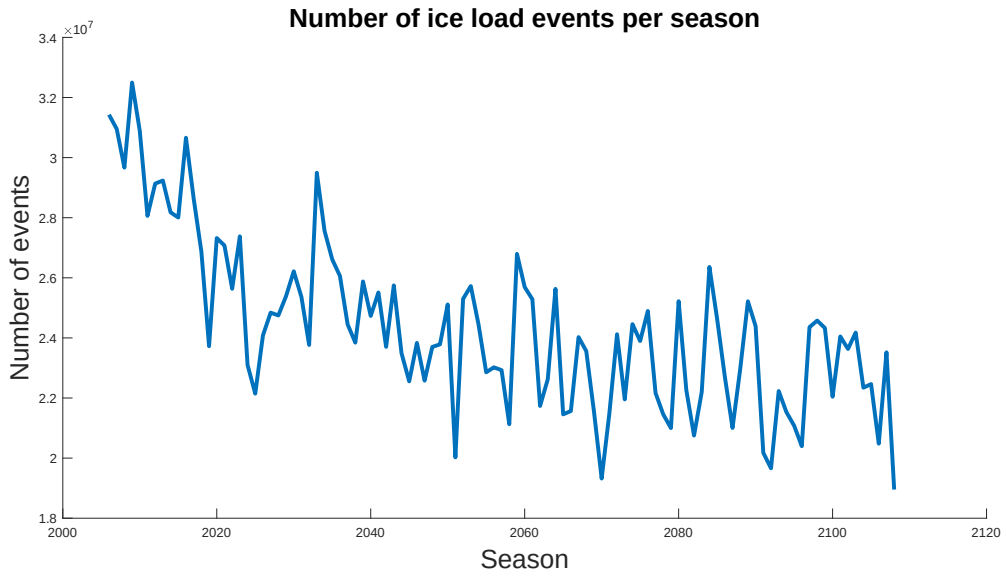

Figure 9.9: Number of ice load events for each season in the considered time period for RCP2.6.

9.1.10. Extremal distributions

The extremal distributions are calculated using the long-term parent distribution and the number of events of each season as described in Section 5.1. First the cumulative distribution function of the parent distribution is determined. Then, this distribution is raised to the power of the number of events corresponding to the season to obtain the extremal cumulative distribution function. The probability density function of the extremal distribution is based on this cumulative distribution.

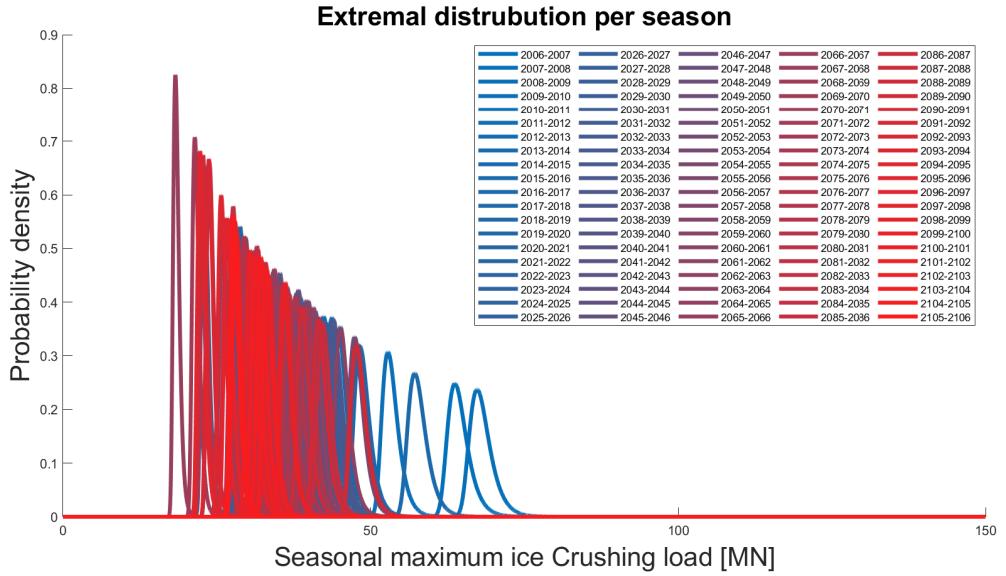

Figure 9.10: Extremal distribution for each season in the considered time period for RCP2.6.

The extremal distributions are plotted in Figure 9.10. The colors of the distributions fade from blue into red as time progresses. As can be seen in the figure, the distributions at the end of the interval tend to be on the left hand side of the distributions at the beginning of the interval. In Figure 9.11, the $CDF = 0.95$ (median), $CDF = 0.95$ and $CDF = 0.99$ ice loads according to the extremal distribution are plotted for all seasons. All show a downward trend.

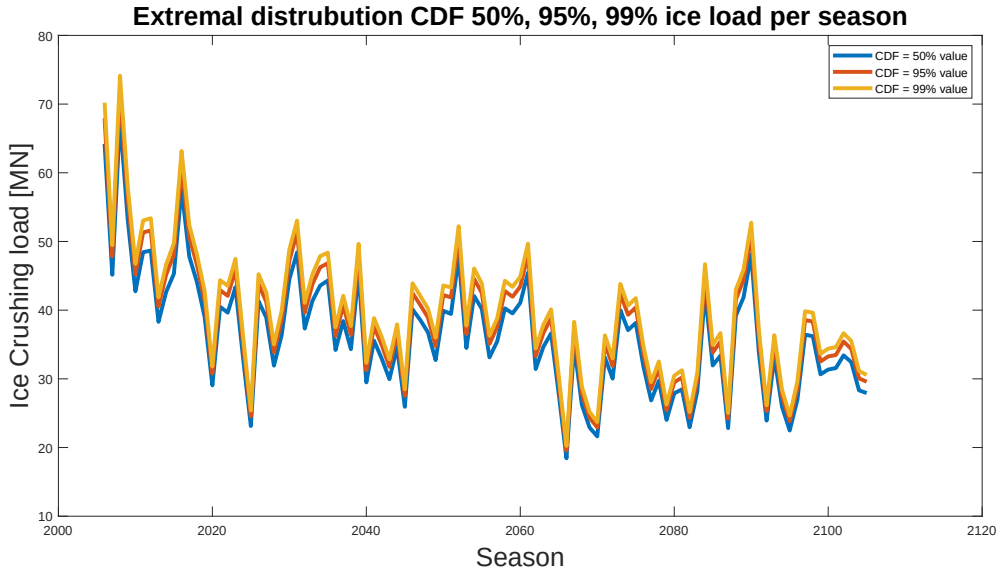

Figure 9.11: Median, 95% and 99% ice loads according to the extremal distribution for each season in the considered time period for RCP2.6.

9.1.11. Design load

Now the extremal distributions are known, the ULS design load can be determined using the method described in Section 4.3. In Figure 9.12, the expected number of exceedances of ice loads in the 100 years time interval are plotted. The ULS design load corresponds to the load with an expected number of exceedances of one. According to this method, the ULS design load is equal to 66.2 MN.

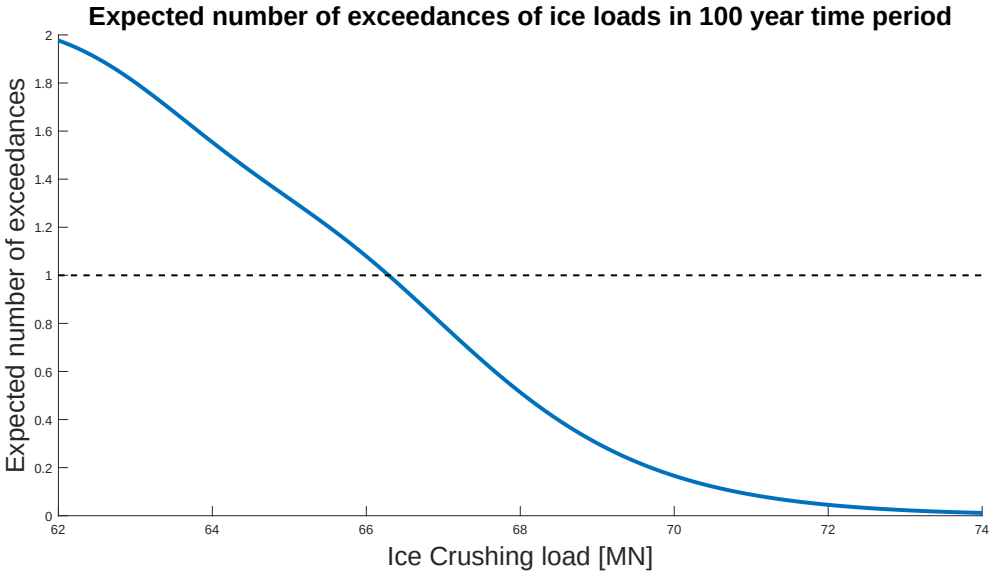

Figure 9.12: Expected number of occurrences of ice loads in the 100 years time interval for RCP2.6.

9.2. RCP8.5

The process of Section 9.1 is repeated for the RCP8.5 scenario. In this case, the same location is considered and the same assumptions hold. In this section, the climate model data and the results are presented.

For the RCP8.5 scenario, climate change forcing is the highest from all RCP scenarios. According to this scenarios, coal and natural gas usage has increased by 2100 and oil usage is more or less the same. This scenario assumes no climate policy and therefore a big increase in greenhouse gas emissions.

9.2.1. Ice conditions

In Figure 9.13, surface air temperature and the sea ice properties are plotted during different seasons according to the RCP8.5 scenario. At the end of the interval, there is barely any ice at the considered location.

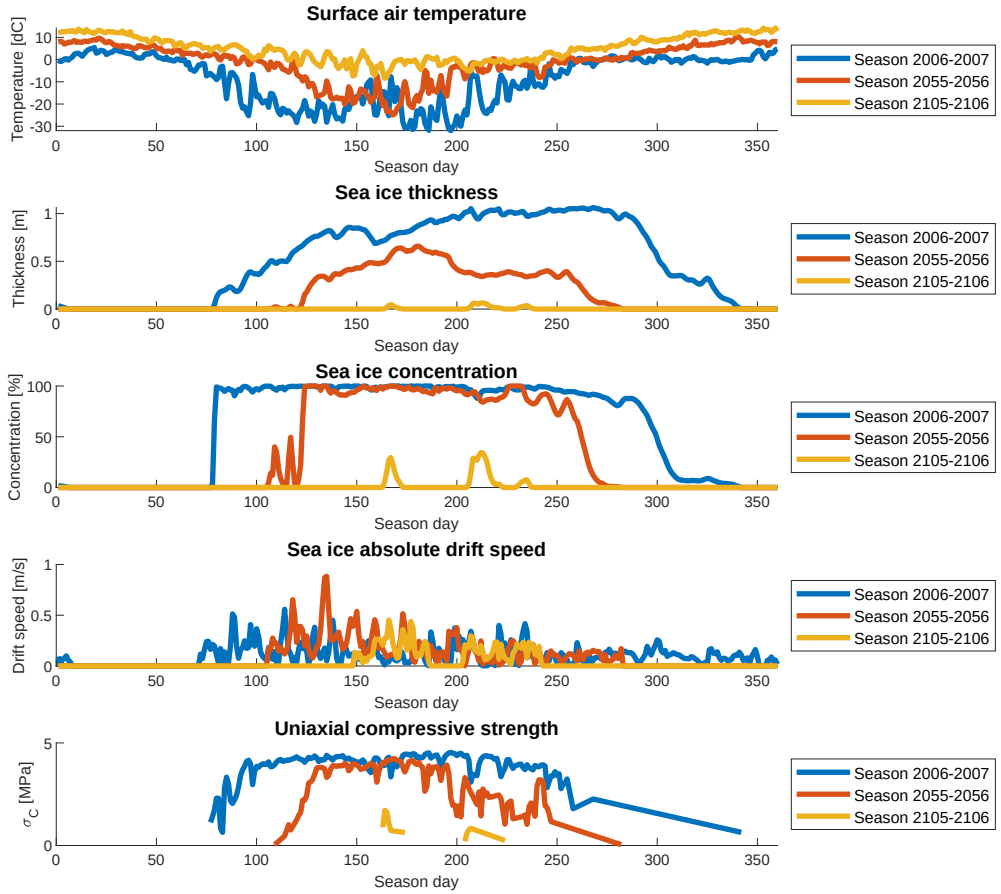

Figure 9.13: Overview of sea ice properties according to earth system climate model from the Met Office Hadley Centre for RCP8.5 [45].

In Figure 9.14, the seasonal mean value is plotted for all seasons. The surface air temperature shows an upward trend and ice thickness, concentration, drift speed and compressive strength show a downward trend. Also, the length of the freezing period is determined. This period includes all days when there is sea ice that could interact with the structure. For the number of days with sea ice per season, see Figure 9.15.

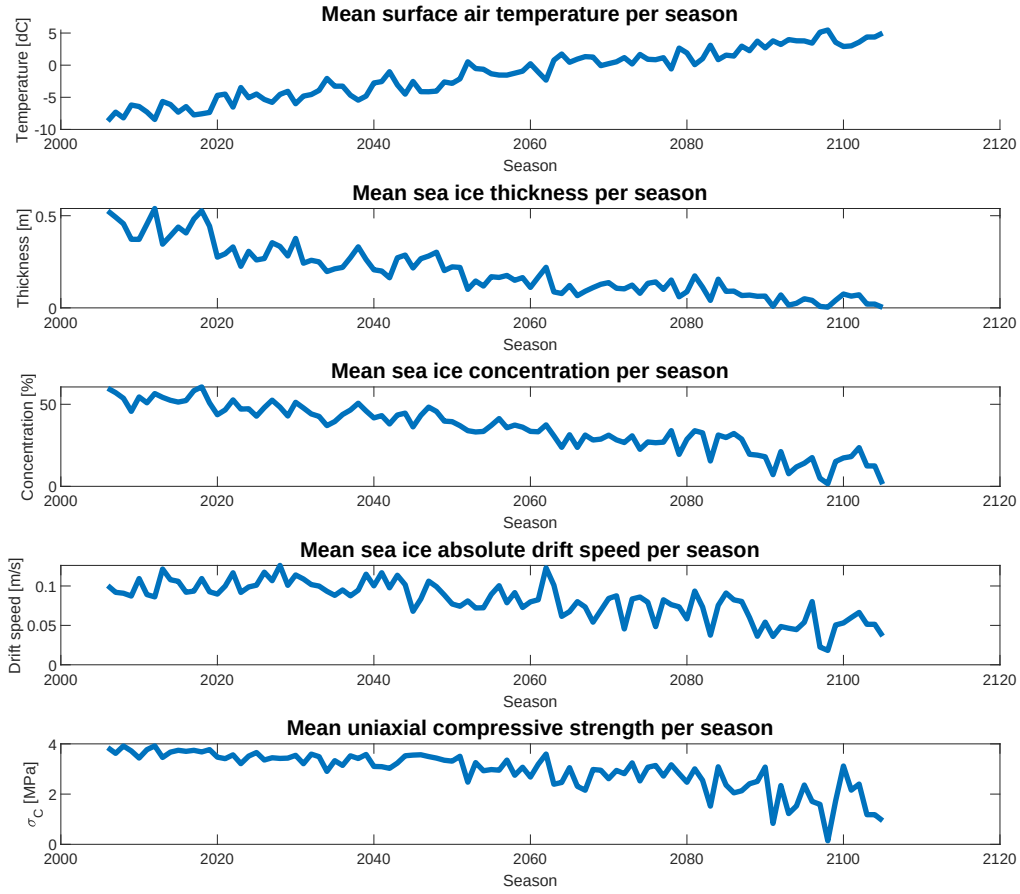

Figure 9.14: Seasonal mean of the sea ice properties according to earth system coupled climate model from the Met Office Hadley Centre for RCP8.5 [45].

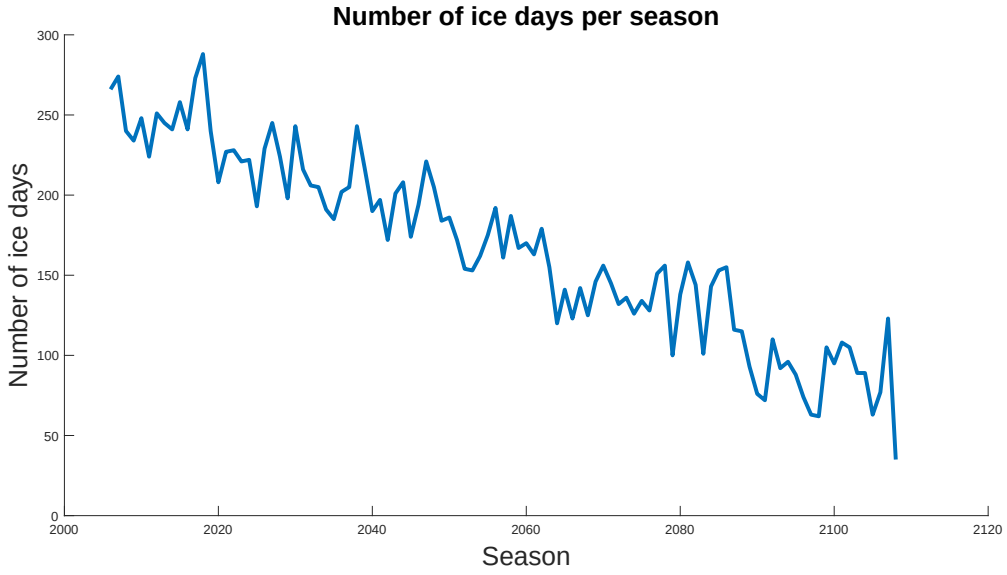

Figure 9.15: Number of days with sea ice for each season for RCP8.5.

9.2.2. Long-term parent distribution and number of events

Using the sea ice conditions, the long-term parent distribution and seasonal number of events are determined for each season. In Figure 9.16, the $CDF = 0.50$ (median), $CDF = 0.95$ and $CDF = 0.99$ ice loads according to the parent distribution are plotted for each season. All show a downward trend in the ice loads.

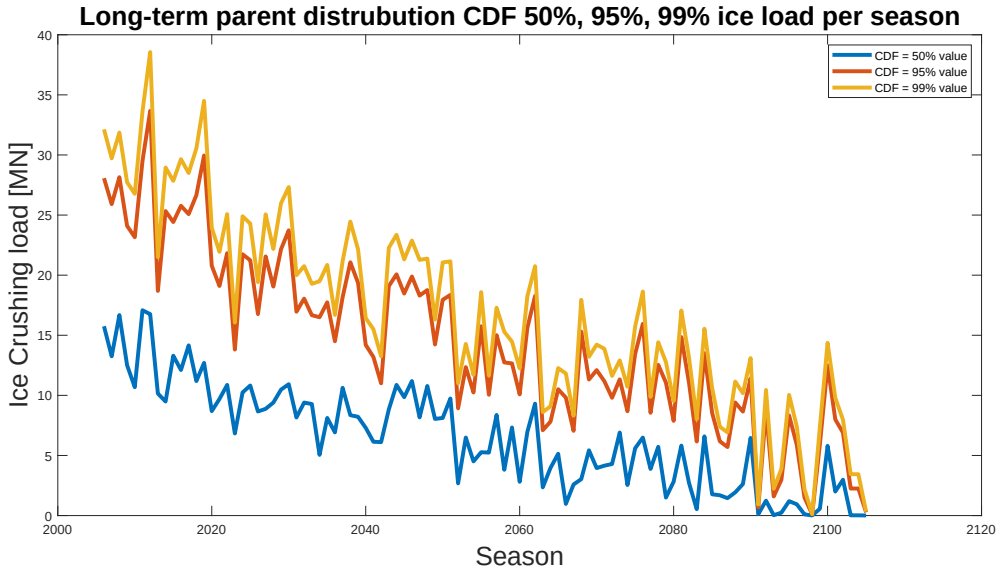

Figure 9.16: Median, 95% and 99% ice loads for each season in the considered time period for RCP8.5.

In Figure 9.17, the number of events per season are presented. In this case, the number of events per season also shows a downward trend.

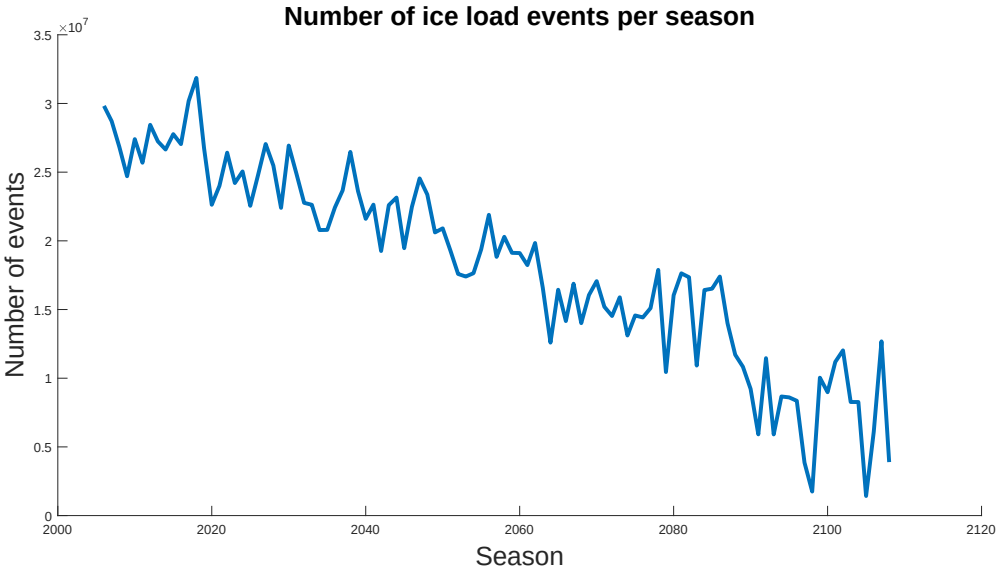

Figure 9.17: Number of ice load events for each season in the considered time period for RCP8.5.

9.2.3. Extremal distributions

The extremal distributions are calculated using the long-term parent distribution and the number of events of each season. In Figure 9.18, the $CDF = 0.95$ (median), $CDF = 0.95$ and $CDF = 0.99$ ice loads according to the extremal distribution are plotted for all seasons. All show a downward trend.

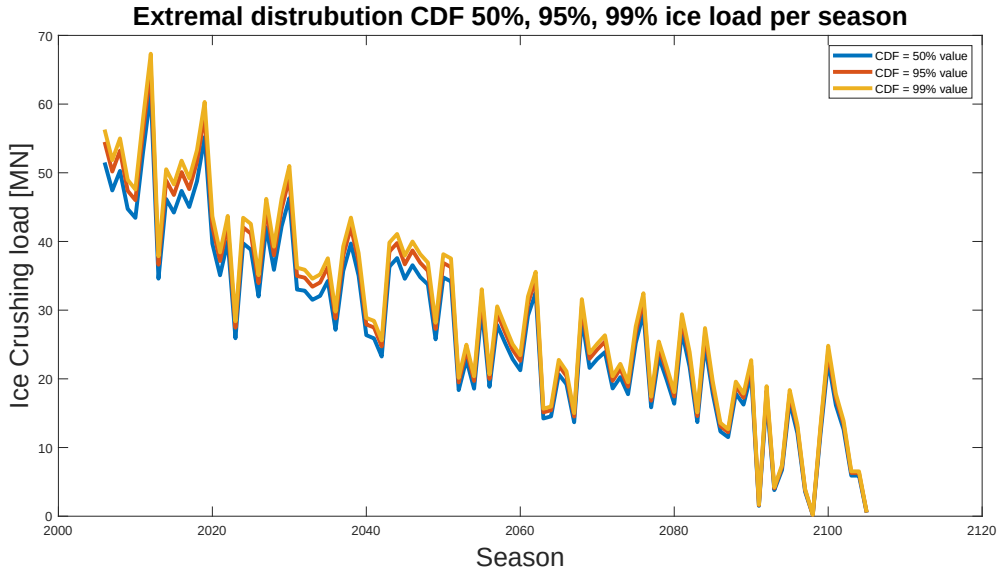

Figure 9.18: Median, 95% and 99% ice loads according to the extremal distribution for each season in the considered time period for RCP8.5.

9.2.4. Design load

In Figure 9.19 the expected number of exceedances of ice loads in the 100 years time interval are plotted. The ULS design ice load for the RCP8.5 scenario is equal to 59.28 MN.

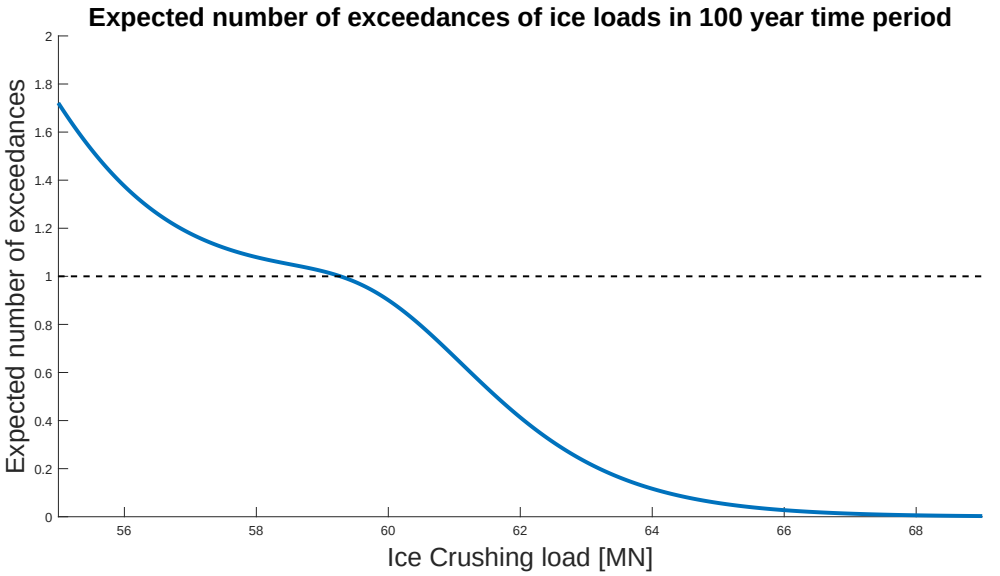

Figure 9.19: Expected number of occurrences of ice loads in the 100 years time interval for RCP8.5.

9.3. Conventional method

According to the conventional way, design loads are based on historical data. The extremal distribution of the first season could be used to represent the lower bound of the historical data. If, for example, an interval of 20 years of most recent historical data is used for the conventional way, the ice loads according to the extremal distribution of this interval are expect to be around or greater than the ice loads according to the extremal distribution of the first season because of the downward trend in ice loads due to climate change. So, the design load according to the historical data is expected to be

greater than the design load according to the first season. According to the conventional way, the ice load corresponding to $CDF = 0.99$ is the ULS design load. The ULS design ice load according to season 2006-2007 is equal to 70.20 MN, see Figure 9.20.

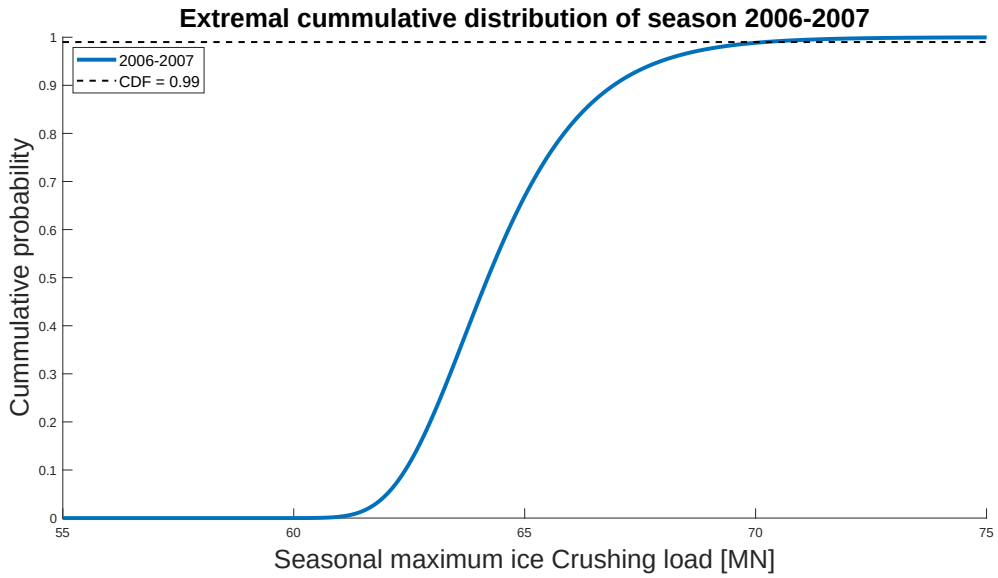

Figure 9.20: Extremal cumulative distribution function of season 2006-2007.

9.4. ISO 19906 method

For comparison, the ULS design ice load is also calculated according to the method suggested by ISO 19906 [5]. This method is discussed in Appendix B.7. ISO 19906 suggests to combine the ice strength coefficient (C_R) with a return period of 100 years with the annual maximum ice thickness to determine the ULS design ice load. According to ISO 19906, $C_R = 2.3$ MPa. The annual maximum ice thickness of the first season is used which is equal to 1.30 m. This results in a ULS design ice load of 77.19 MN.

9.5. Comparison

In Table 9.1, the ULS design loads for the different methods are compared. The design ice load according to the new method are lower for both RCP scenarios compared to the conventional method. The ULS design ice load according to the method suggested by ISO 19906 is higher compared to all other methods.

Method	ULS design ice load	Relative to conventional method
Conventional method	70.20 MN	-
RCP2.6 new method	66.20 MN	-5.7 %
RCP8.5 new method	59.28 MN	-15.6 %
ISO 19906 method	77.19 MN	$+10.0$ %

Table 9.1: Design ice loads according to different methods.

9.6. Sensitivity analysis

In this section, the individual impact of change in ice properties on design loads is studied. To do this, the data of the 2005-2006 season of the earth system climate model of the Met Office Hadley Centre corresponding to the RCP2.6 scenario is used [45]. To one of the ice properties, different linear trends are applied over an interval of a hundred years while the other ice properties are fixed. Once the data is known, the ULS design load is calculated like in Section 9.1.

How to determine the duration of the ice-structures interactions is yet uncertain and therefore the impact of ice concentration and drift speed is uncertain as well. In this case, the duration of the interactions is calculated using Equation (9.5). However, because the high ice concentrations, the duration is of interaction is limited by one divided by the interaction frequency. Therefore, if a downward trend is applied to the ice concentration, the design ice load will not be affected. In order to prevent this, the ice concentration of the first season is divided by a factor of 3.5.

9.6.1. Concentration

Different linear downward trend are applied to the concentration data. For each season, the ice concentration of the previous season is reduced by a fraction of the ice concentration of the first season so. Linear trends of 1% till 9% of the first season in steps of 1% are considered. In Figure 9.21, the ice concentration of the last season is plotted for each trend.

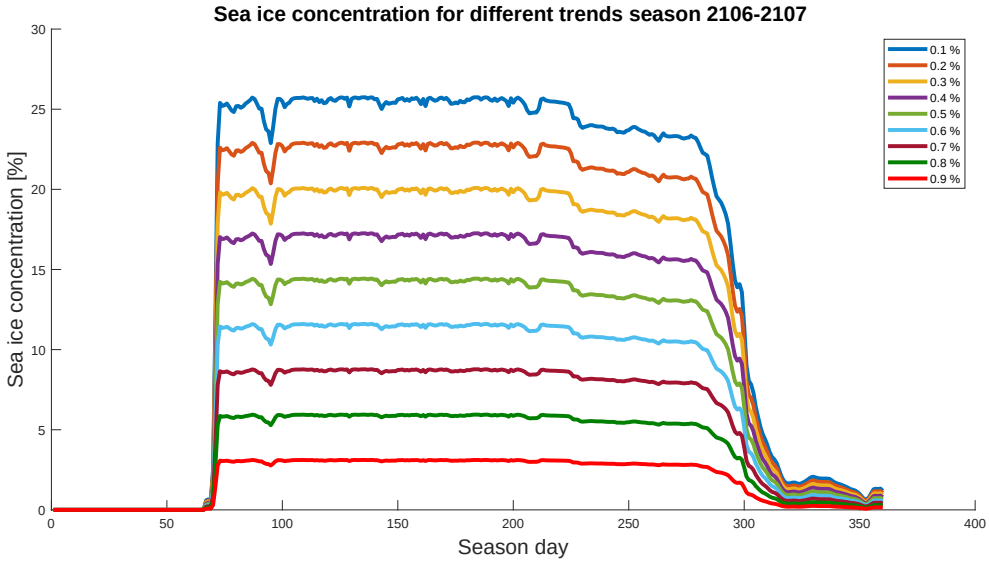

Figure 9.21: Sea ice concentration of the last season for different trends.

For each case with a different trend, the expected number of exceedances of the ice loads is determined, see Figure 9.22. The ice load with one exceedance corresponds to the ULS design ice load.

9.6.2. Ice thickness

For the sea ice thickness, the same trends are applied. For each case with a different trend, the expected number of exceedances of the ice loads is determined, see Figure 9.23. The ice load with one exceedance corresponds to the ULS design ice load.

9.6.3. Compressive strength

The same trend can be applied to the compressive strength. However, because the ice load is calculated using Equation (B.15), the effect of the downward trend in compressive strength on the ice loads is exactly the same as the effect of the downward trend in ice thickness. Therefore, the design loads

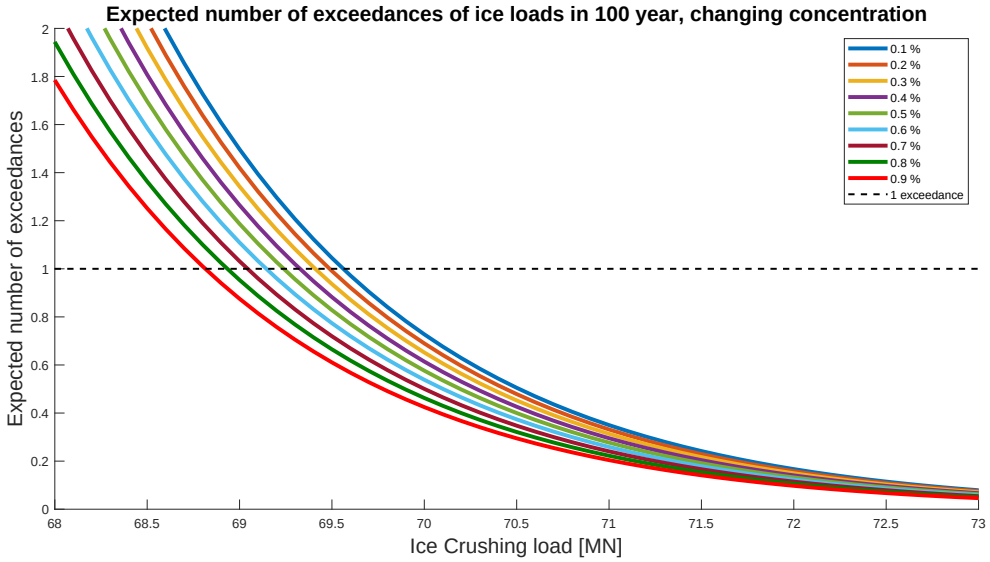

Figure 9.22: Expected number of exceedances for changing sea ice thickness.

corresponding to compressive strength having a trend are the same as the design loads corresponding the ice thickness having the same trend. So, Figure 9.23 looks the same for compressive strength having a trend.

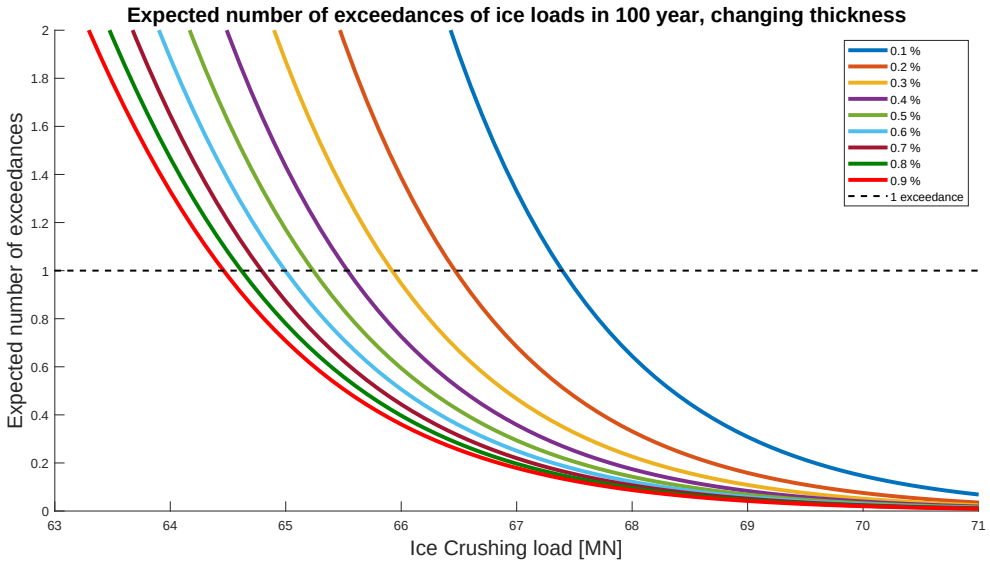

Figure 9.23: Expected number of exceedances for changing sea ice thickness.

9.6.4. Drift speed

In Section 9.1, the interaction frequency and the duration of the interactions are calculated as function of the drift speed. Because the assumption is made that the drift speed maintains its speed during the interaction, the drift speed cancels out when calculating the time fraction of ice-structure interaction during the ice state. Therefore, the design loads will be not be impacted by changing drift speeds. Before the impact of drift speed on design ice loads can be determined, the dependency of interaction duration on drift speed needs to be determined.

9.6.5. Overview

In Figure 9.24, an overview of the ULS design ice loads as function of the applied trends is presented. According to this method, a downward trend in ice thickness and compressive strength have more impact on the design ice loads compared to the ice concentration.

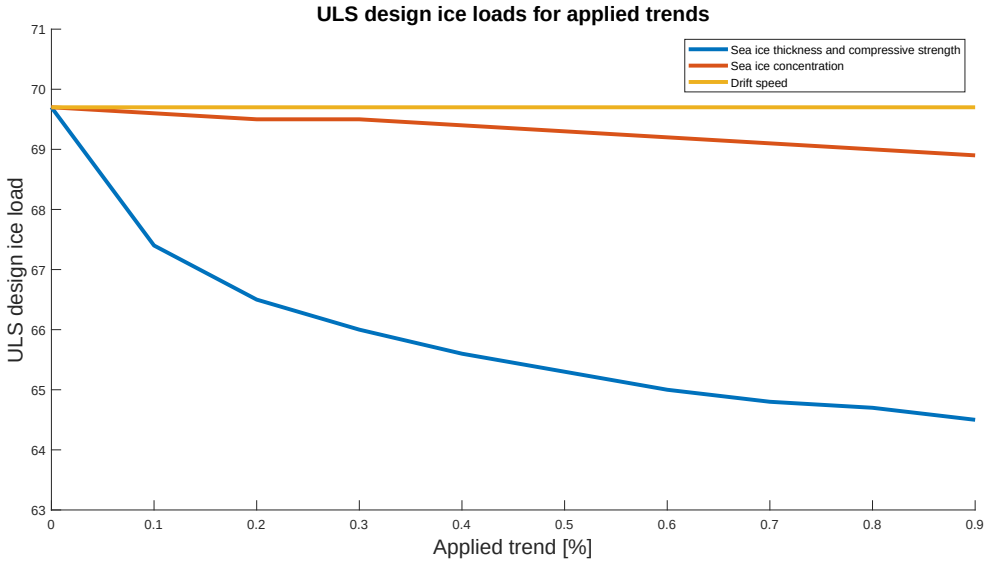

Figure 9.24: ULS design ice loads for changing sea ice properties.

10

Conclusion

In this thesis a new method is proposed to determine the design ice loads of Arctic offshore structures. This method enables to take the effect of climate change on the design loads into account.

Common practice to determine design ice loads is fitting an extremal distribution directly to historical data. This method is not suitable if climate change is considered because the design ice loads are based on historical data and the change in ice loads due to climate change is not properly included in the one extremal distribution.

Because of climate change, a trend is to be expected in ice loads. Therefore, also the seasonal extreme loads will be affected by climate change. Because of changing ice loads, extremal distributions based on historical data cannot represent the probability of future extreme ice loads.

Because environmental conditions change each season due to climate change, the probability distribution for ice loads also changes each season. This means that the extremal distribution also differs each season. In order to capture the effect of climate change, for each season an extremal distribution needs to be determined. So, one extremal distribution based on historical data is not suitable to determine design ice loads if climate change is considered.

A new method is required to be able to determine design loads considering climate change. The proposed method enables this because design loads are based on multiple extremal distributions and the extremal distributions are determined for each season individually.

Instead of fitting an extremal distribution to extreme ice loads, the extremal distribution is derived from the parent distribution and the expected number of ice load event during that season. The parent distribution represents the probability of all ice loads a structure may be exposed to in one season.

To be able to determine the parent distribution and the seasonal number of events, a concept referred to as an 'ice state' is introduced. Ice states describe time intervals where governing ice conditions are assumed to be constant. Because conditions are constant, for each ice state the short-term ice load distribution and the ice load event frequency can be determined. Each ice state is weighted in order to obtain the parent distribution based on the short-term distributions and the seasonal number of events based on the ice load event frequencies of the ice states.

The short-term distribution depends on the magnitude of ice load events and is therefore impacted by ice thickness and ice strength. The ice load event frequency of the ice state depends on the exposure rate to sea ice and is therefore impacted by ice concentration, ice drift speed and the dimensions of the ice features.

11

Recommendations

In the proposed method, ice states are used to determine both the parent distribution and number of events for a full season. In order to do this, for all ice states the short-term ice load distribution and the ice load event frequency needs to be known.

The short-term distribution represents the probability of all ice load events during the ice state. How to determine the short-term distribution according to the ice conditions is not yet fully understood. First of all, which ice load should be selected as events is unclear and therefore needs to be addressed. Once this is known, the impact ice conditions on short-term distribution can be determined.

The ice load event frequency represents the number of ice loads events per unit of time during the ice state. Like the short-term distribution, the event frequency is also impacted by how the ice load events are selected.

Besides the definition of an ice load event, the exposure rate to sea ice during the ice state also impacts the event frequency. The exposure rate indicates the fraction of time the structure is exposed to ice during the ice states. How the exposure rate depends on the ice conditions is uncertain. A proper method to determine the exposure rate needs be developed.

Before the proposed method is used to determine the design ice loads, a study dedicated to ice states and the corresponding short-term distributions and ice load event frequencies is recommended. Once is known how the short-term distribution and the ice load event frequency depend on the ice conditions, the design loads can be properly determined.

A

Resolute Bay Data

For the purpose of illustration, data from Resolute Bay in Canada is used in this report. Assessment of the data is provided in this appendix. The sea ice thickness data is obtained from Environment and Climate Change Canada [72], surface air temperature data is obtained from NOAA National Climatic Data Center [73].

A.1. Sea ice thickness

This dataset provides weekly measurements of ice thickness since 1947. Annual maximum ice thickness is plotted in Figure A.1. The measurements have been only executed if the ice was thick enough to walk on safely. For a one person, that corresponds to thickness of roughly 80 mm [74]. Season 2001/2002 is missing and the season 1951/1952 is omitted because the measured ice thickness is much lower than expected according to the temperature data.

The ice thickness data is collected manually. The measuring site is selected by a degree of judgement. For each measurement, new holes are drilled at sites where the water depth is deeper than the expected annual maximum ice thickness. The exact locations of the measurements are unknown. Because of possible changes in personnel, changes in measurement location and disturbances in the measurement area, quality of data may vary somewhat [75].

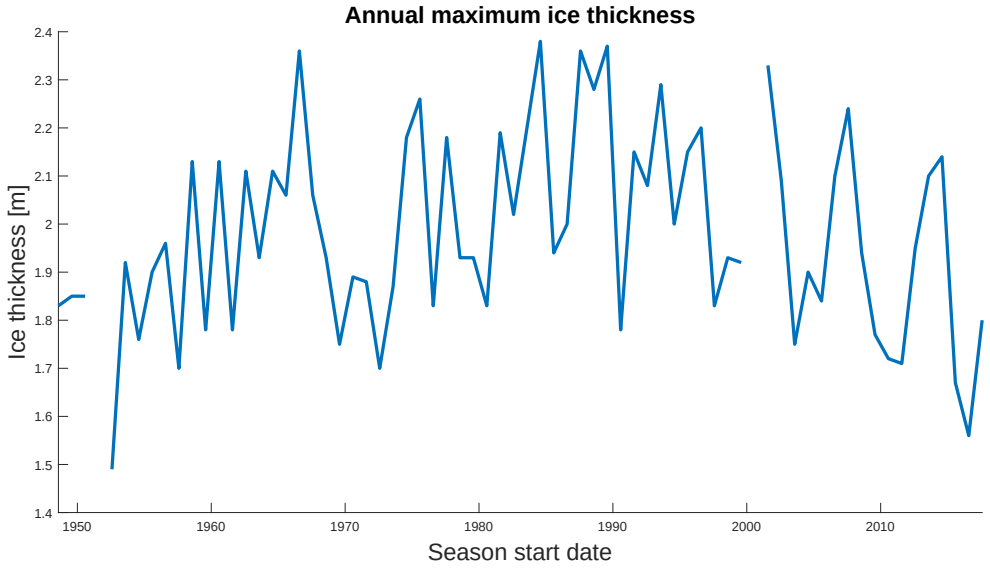

Figure A.1: Maximum measured ice thickness at Resolute Bay.

A.2. Air temperature

Besides the sea ice thickness data, also daily minimum and maximum surface air temperature data is available covering the same time period. Annual maximum and minimum temperatures are plotted in Figure A.2. Average temperatures are incomplete and are therefore estimated as the average of the minimum and maximum temperature. For the first measurements of air temperature, the location of the official Resolute Bay Airport is given, this location is 74.7167°N, 94.9667°W. Whether this is the exact location of the measurements, is unknown. Since 27 October 2002 the location is given at 74°42'57.005"N, 94°58'59.007"W.

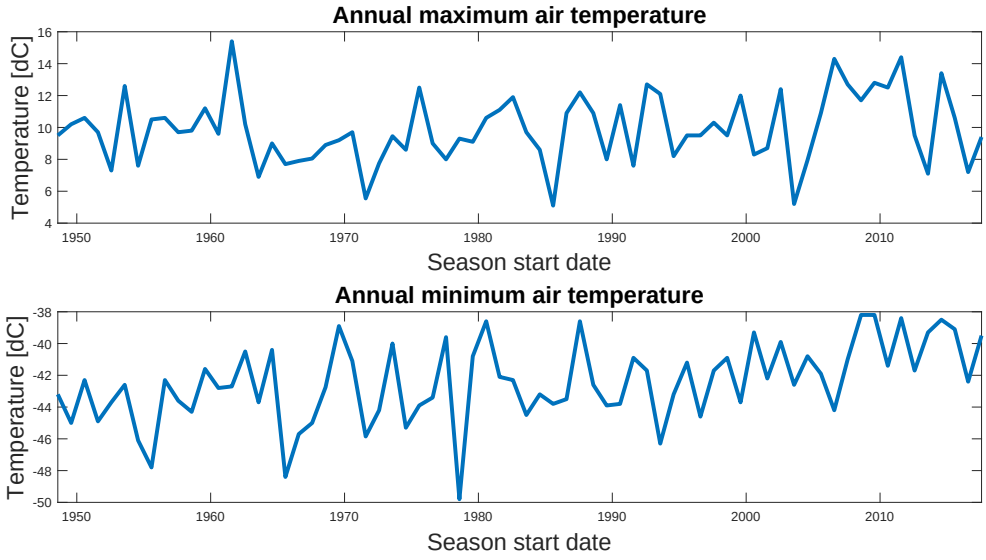

Figure A.2: Minimum and maximum annual air temperature at Resolute Bay.

A.3. Data evaluation

In order to check whether the data seems reliable, the Freezing Degree Days (FDD) and the corresponding theoretical ice thickness is calculated based on the temperature data of Resolute Bay. The method used is discussed in Appendix B.1. The theoretical thickness is compared to the measured thickness to see if they match reasonably well. For the freezing temperature of sea water this method suggests $T_f = -1.8\,°C$. The cumulative sum of FDD starts once the temperature gets below T_f and for temperatures above T_f, FDD remains constant.

The method does not include the melting of ice as soon as the melt season starts. However, this dataset also contains data points where the ice already started melting. For these data points FDD should not be zero because ice thickness is non-zero. On the other hand, the FDD should be smaller than the FDD at the end of the freezing season because the ice is thinner because of melting. For the purpose of evaluation of the data, the FDD is set to decline to zero proportionally with the temperature. This starts as soon as the average temperature has been positive for four days, see Figure A.3. This way, these data point do not indicate any false inadequacy.

The thickness is calculated as function of FDD, see Equation (B.2). The initial thickness (h_0) is set to zero because in Resolute Bay almost only first year ice exists. Snow is not considered here, because there is limited snow data available and the point of calculating the theoretical ice thickness is only to check if the measured thickness corresponds reasonably well with the measured temperature. Because snow is not considered, m is zero. Equation (B.3) is used to calculate α and the following values are used as suggested by ISO 19906:

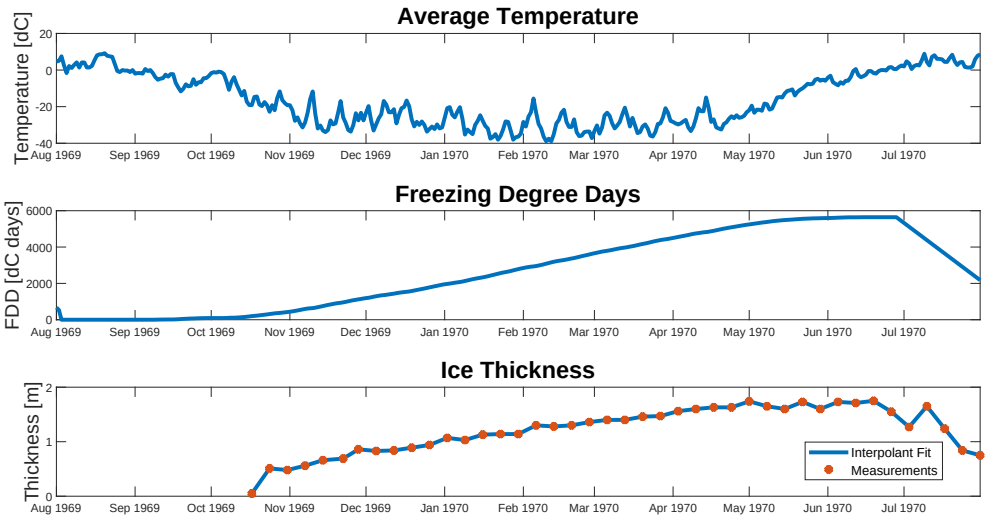

Figure A.3: Calculation of FDD compared to the measured thickness.

$k_i = 2.3\,\mathrm{Wm^{-1}°C^{-1}}$ (thermal conductivity of ice)

$\rho = 900\,\mathrm{kgm^{-1}m^{-3}}$ (ice density)

$l = 334 \times 10^3\,\mathrm{Jkg^{-1}}$ (latent heat of fusion for ice)

For ω a range between 0.3 and 0.7 is suggested. This range can be used as lower and upper bound to verify whether the measured thicknesses are within these bounds, see Figure A.4. Of the measured thickness, 86% of the data points is within the bounds of the theoretical thickness. So the measurements seem adequate.

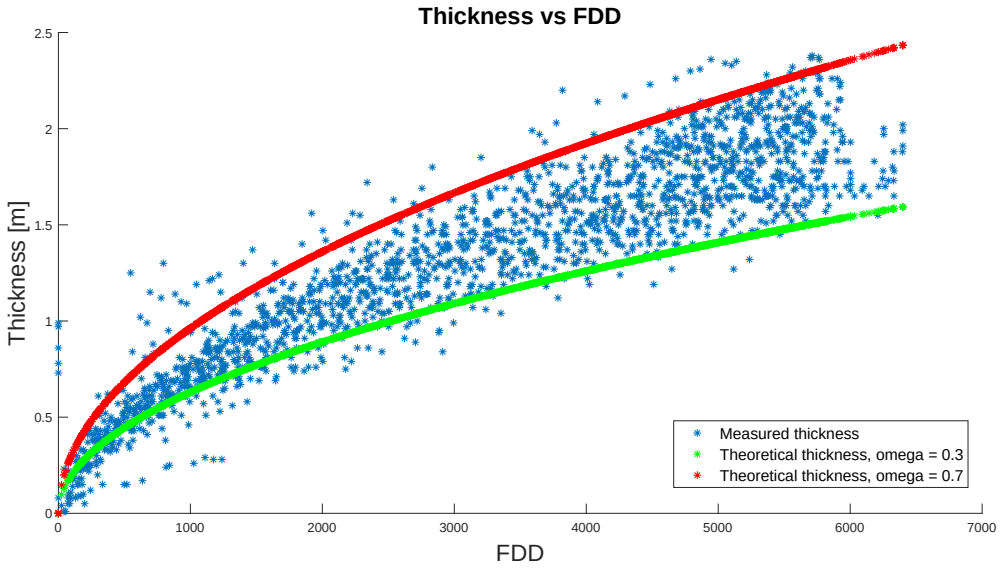

Figure A.4: Measured and theoretical upper and lower bound ice thickness for all data from Resolute Bay.

A.4. Crushing load

Using the daily temperature and thickness data the daily compressive strength is calculated using the method described in Appendix B.7. The global load is estimated using the method described in Appendix B.6, see Figure A.5.

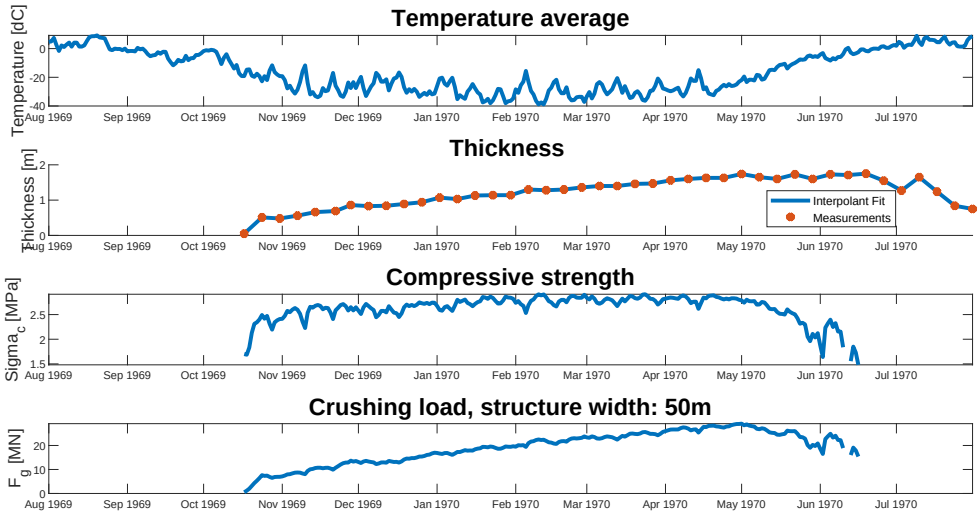

Figure A.5: Uni-axial compressive strength and estimated crushing load according to daily data from Resolute Bay.

A.5. Crushing load with trend

For the purpose of illustrating the effect of ice loads having a trend, a linear trend is applied to the seasonal maximum loads of Resolute Bay data. To do this, first the existing trend is removed. The data does not show a strong linear trend but does show a second order polynomial trend, see Figure A.6. Both curves are fitted using the least square error method.

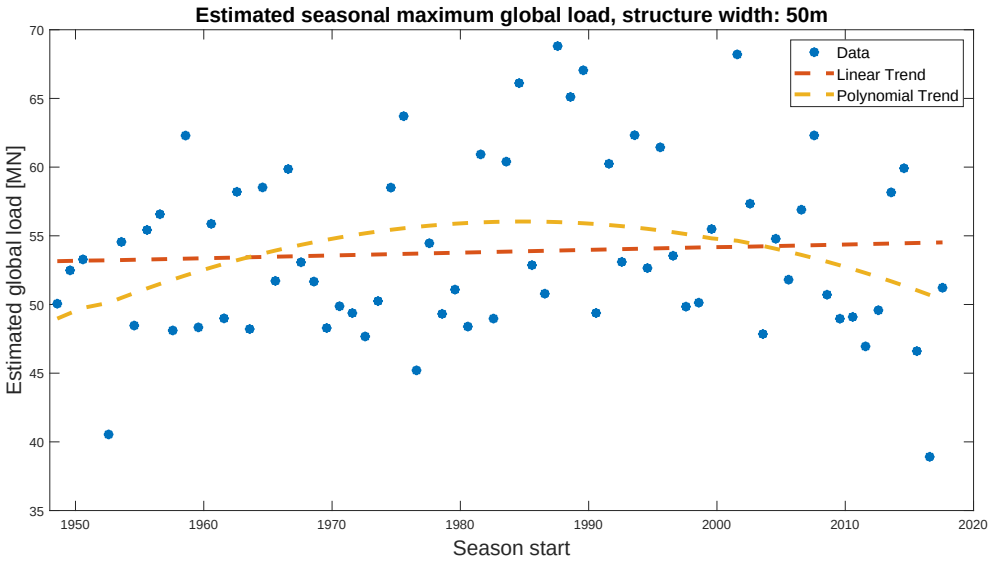

Figure A.6: Seasonal maximum estimated crushing ice load from Resolute Bay with linear and polynomial curve fit.

To apply a the linear trend, first the polynomial fitted curve is subtracted and the original ice load of the first data point (48.97 MN) is added up to all the data point. Then, a linear trend of −0.3 MN per season is applied, see Figure A.7.

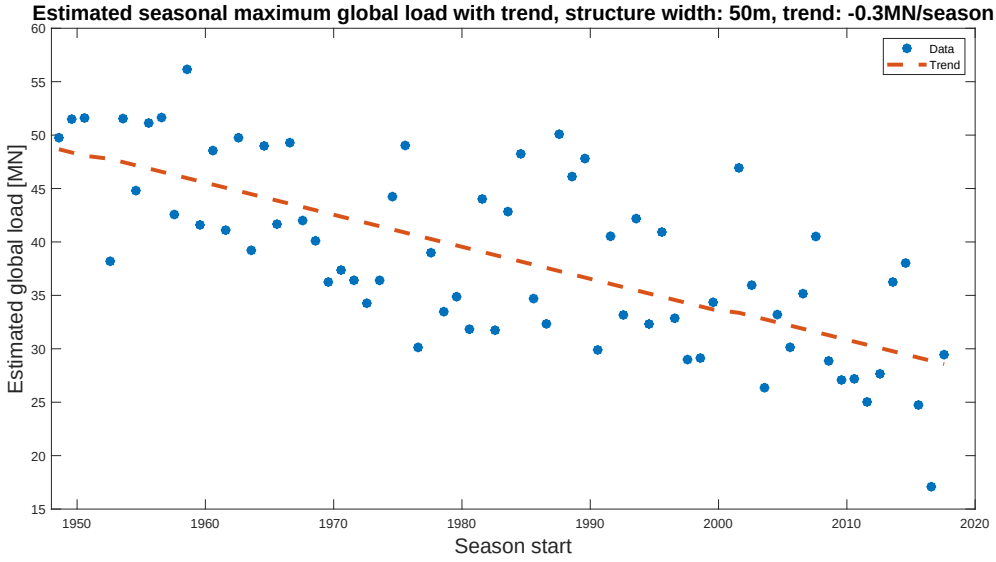

Figure A.7: Seasonal maximum estimated crushing ice load from Resolute Bay with trend.

B

Methodology

In this appendix, details of the method used to calculated various ice properties and ice loads are provided.

B.1. Ice thickness

Stefan's law is used to calculate the ice thickness for first-year ice [31]. This method is also suggested in ISO 19906. The Freezing Degree Days (FDD) can be calculated using Equation (B.1), where the sum should include all days of the considered freezing period.

$$FDD = \left| \sum (T_a - T_f) \right| \quad \text{for } T_a < T_f \tag{B.1}$$

Where T_a is the average daily air temperature and T_f is the freezing temperature of the sea water. ISO 19906 suggests a freezing temperature of T_f = −1.8 °C. Finally, the ice thickness can be determined using Equation (B.2):

$$h^2 - h_0^2 + m(h - h_0) = \alpha C_{FDD} \tag{B.2}$$

Here, h is the sea ice thickness in meters, h_0 is the initial ice thickness in meters and α is given by Equation (B.3):

$$\alpha = \omega \frac{2k_i}{\rho_i l} \tag{B.3}$$

Where ω is a given empirical coefficient, k_i is the thermal conductivity of ice, ρ_i is the density of ice and l is the latent heat of fusion for ice. Parameter m takes snow into account. Equation (B.4) is given to calculate m, in case of no snow $m = 0$.

$$m = \frac{2h_s k_i}{k_s} \tag{B.4}$$

Where h_s is the snow thickness in meters and k_s is the thermal conductivity of snow. For the input variables, values are suggested in ISO 19906.

B.2. Ice temperature

The bottom temperature (T_b) of ice is generally assumed to be equal to the freezing temperature of the sea water, so roughly −1.8 °C. The surface ice temperature (T_s) is linked to the surface air temperature (T_a), according to Equation (B.5) [65]:

$$T_s = \begin{cases} T_a, & \text{if } -2\,^\circ\text{C} \geq T_a \geq -10\,^\circ\text{C} \\ 0.6T_a - 4, & \text{if } T_a < -10\,^\circ\text{C} \end{cases} \tag{B.5}$$

For the method of calculating the compressive strength of ice, described in Appendix B.5, the ice is divided into several layers and for each layer the average temperature must be determined. According to this method, the average temperature of layer n for a total of N layers can be calculated using Equation (B.6) , under the assumption that the temperature profile is linear.

$$T_n = T_s - \frac{T_s - T_b}{2N} - (n-1)\frac{(T_s - T_b)}{N} \tag{B.6}$$

B.3. Salinity

Salinity is calculated using Equation (B.7) [61].

$$S_b = 4.606 + \frac{91.603}{100h} \tag{B.7}$$

Here, S_b is the bulk salinity as mass fraction in parts per thousand (ptt) and h is the ice thickness in metres.

B.4. Porosity

The total porosity (ν_t) can be calculated as the sum of the relative brine volume(ν_b) and the relative air volume (ν_a).

$$\nu_t = \nu_b + \nu_a \tag{B.8}$$

The relative brine volume and relative air temperature are determined as functions of salinity (S_i), temperature (T_i) and density (ρ) [62]. The relative brine volume is given by Equation (B.9):

$$\nu_b = \frac{\rho S_i}{F_1(T_i)} \tag{B.9}$$

Where,

$$F_1(T_i) = \begin{cases} -4.732 - 22.45T_i - 0.6397T_i^2 - 0.01074T_i^3, & \text{for } -2\,°\text{C} \geq T_i \geq -22.9\,°\text{C} \\ 9899 + 1309T_i + 55.27T_i^2 + 0.716T_i^3, & \text{for } -22.9\,°\text{C} \geq T_i \geq -30\,°\text{C} \end{cases}$$

And the relative air volume is given by Equation (B.10):

$$\nu_a = 1 - \frac{\rho}{\rho_i(T_i)} + \frac{\rho S_i F_2(T_i)}{F_1(T_i)} \tag{B.10}$$

Where,

$$F_2(T_i) = \begin{cases} 8.903 \cdot 10^{-2} - 1.763 \cdot 10^{-2}T_i - 5.33 \cdot 10^{-4}T_i^2 - 8.801 \cdot 10^{-6}T_i^3, & \text{for } -2\,°\text{C} \geq T_i \geq -22.9\,°\text{C} \\ 8.547 + 1.089T_i + 4.158 \cdot 10^{-2}T_i^2 + 5.849 \cdot 10^{-4}T_i^3, & \text{for } -22.9\,°\text{C} \geq T_i \geq -30\,°\text{C} \end{cases}$$

$$\rho_i(T_i) = 917 - 1.403 \cdot 10^{-1}T_i$$

Furthermore, for these equations, S_i is in ppt, T_i in °C, ρ in kgm^{-3} and ν_t as volume fraction ([-]). The temperature of the ice can be calculated using Equation (B.6).

In ISO 19906, a more simple method is suggested to calculate the relative brine volume, see Equation (B.11) [76]. This method is valid for temperatures between -0.5 °C and -22.9 °C and can be used if the density is not well known.

$$\nu_b = S_i\left(\frac{49.185}{|T_i|} + 0.532\right) \tag{B.11}$$

For this equation the same units hold. No equation for relative air volume is given in ISO 19906.

B.5. Uni-axial compressive strength

The uni-axial compressive strength is calculated according to the method of Timco and Frederking [65]. For this method, only the average air temperature (T_a), ice thickness (h_i) and strain rate ($\dot{\epsilon}$) are needed. This method is valid for air temperatures between $-2\,°C$ and $-30\,°C$. The method suggests that the ice is divided in nine layers, see Figure 3.6. The top layer is assumed to be made of granular ice and the other layers of columnar ice. The compressive strength for the top granular layer can be calculated according to Equation (B.12):

$$\sigma_c = 49\dot{\epsilon}^{0.22}\left(1+\sqrt{\frac{\nu_t}{0.280}}\right) \tag{B.12}$$

And the compressive strength for the other horizontally-loaded columnar ice layers can be calculated according to Equation (B.13):

$$\sigma_c = 37\dot{\epsilon}^{0.22}\left(1+\sqrt{\frac{\nu_t}{0.270}}\right) \tag{B.13}$$

The compressive strength of the ice sheet is calculated as the average compressive strength of all ice layers. This method is valid for a strain rate range from $\dot{\epsilon} = 10^{-7}\,s^{-1}$ till $\dot{\epsilon} = 10^{-3}\,s^{-1}$. For design purpose, usually a strain rate of $\dot{\epsilon} = 10^{-3}\,s^{-1}$, corresponding to the highest compressive strength values, is used.

The porosity is calculated as volume fraction according to the method of Cox and Week. For the bulk density a value of $907\,kgm^{-3}$ is suggested, based on measurements from the Beaufort Sea. The ice salinity is calculated according to Equation (B.14) in parts per thousand:

$$S_i = \begin{cases} 134 - 17.4h_i, & \text{for } h \leq 0.34\,m \\ 8.0 - 1.62h_i, & \text{for } h \geq 0.34\,m \end{cases}$$

B.6. Crushing load estimation

To estimate the global crushing load, the following method is devised. The global crushing load resulting from this method is a rough estimate based on experience. The load is estimated using the uni-axial compressive strength of the ice and the contact area. For crushing, the actual contact area can be estimated using Equation (B.14):

$$A_{contact} = C_{NS}C_G wh \tag{B.14}$$

Values for C_{NS} and C_G are suggested in Section 3.5.3. The global load can be estimated using Equation (B.15):

$$F_G = \sigma_c A_{contact} \tag{B.15}$$

B.7. ISO 19906 Design Crushing load

The following method is suggested by ISO 19906 to calculate the ULS global crushing load. Using Equation (B.16), this global ice load (F_G) can be calculated as function of the global pressure (p_G), the ice thickness (h) and the structure width (w). The global ice pressure (p_G) can be calculated according Equation (B.17) as function of an ice strength coefficient (C_R), a reference thickness ($h_1 = 1\,m$), empirical term (f_{AR}) and two empirical coefficients ($m = -0.16$) and ($n = -0.50 + \frac{h}{5}$ for $h < 1.0\,m$ or $n = -0.30$ for $h \geq 1.0\,m$).

$$F_G = p_G wh \tag{B.16}$$

$$p_G = C_R\left(\left(\frac{h}{h_1}\right)^n\left(\frac{w}{h}\right)^m + f_{AR}\right) \tag{B.17}$$

The empirical term (f_{AR}) is given by Equation (B.18) but can be disregarded for aspect ratios of $w/h > 5$.

$$f_{AR} = \exp \frac{-w}{3h} \sqrt{1 + 5\frac{h}{w}} \tag{B.18}$$

Bibliography

[1] Mikael Höök and Xu Tang. Depletion of fossil fuels and anthropogenic climate change—a review. *Energy Policy*, 52:797 – 809, 2013. ISSN 0301-4215. doi:10.1016/j.enpol.2012.10.046. Special Section: Transition Pathways to a Low Carbon Economy.

[2] Stocker T.F., D. Qin, G.-K. Plattner, M. Tignor, S.K. Allen, J. Boschung, A. Nauels, Y. Xia, V. Bex and P.M. Midgley (eds.). Climate change 2013: The physical science basis. contribution of working group i to the fifth assessment report of the intergovernmental panel on climate change. *IPCC, 2013*, Cambridge University Press, Cambridge, United Kingdom and New York, NY, USA:1535, 2014. doi:10.1017/CBO9781107415324.

[3] Mark C. S. and Roger G. B., title = Processes and impacts of Arctic amplification: A research synthesis, journal = Global and Planetary Change, volume = 77, number = 1, pages = 85 - 96, year = 2011, issn = 0921-8181, doi = 10.1016/j.gloplacha.2011.03.004,.

[4] Fetterer, F., K. Knowles, W. N. Meier, M. Savoie, and A. K. Windnagel. Sea ice index, version 3. *National Snow and Ice Data Center*, 2017. doi:10.7265/N5K072F8.

[5] ISO 19906:2019. Petroleum and natural gas industries — Arctic offshore structures. Design standard, International Organization for Standardization, Geneva, Switzerland, 2019. URL `https://www.iso.org/standard/65477.html`.

[6] DNVGL-OS-C101. Design of offshore steel structures, general lrfd method. Design standard, DNV GL, Høvik, Norway, 2015.

[7] Pithan F., Mauritsen T. Arctic amplification dominated by temperature feedbacks in contemporary climate models. *Nature Geosci*, 7:181–184, 2014. doi:10.1038/ngeo2071.

[8] Johannessen O.M., Bengtsson L., Miles M.W., Kuzmina S.I., Semenov V.A., Alekseev G.V., Nagurnyi A.P., Zakharov V.F., Bobylev L.P., Pettersson L.H., Hasselmann K., Cattle H.P. Arctic climate change: observed and modelled temperature and sea-ice variability. *Tellus A: Dynamic Meteorology and Oceanography*, 56(4):328–341, 2004. doi:10.3402/tellusa.v56i4.14418.

[9] Rajmund P. Temporal and spatial variation of surface air temperature over the period of instrumental observations in the arctic. *International Journal of Climatology*, 20(6):587–614, 2000. URL `https://doi.org/10.1002/(SICI)1097-0088(200005)20:6%3C587::AID-JOC480%3E3.0.CO;2-H`.

[10] van Vuuren, D., M. den Elzen, P. Lucas, B. Eickhout, B. Strengers, B. van Ruijven, S. Wonink, R. van Houdt. Stabilizing greenhouse gas concentrations at low levels: an assessment of reduction strategies and costs. *Climatic Change*, 2007. doi:10.1007/s10584-006-9172-9.

[11] Clarke, L., J. Edmonds, H. Jacoby, H. Pitcher, J. Reilly, R. Richels. Scenarios of greenhouse gas emissions and atmospheric concentrations. sub-report 2.1a of synthesis and assessment product 2.1. *U.S. Climate Change Science Program and the Subcommittee on Global Change Research*, 2007.

[12] Smith, S.J. and T.M.L. Wigley. Multi-gas forcing stabilization with the minicam. *Energy Journal (Special Issue 3)*, 2006. doi:10.5547/ISSN0195-6574-EJ-VolSI2006-NoSI3-19.

[13] Wise, MA, KV Calvin, AM Thomson, LE Clarke, B Bond-Lamberty, RD Sands, SJ Smith, AC Janetos, JA Edmonds. Implications of limiting co2 concentrations for land use and energy. *Science*, pages 324:1183–1186, 2009. doi:10.1126/science.1168475.

[14] Fujino, J., R. Nair, M. Kainuma, T. Masui, Y. Matsuoka. Multi-gas mitigation analysis on stabilization scenarios using aim global model. *The Energy Journal Special Issue.*, 2006. doi:10.5547/ISSN0195-6574-EJ-VolSI2006-NoSI3-17.

[15] Hijioka, Y., Y. Matsuoka, H. Nishimoto, M. Masui, and M. Kainuma. Global ghg emissions scenarios under ghg concentration stabilization targets. *Journal of Global Environmental Engineering*, 13, 97-108.

[16] Riahi, K. Gruebler, A. and Nakicenovic N. Scenarios of long-term socio-economic and environmental development under climate stabilization. *Technological Forecasting and Social Change*, 74:887–935, 2007. doi:10.1016/j.techfore.2006.05.026.

[17] H.O. Portner, D.C. Roberts, V. Masson-Delmotte, P. Zhai, M. Tignor, E. Poloczanska, K. Mintenbeck, A. Alegria, M. Nicolai, A. Okem, J. Petzold, B. Rama, N.M. Weyer (eds.). Ipcc special report on the ocean and cryosphere in a changing climate. *IPCC, 2019*, 2019.

[18] van Vuuren, D.P., Edmonds, J., Kainuma, M. et al. The representative concentration pathways: an overview. *Climatic Change*, 109, 2011. doi:10.1007/s10584-011-0148-z.

[19] International Institute for Applied Systems Analysis. Rcp database. URL `https://tntcat.iiasa.ac.at/RcpDb/dsd?Action=htmlpage&page=welcome`.

[20] Stroeve J., Holland M. M., Meier W., Scambos T. and Serreze, Mark. Arctic sea ice decline: Faster than forecast. *Geophysical Research Letters*, 34(9), 2007. doi:10.1029/2007GL029703.

[21] Taylor, Karl E. and Stouffer, Ronald J. and Meehl, Gerald A. An overview of cmip5 and the experiment design. *Bulletin of the American Meteorological Society*, 93(4):485–498, 2012. doi:10.1175/BAMS-D-11-00094.1.

[22] Peter Lemke, Hans-Werner Jacobi. Arctic climate change, the acsys decade and beyond. 2012. doi:10.1007/978-94-007-2027-5.

[23] Chapman, William L. and Walsh, John E. Simulations of arctic temperature and pressure by global coupled models. *Journal of Climate*, 20(4):609–632, 2007. doi:10.1175/JCLI4026.1.

[24] Liston, Glen E. and Hiemstra, Christopher A. The changing cryosphere: Pan-arctic snow trends (1979–2009). *Journal of Climate*, 24(21):5691–5712, 2011. doi:10.1175/JCLI-D-11-00081.1.

[25] Spreen, Gunnar and Kwok, Ron and Menemenlis, Dimitris. Trends in arctic sea ice drift and role of wind forcing: 1992–2009. *Geophysical Research Letters*, 38(19), 2011. doi:10.1029/2011GL048970.

[26] Rigor, Ignatius G. and Wallace, John M. and Colony, Roger L. Response of sea ice to the arctic oscillation. *Journal of Climate*, 15(18):2648–2663, 2002. doi:10.1175/1520-0442(2002)015<2648:ROSITT>2.0.CO;2.

[27] Armitage, T. W. K. and Bacon, S. and Ridout, A. L. and Petty, A. A. and Wolbach, S. and Tsamados, M. Arctic ocean surface geostrophic circulation 2003–2014. *The Cryosphere*, 11(4):1767–1780, 2017. doi:10.5194/tc-11-1767-2017.

[28] G.W. Timco and W.F. Weeks. A review of the engineering properties of sea ice. *Cold Regions Science and Technology*, 60(2):107 – 129, 2010. ISSN 0165-232X. doi:10.1016/j.coldregions.2009.10.003.

[29] Matti Leppäranta. A review of analytical models of sea□ice growth. *Atmosphere-Ocean*, 31(1): 123–138, 1993. doi:10.1080/07055900.1993.9649465.

[30] F.J. Millero. Freezing point of seawater. *Annex 6, Eight report of the Joint Panel on Oceanographic Tables and Standards (JPOTS)*, pages 29–35, 1978.

[31] Stefan, J. Ueber die theorie der eisbildung, insbesondere über die eisbildung im polarmeere. *Annalen der Physik*, 278(2):269–286, 1891. doi:10.1002/andp.18912780206.

[32] Kwok, R. and Rothrock, D. A. Decline in arctic sea ice thickness from submarine and icesat records: 1958–2008. *Geophysical Research Letters*, 36(15), 2009. doi:10.1029/2009GL039035.

[33] Deser, Clara and Teng, Haiyan. Evolution of arctic sea ice concentration trends and the role of atmospheric circulation forcing, 1979–2007. *Geophysical Research Letters*, 35(2), 2008. doi:10.1029/2007GL032023.

[34] Vinnikov, Konstantin Y. and Robock, Alan and Stouffer, Ronald J. and Walsh, John E. and Parkinson, Claire L. and Cavalieri, Donald J. and Mitchell, John F. B. and Garrett, Donald and Zakharov, Victor F. Global warming and northern hemisphere sea ice extent. *Science*, 286(5446):1934–1937, 1999. ISSN 0036-8075. doi:10.1126/science.286.5446.1934.

[35] Stroeve, J.C., Serreze, M.C., Holland, M.M. et al. The arctic's rapidly shrinking sea ice cover: a research synthesis. *Climatic Change*, 110:1005–1027, 2012. doi:10.1007/s10584-011-0101-1.

[36] Melling, Humfrey and Riedel, David A. and Gedalof, Ze'ev. Trends in the draft and extent of seasonal pack ice, canadian beaufort sea. *Geophysical Research Letters*, 32(24), 2005. doi:10.1029/2005GL024483.

[37] Vinje, Torgny and Nordlund, Nina and Kvambekk, Ånund. Monitoring ice thickness in fram strait. *Journal of Geophysical Research: Oceans*, 103(C5):10437–10449, 1998. doi:10.1029/97JC03360.

[38] Lindsay, R. and Schweiger A. Unified sea ice thickness climate data record, 1947 onward, version 1. *National Snow and Ice Data Center*, 2017. doi:10.7265/N5D50JXV.

[39] Lindsay, R. and Schweiger, A. Arctic sea ice thickness loss determined using subsurface, aircraft, and satellite observations. *The Cryosphere*, 9(1):269–283, 2015. doi:10.5194/tc-9-269-2015.

[40] Kwok,Ronald and Untersteiner,Norbert. The thinning of arctic sea ice. *Physics Today*, 64(4): 36–41, 2011. doi:10.1063/1.3580491.

[41] Barber, D. G., McCullough, G., Babb, D. G., Komarov, A. S., Candlish, L. M., Lukovich, J. V., et al. Climate change and ice hazards in the beaufort sea. *Elem. Sci. Anth*, 2014. doi:10.12952/journal.elementa.000025.

[42] Kwok, R. and Cunningham, G. F. Variability of arctic sea ice thickness and volume from cryosat-2. *Philosophical Transactions of the Royal Society A: Mathematical, Physical and Engineering Sciences*, 373(2045), 2015. doi:10.1098/rsta.2014.0157.

[43] Rampal, P. and Weiss, J. and Marsan, D. Positive trend in the mean speed and deformation rate of arctic sea ice, 1979–2007. *Journal of Geophysical Research: Oceans*, 114(C5), 2009. doi:10.1029/2008JC005066.

[44] Shu, Q. and Song, Z. and Qiao, F. Assessment of sea ice simulations in the cmip5 models. *The Cryosphere*, 9(1):399–409, 2015. doi:10.5194/tc-9-399-2015.

[45] Collins, W.J., N. Bellouin, M. Doutriaux-Boucher, N. Gedney, T. Hinton, C. D. Jones, S. Liddicoat, G. Martin, F. O'Connor, J. Rae, C. Senior, I. Totterdell, S. Woodward, T. Reichler, J. Kim,. Met office hadley centre technical note no. hctn 74. *HadGEM2-ES*, 2008. URL `https://esgf-node.llnl.gov/projects/cmip5/`.

[46] API RP 2N. Planning, designing, and constructing structures and pipelines for arctic conditions. Design standard, American Petroleum Institute, Washington, DC, United States of America, 2015.

[47] CAN/CSA-S471-04 (R2008). General Requirements, Design Criteria, the Environment, and Loads. Design standard, Canadian Standards Association, Ontario, Canada, 2008.

[48] SNiP 2.06.04-82. Loads and actions on hydraulic engineering constructions (wave and ice generated and from ships). Design standard, Ministry of Construction of Russia, Moscow, Russia, 1995.

[49] Spring W., McKenna R. F., Thomas G. A. N., Blanchet D. Iso 19906 - an international standard for arctic offshore structures. *Proceedings of the International Conference on Port and Ocean Engineering under Arctic Conditions*, 61, 2011. ISSN 2077-7841. URL http://www.poac.com/PapersOnline.html.

[50] Kaj Riska and Robert Bridges. Limit state design and methodologies in ice class rules for ships and standards for arctic offshore structures. *Marine Structures*, 63:462 – 479, 2019. ISSN 0951-8339. doi:10.1016/j.marstruc.2017.09.005.

[51] Roeder, C. W. Comparison of lrfd and allowable stress design methods for steel structures. *5th Seminario de Ingenieria Estructural, San Jose, Costa Rica*, 1990.

[52] Galambos, T. V. Eight collected papers on load and resistance factor. *Journal of the Structural Division, ASCE*, 104, 1978.

[53] Dayong Zhang and Guojun Wang and Qianjin Yue. Evaluation of ice-induced fatigue life for a vertical offshore structure in the bohai sea. *Cold Regions Science and Technology*, 154:103 – 110, 2018. ISSN 0165-232X. doi:10.1016/j.coldregions.2018.05.012.

[54] Devinder S. Sodhi and Robert B. Haehnel. Crushing ice forces on structures. *Journal of Cold Regions Engineering*, 17(4):153–170, 2003. doi:10.1061/(ASCE)0887-381X(2003)17:4(153).

[55] G. W. Timco. Laboratory observations of macroscopic failure modes in freshwater ice. *Proceedings 6th International Cold Regions Engineering Conference*, 17(4):605–614, 1991.

[56] Hayo Hendrikse and Andrei Metrikine. Ice-induced vibrations and ice buckling. *Cold Regions Science and Technology*, 131:129 – 141, 2016. ISSN 0165-232X. doi:10.1016/j.coldregions.2016.09.009.

[57] Riska, Kaj. Ice edge failure process and modelling ice pressure. *Philosophical Transactions of the Royal Society A: Mathematical, Physical and Engineering Sciences*, 376(2129):20170340, 2018. doi:10.1098/rsta.2017.0340.

[58] Palmer, A.C. and Goodman, D. J. and Ashby, M. F. and Evans, A. G. and Hutchinson, J.W. and Ponter, A. R. S. Fracture and its role in determining ice forces on offshore structures. *Annals of Glaciology*, 4:216–221, 1983. doi:10.3189/S0260305500005504.

[59] Takeuchi, Takahiro and Sakai, Masafumi and Akagawa, Satoshi and Nakazawa, Naoki and Saeki, Hiroshi. On the factors influencing the scaling of ice forces. In Dempsey, J. P. and Shen, H. H., editors, *IUTAM Symposium on Scaling Laws in Ice Mechanics and Ice Dynamics*, pages 149–160, Dordrecht, 2001. Springer Netherlands. ISBN 978-94-015-9735-7.

[60] Hayo Hendrikse and Andrei Metrikine. Interpretation and prediction of ice induced vibrations based on contact area variation. *International Journal of Solids and Structures*, 75-76:336 – 348, 2015. ISSN 0020-7683. doi:doi.org/10.1016/j.ijsolstr.2015.08.023.

[61] Austin Kovacs. Sea ice. part i. bulk salinity versus ice floe thickness. 1996. URL https://apps.dtic.mil/dtic/tr/fulltext/u2/a312027.pdf.

[62] Cox, G. F. N. and Weeks, W. F. Equations for determining the gas and brine volumes in sea-ice samples. *Journal of Glaciology*, 29(102):306–316, 1983. doi:10.3189/S0022143000008364.

[63] G.W Timco and R.M.W Frederking. An investigation of the failure envelope of granular/discontinuous-columnar sea ice. *Cold Regions Science and Technology*, 9(1):17 – 27, 1984. ISSN 0165-232X. doi:doi.org/10.1016/0165-232X(84)90044-2.

[64] G.W. Timco and R. Frederking. Confined compressive strength of sea ice. *The Seventh International Conference on Port and Ocean Engineering under Arctic Conditions*, 1:243–253, 1983. ISSN 0357-9387.

[65] G.W. Timco and R.M.W. Frederking. Compressive strength of sea ice sheets. *Cold Regions Science and Technology*, 17(3):227 – 240, 1990. ISSN 0165-232X. doi:10.1016/S0165-232X(05)80003-5.

[66] Philippe Cambos, Ken Croasdale, Maxim Yazarov, Kaj Riska and Robert Bridges. Impact of climate change on design and operation of arctic ships and offshore units. *Proceedings of the International Conference on Port and Ocean Engineering under Arctic Conditions*, 2019. ISSN 2077-7841. URL http://www.poac.com/PapersOnline.html.

[67] Ochi, M. K. Principles of extreme value statistics and their application. *Proc, Extreme Loads Response Sypmosium*, pages 15–30, 1981.

[68] Mark Fuglem and Ian Jordaan and Greg Crocker and Gus Cammaert and Bruce Berry. Environmental factors in iceberg collision risks for floating systems. *Cold Regions Science and Technology*, 24(3):251 – 261, 1996. ISSN 0165-232X. doi:10.1016/0165-232X(95)00013-2.

[69] Mikko Suominen and Pentti Kujala and Jani Romanoff and Heikki Remes. Influence of load length on short-term ice load statistics in full-scale. *Marine Structures*, 52:153 – 172, 2017. ISSN 0951-8339. doi:10.1016/j.marstruc.2016.12.006.

[70] Torodd S. Nord and Ilija Samardžija and Hayo Hendrikse and Morten Bjerkås and Knut V. Høyland and Hongtao Li. Ice-induced vibrations of the norströmsgrund lighthouse. *Cold Regions Science and Technology*, 155:237 – 251, 2018. ISSN 0165-232X. doi:https://doi.org/10.1016/j.coldregions.2018.08.005.

[71] Google. (n.d.). Kara sea google maps. 2020. URL https://www.google.com/maps.

[72] Environment and Climate Change Canada. Ice thickness program collection, 1947-2002. 2015. URL http://donnees.ec.gc.ca/data/ice/products/ice-thickness-program-collection/.

[73] Menne, M.J., I. Durre, B. Korzeniewski, S. McNeal, K. Thomas, X. Yin, S. Anthony, R. Ray, R.S. Vose, B.E.Gleason, and T.G. Houston. Global historical climatology network - daily (ghcn-daily). *NOAA National Climatic Data Center*, 2012. doi:10.7289/V5D21VHZ.

[74] M. Shokr , N. Sinha. *Sea Ice: Physics and Remote Sensing*, chapter 1, pages 1–25. American Geophysical Union (AGU), 2015. ISBN 9781119028000. doi:10.1002/9781119028000.ch1.

[75] Ross D. Brown and Phil Cote. Interannual variability of landfast ice thickness in the canadian high arctic, 1950-89. *Arctic*, 45(3):273–284, 1992. ISSN 00040843.

[76] Frankenstein, Guenther and Garner, Robert. Equations for determining the brine volume of sea ice from minus 0.5 to minus 22.9 degree celsius. *Journal of Glaciology*, 6(48):943–944, 1967. doi:10.3189/S0022143000020244.